USE OF A MASS SPECTROMETER TO DETERMINE THE COMPOSITION OF THE UNDISTURBED MARTIAN ATMOSPHERE FROM A HYPERSONIC ENTRY VEHICLE

by

M. H. Bortner, R. P. Fogaroli, H. L. Friedman, H. W. Goldstein,
R. E. Simons, and P. D. Zavitsanos

FINAL REPORT

October 25, 1965

Prepared under Contract No. NAS5-9602 by

General Electric Company
Missile and Space Division
King of Prussia, Pennsylvania

for

NATIONAL AERONAUTICS AND SPACE ADMINISTRATION
Goddard Space Flight Center
Greenbelt, Maryland

USE OF A MASS SPECTROMETER TO DETERMINE THE COMPOSITION OF THE UNDISTURBED MARTIAN ATMOSPHERE FROM A HYPERSONIC ENTRY VEHICLE

by

M. H. Bortner, R. P. Fogaroli, H. L. Friedman, H. W. Goldstein,
R. E. Simons, and P. D. Zavitsanos

FINAL REPORT

October 25, 1965

Prepared under Contract No. NAS5-9602 by

General Electric Company
Missile and Space Division
King of Prussia, Pennsylvania

for

NATIONAL AERONAUTICS AND SPACE ADMINISTRATION
Goddard Space Flight Center
Greenbelt, Maryland

TABLE OF CONTENTS

LIST OF ILLUSTRATIONS

LIST OF ILLUSTRATIONS (Cont'd)

LIST OF ILLUSTRATIONS (Cont'd)

LIST OF ILLUSTRATIONS (Cont'd)

LIST OF TABLES

INTRODUCTION

The purpose of this research is to examine various aspects of using a mass spectrometer to determine the chemical composition of the Martian atmosphere when this instrument is carried aboard a hypersonic entry vehicle having the configuration shown in Figure 1 and a heat shield made of ATJ graphite. The mass spectrometer entrance chamber will be mounted within the vehicle and will be connected to the exterior of the vehicle by means of a circular orifice. The pressure response time constant of the chamber is less than 0.05 seconds and the chamber will be flushed at a rate of from one to twenty times persecond. Trajectories and atmosphere profiles are shown in Figures 2-7 for minimum and maximum engineering models of the Mars atmosphere similar to those given in NASA TN D-2525. The chemical composition of each model is given in Table 1. The angle of attack of the vehicle is assumed to be zero. Vehicle speeds given in this report fall into two groups corresponding to nominal impact speeds of 26,000 ft/s and 22,000 ft/s on Mars surface for the case of no atmospheric retardation.

When the mass spectrometric data are received, it will be necessary to convert them to chemical composition at the inlet leak of the mass spectrometer and then to chemical composition

MARS ENTRY VEHICLE CONFIGURATION

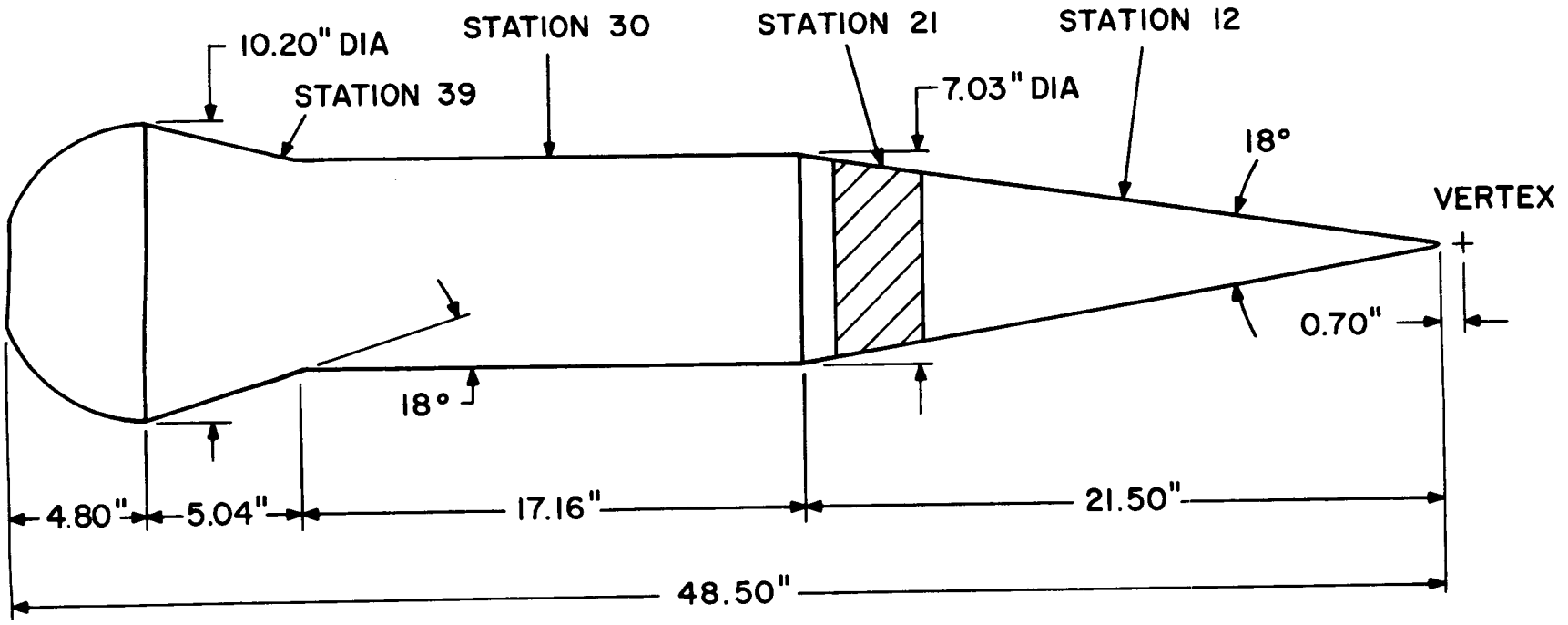

FIGURE 1

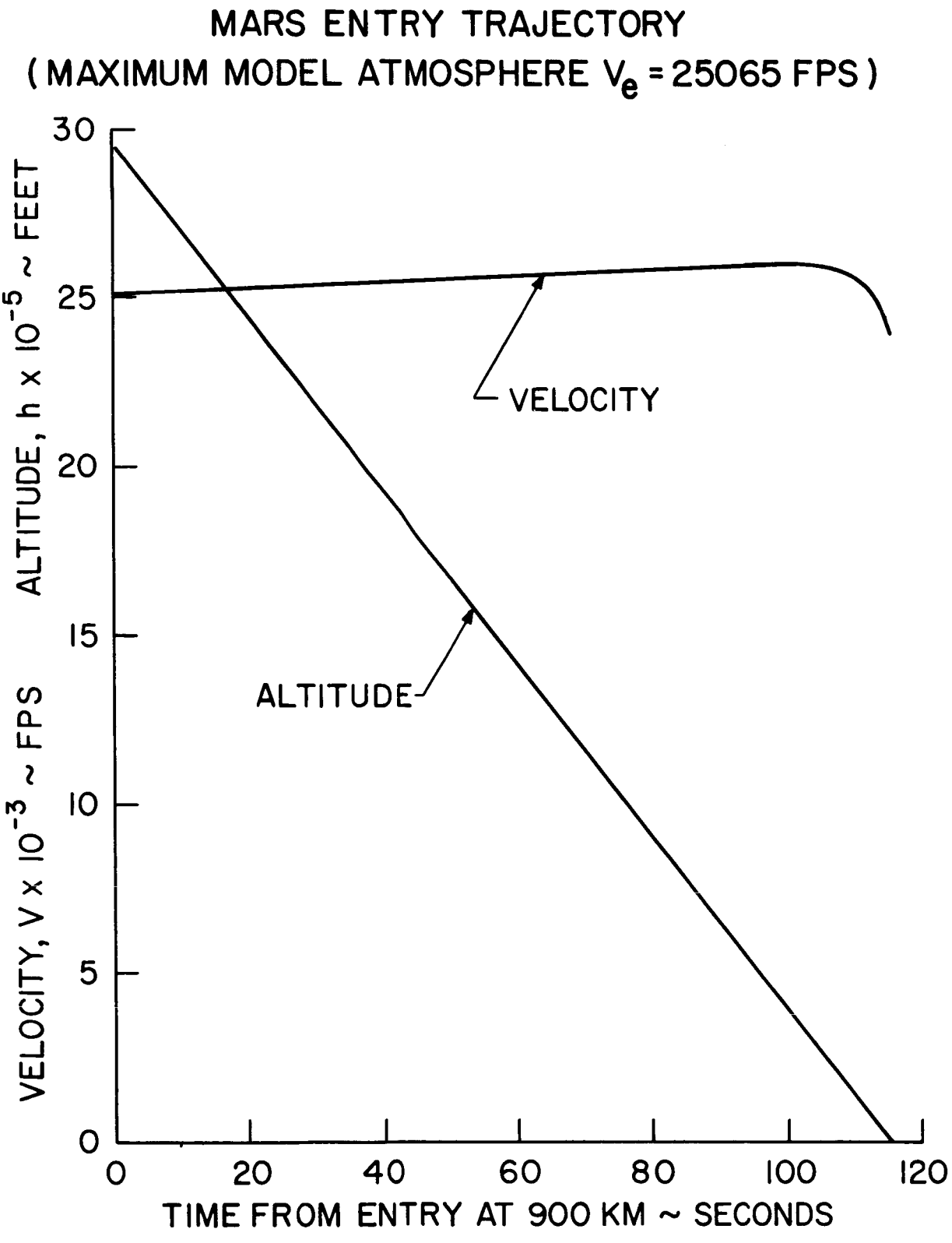
MARS ENTRY TRAJECTORY
(MAXIMUM MODEL ATMOSPHERE V_e = 25065 FPS)
VELOCITY, V x 10^{-3} ~ FPS
ALTITUDE, h x 10^{-5} ~ FEET
30
25
20
15
10
5
0
VELOCITY
ALTITUDE
0
20
40
60
80
100
120
TIME FROM ENTRY AT 900 KM ~ SECONDS

FIGURE 2

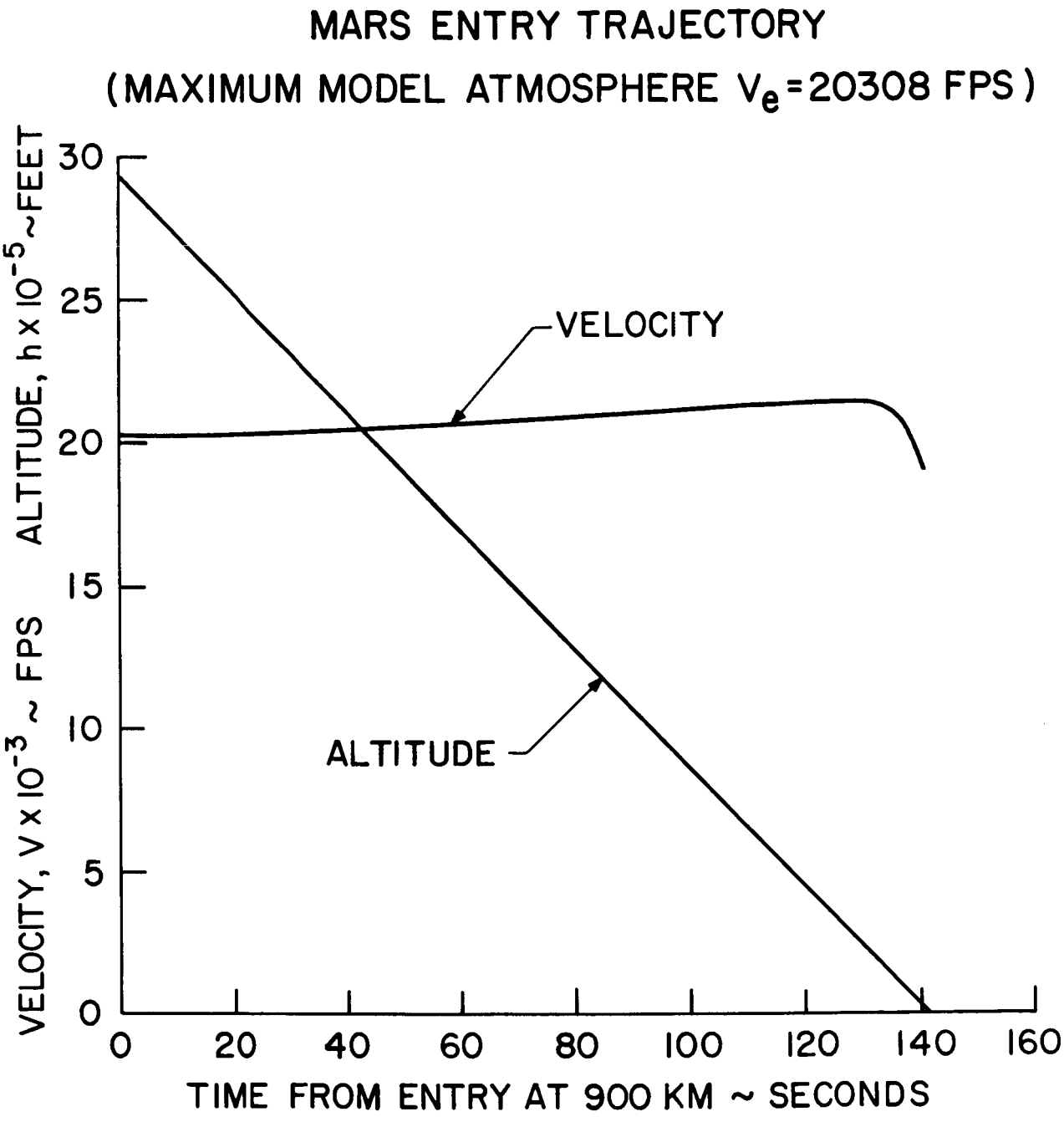
MARS ENTRY TRAJECTORY
(MAXIMUM MODEL ATMOSPHERE V_e = 20308 FPS)
VELOCITY, V x 10^-3 ~ FPS
ALTITUDE, h x 10^-5 ~ FEET
30
25
20
15
10
5
0
VELOCITY
ALTITUDE
0
20
40
60
80
100
120
140
160
TIME FROM ENTRY AT 900 KM ~ SECONDS

FIGURE 3

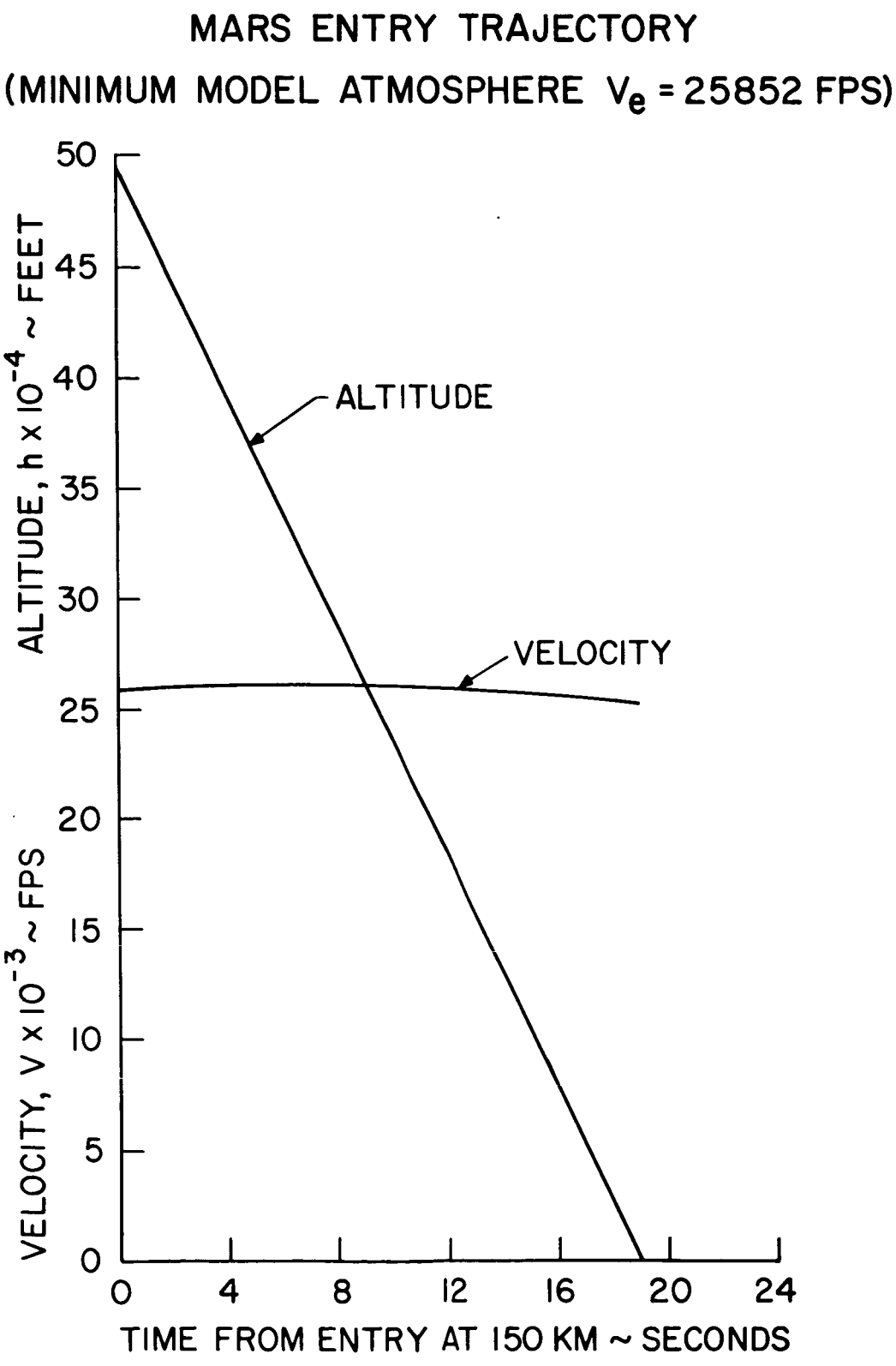
MARS ENTRY TRAJECTORY
(MINIMUM MODEL ATMOSPHERE V_e = 25852 FPS)
ALTITUDE, h x 10^{-4} ~ FEET
VELOCITY, V x 10^{-3} ~ FPS
ALTITUDE
VELOCITY
50
45
40
35
30
25
20
15
10
5
0
0
4
8
12
16
20
24
TIME FROM ENTRY AT 150 KM ~ SECONDS

FIGURE 4

MARS ENTRY TRAJECTORY

(MINIMUM MODEL ATMOSPHERE V_e = 21292 FPS)

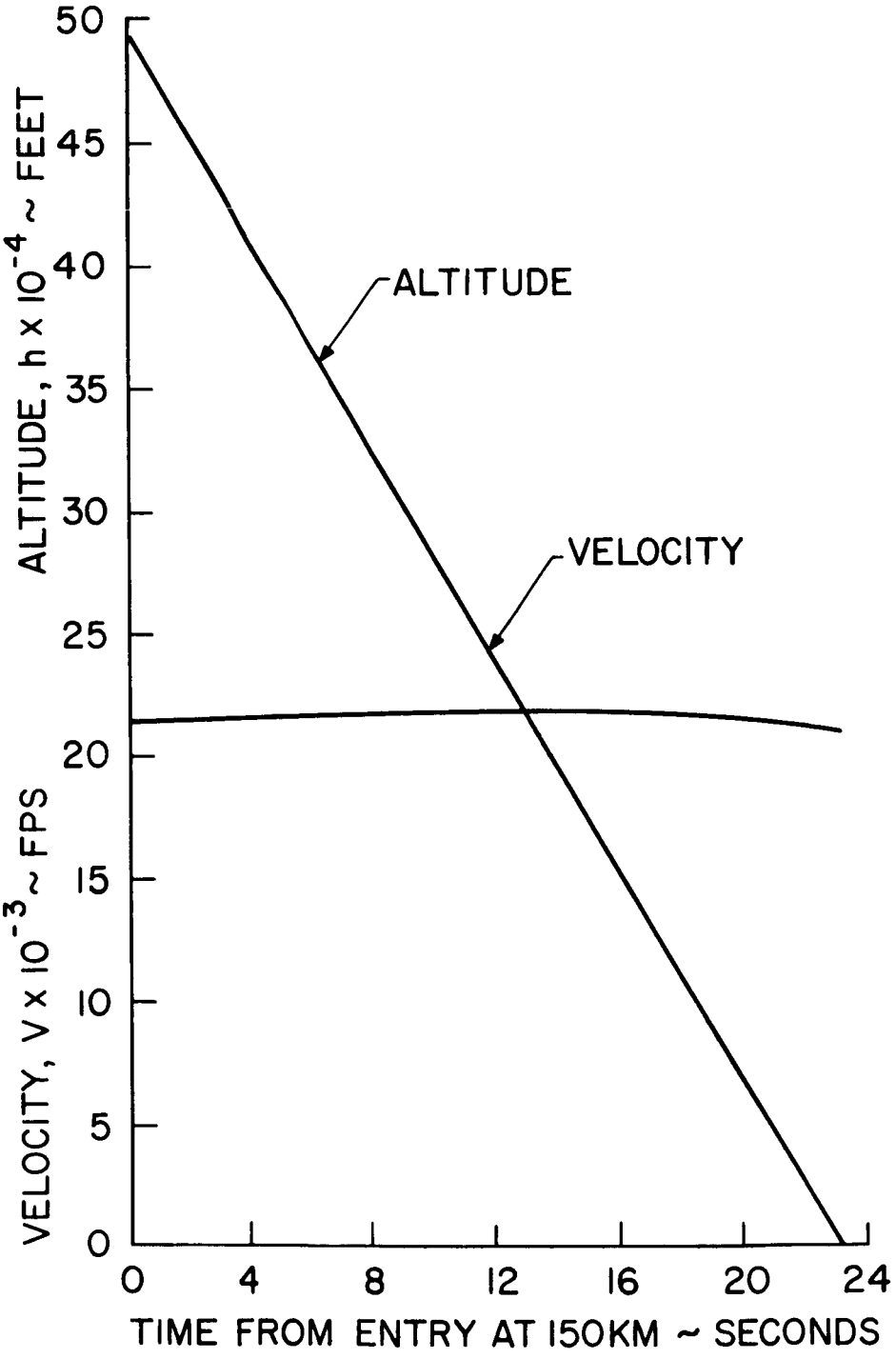

FIGURE 5

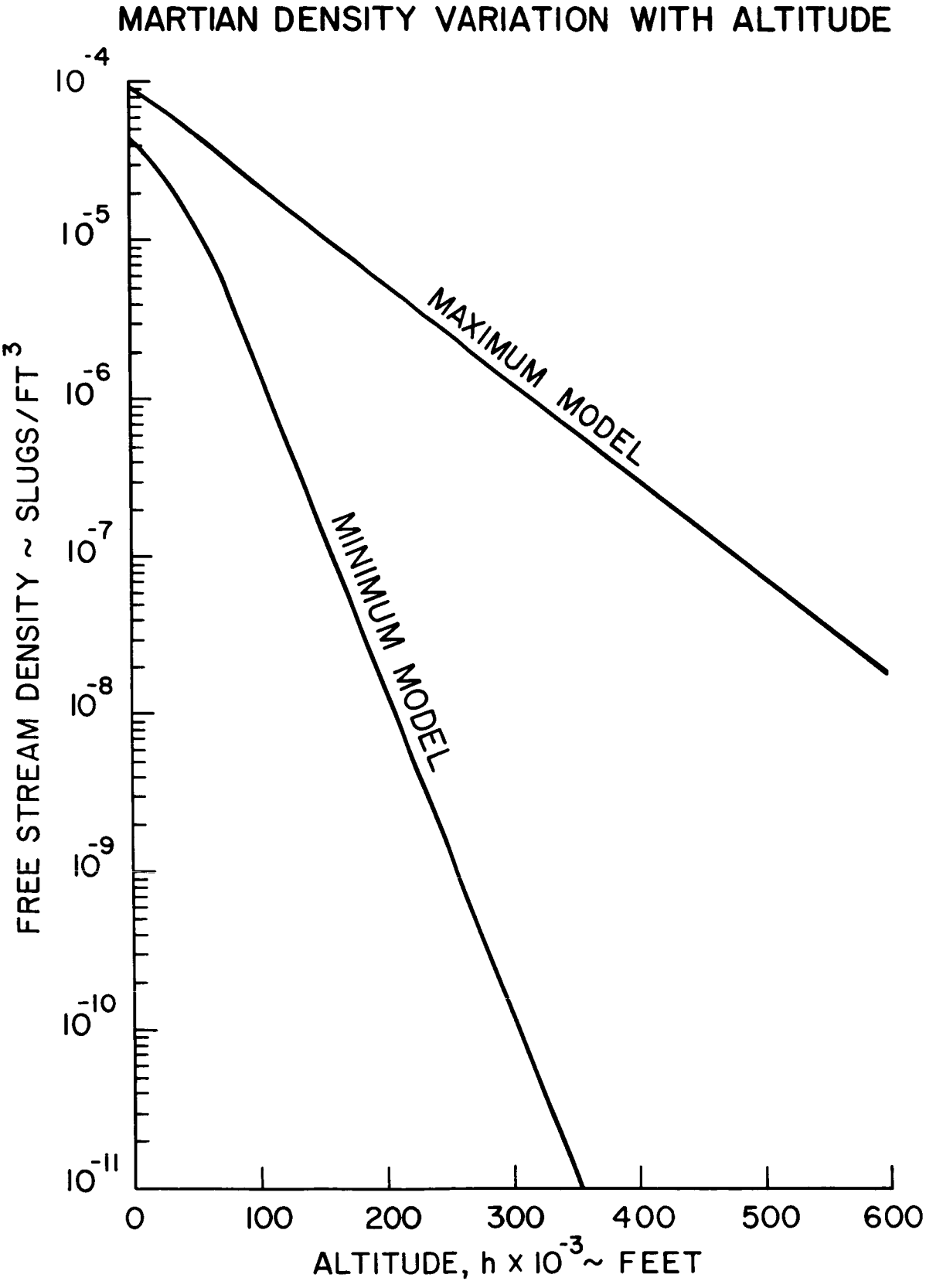
MARTIAN DENSITY VARIATION WITH ALTITUDE
FREE STREAM DENSITY ~ SLUGS/FT^3
10^{-4}
10^{-5}
10^{-6}
10^{-7}
10^{-8}
10^{-9}
10^{-10}
10^{-11}
MAXIMUM MODEL
MINIMUM MODEL
0
100
200
300
400
500
600
ALTITUDE, h x 10^{-3} ~ FEET

FIGURE 6

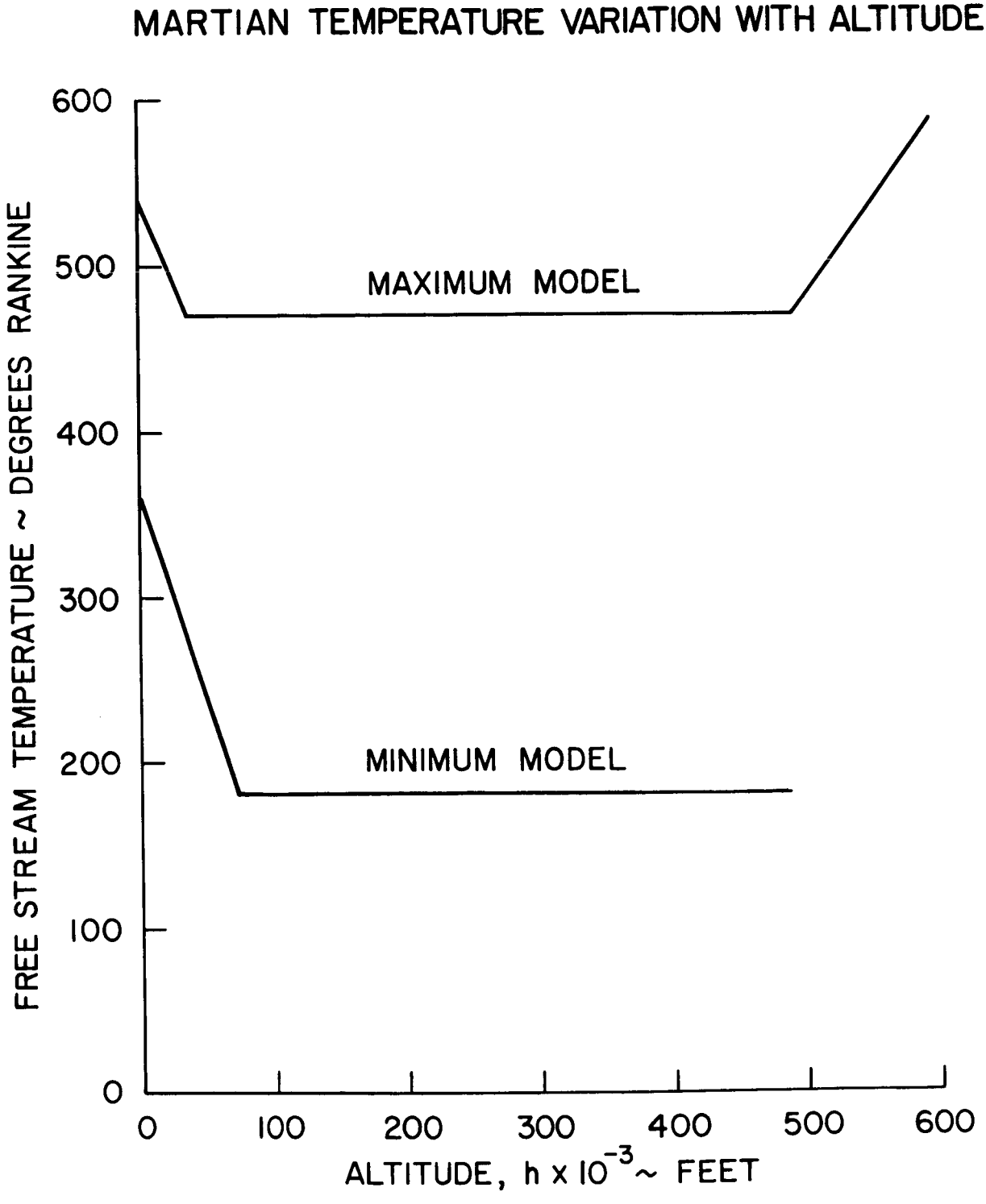
MARTIAN TEMPERATURE VARIATION WITH ALTITUDE
600
500
400
300
200
100
0
FREE STREAM TEMPERATURE ~ DEGREES RANKINE
MAXIMUM MODEL
MINIMUM MODEL
0
100
200
300
400
500
600
ALTITUDE, h x 10^-3 ~ FEET

FIGURE 7

TABLE 1

CHEMICAL COMPOSITION OF MARS ATMOSPHERES MODELS

Component	Volume Percent	
	Maximum	Minimum
CO_2	5	49
A	1	1
O_2	1	1
H_2O	1	1
N_2	92	48

of the undisturbed Martian atmosphere since during entry, the atmospheric gases will change in composition because of boundary layer heating and interaction with the graphite surface. The gases that enter the surface orifice will change further as they travel to the inlet leak of the mass spectrometer. Placement of the surface orifice must be selected so as to provide the most accurate analysis of the atmosphere. Since the heat shield of the vehicle is made of carbon, and since carbon is expected to be a major component of the atmosphere, one must look for conditions of possible interference. If such interference occurs, better accuracy could be achieved if the carbon from each source could be accounted for. Another possible source of interference could arise from impurities in the graphite. Successful use of graphite means fabricating it to be free of impurities and to retain this state until launched near Mars. An investigation must also be made of the possibility of error in measurement arising from condensation of carbon in the sampling volume as the gases travel to the mass spectrometer leak.

During this research, it was necessary to carry out several interrelated studies. First, the heating of the entry vehicle (Figure 1) was calculated using the Ablation Design Program as

modified for Martian entry. These calculations were performed throughout entry at (1) the stagnation point, (2) the cone (12 in. along the axis from the stagnation point), (3) the cylinder (30 in. from the stagnation point) and (4) the flare (39 in. from the stagnation point, which is about 0.34 in. past the point where the cylinder meets the flare). These results were used to determine the corresponding thermal response of the graphite, as characterized by mass losses and temperature changes, through the use of REKAP*. Then the predicted surface temperatures, local pressures, and mass losses were used to determine the quantity of equilibrium boundary layer species as a function of altitude by means of the Chemically Reacting Boundary Layer Program**. The quantity of ablation products carried back in the boundary layer from the region in front of each of stations 12, 30, and 39 was then estimated and added to the results of the Chemically Reacting Boundary Layer Program, when significant. The latest chemical kinetic information was used to determine the actual (non-equilibrium) composition of the

---

* General Electric Re-Entry Systems Department's Reaction Kinetics Ablation Program. Note that the influence of the upstream atmosphere gases are taken into account in these calculations.

** The assumption of chemical equilibrium is reasonable for these conditions.

boundary layer and then the changes that would be expected to occur when the gases flow from the surface orifice to the mass spectrometer leak. The compositions of gases that enter the mass spectrometer were then studied to determine the factors that would influence accuracy of analysis and relating the results to the chemical composition of the atmosphere. Descriptions of the various treatments are presented in the following sections.

NOMENCLATURE FOR AERODYNAMIC CALCULATIONS

Symbols

B	Dimensionless mass loss parameter $(\dot{m}_W/\rho_e U_e C_{HO})$
C_p	Specific heat (Btu/lb^oR)
h	Enthalpy (Btu/lb)
K	Thermal conductivity (Btu/ft sec^oR)
K_p	Equilibrium constant
$\dot{m}$	Mass flow rate (lb/ft^{2}sec)
P	Pressure (lb/ft^2)
$\dot{q}$	Heat flux (Btu/ft^{2}sec)
R_s	Shock radius (ft)
s	Sublimation correlation factor, or wetted length (ft)
T	Temperature (^oR)
t	Time (sec)
U	Velocity (ft/sec)
x	Depth from original frontface of heat shield (ft)
y	Radius of E/V (ft)
δ	Boundary layer velocity thickness (ft)
δ^*	Boundary layer displacement thickness (ft)
ρ	Density (lb/ft^3)
θ_s	Shock angle (degrees)

μ	Viscosity (lb/ft sec)

Subscripts

BF	Backface
BL	Boundary layer conditions
e	Edge of boundary layer conditions
o	Stagnation conditions
HGR	Hot gas radiation
L	Laminar
RR	Reradiation
r	Recovery conditions
T	Turbulent
W	Wall (surface) conditions
∞	Free stream conditions

Superscripts

*	Properties evaluated at Eckert's reference enthalpy

AERODYNAMIC HEATING CALCULATIONS

The Martian entry environment (in terms of local pressures and heat transfer rates) was evaluated using the Ablation Design Program[1,2] as modified for planetary entry. This version of the program differed from that which is normally used for Earth re-entry in that provisions were made for supplying as inputs:

1) A planetary model atmosphere in terms of free stream density, pressure, and temperature variation with altitude.

2) The thermodynamic state properties (pressure, temperature, density, and enthalpy) in the form of a Mollier diagram for the given chemical constituents of the model atmosphere.

The chemical composition of the model atmospheres considered during this study was

	Mass Fraction*				
Model Atmosphere	N_2	CO_2	A	O_2	H_2O
Maximum	.893	.076	.014	.011	.006
Minimum	.374	.601	.011	.009	.005

* Volume fractions are given in Table I, Page 9

with the corresponding physical structure provided in Figures 6 and 7.

To calculate the stagnation point heat transfer rates the program employs Lees' theory[3], modified through the use of Eckert's reference enthalpy techniques[4]. The required relationship is of the form

$$\dot{q}_o = \frac{0.778}{P_r^{0.67}} (\rho_e^* \mu_e^*)^{0.5} \left(\frac{U_\infty}{R_N} \frac{\rho_\infty}{\rho_{e^o}} (2 - \frac{\rho_\infty}{\rho_{e^o}})^{0.5} \right)^{0.5} (h_e^o - h_w).$$

To obtain laminar heating rates on the spherical region of the nose (for body angles in excess of thirty degrees), the preceding relationship was employed with Lees' hemispherical distribution[3]. The body angle at the stagnation point was defined as ninety degrees. At body angles equal to or less than thirty degrees, Walker's compressible reference enthalpy equation[5] was used to obtain laminar heat transfer rates

$$\dot{q}_L = \frac{0.384}{P_r^{0.67}} \frac{\rho_e^* \mu_e^* U_e Y}{\left(\int_o^s \rho_e^* \mu_e^* U_e Y^2 \, ds \right)^{0.5}} (h_r - h_w).$$

For turbulent boundary layer conditions a relationship derived by Walker[5], which satisfies both the momentum and energy integral equations and includes the effect of a finite pressure gradient, was employed. The solution to these equations is

obtained by use of Blasius incompressible flat plate skin coefficients modified for compressible flow by the use of Eckert's reference enthalpy

$$\dot{q}_T = \frac{0.296}{P_r^{0.67}} \frac{\rho_e \mu_e^{0.25} U_e (\mu_e^*/\mu_e)^{0.2} (\rho_e^*/\rho_e)^{0.8} Y^{0.25}}{\left(\int_o^s \rho_e U_e \mu_e^{0.25} Y^{1.25} ds\right)^{0.20}} (h_r - h_w)$$

However, before the previous aerodynamic heating equations could be evaluated it was necessary to determine the thermodynamic state properties at the edge of the boundary layer. These properties were obtained from an isentropic expansion of the flow along a streamline from behind the shock wave, the geometry of which is known from inviscid flow field calculations. The angle of the shock through which a particular streamline passes and subsequently reaches the edge of the boundary layer was determined by Nestler's mass balance technique which is expressed mathematically as

$$\dot{m}_{oo} = \pi R_s^2 \rho_{oo} U_{oo} = 2\pi Y \rho_e U_e (\delta - \delta^*) = \dot{m}_{BL}$$

where $\theta = f(R_s)$

and $\rho_e, U_e, \delta, \delta^* = f(\theta_s)$

The preceding relationship was solved through an iteration technique for the shock radius (R_s) with which the associated

shock angle (θ_s) could then be determined. Once the shock angle was known the flow properties immediately behind the shock were calculated from standard equations. The flow was then expanded isentropically to the local body pressure at the point where it entered the boundary layer.

Using the preceding techniques, heat transfer predictions were made for twenty-three distinct locations on the configuration shown in Figure 1, for the four trajectories (Figures 2-5) of interest. The resulting pressure and heating histories (for points at which conduction solutions were later obtained) are shown in Figures 8-11 and 12-15 respectively.

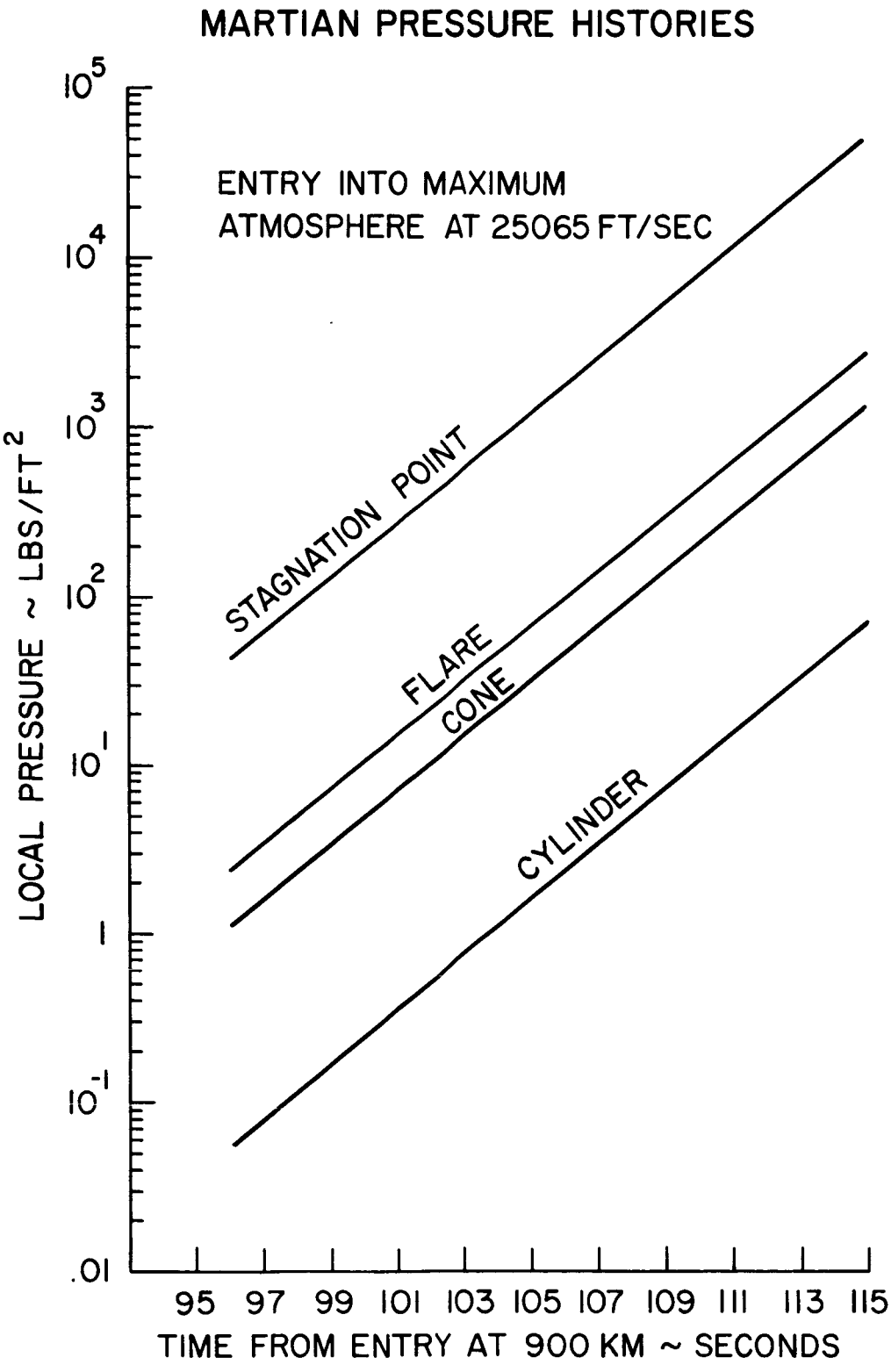
MARTIAN PRESSURE HISTORIES
ENTRY INTO MAXIMUM
ATMOSPHERE AT 25065 FT/SEC
STAGNATION POINT
FLARE CONE
CYLINDER
LOCAL PRESSURE ~ LBS/FT 2
10 5
10 4
10 3
10 2
10 1
1
10 -1
.01
95 97 99 101 103 105 107 109 111 113 115
TIME FROM ENTRY AT 900 KM ~ SECONDS

FIGURE 8

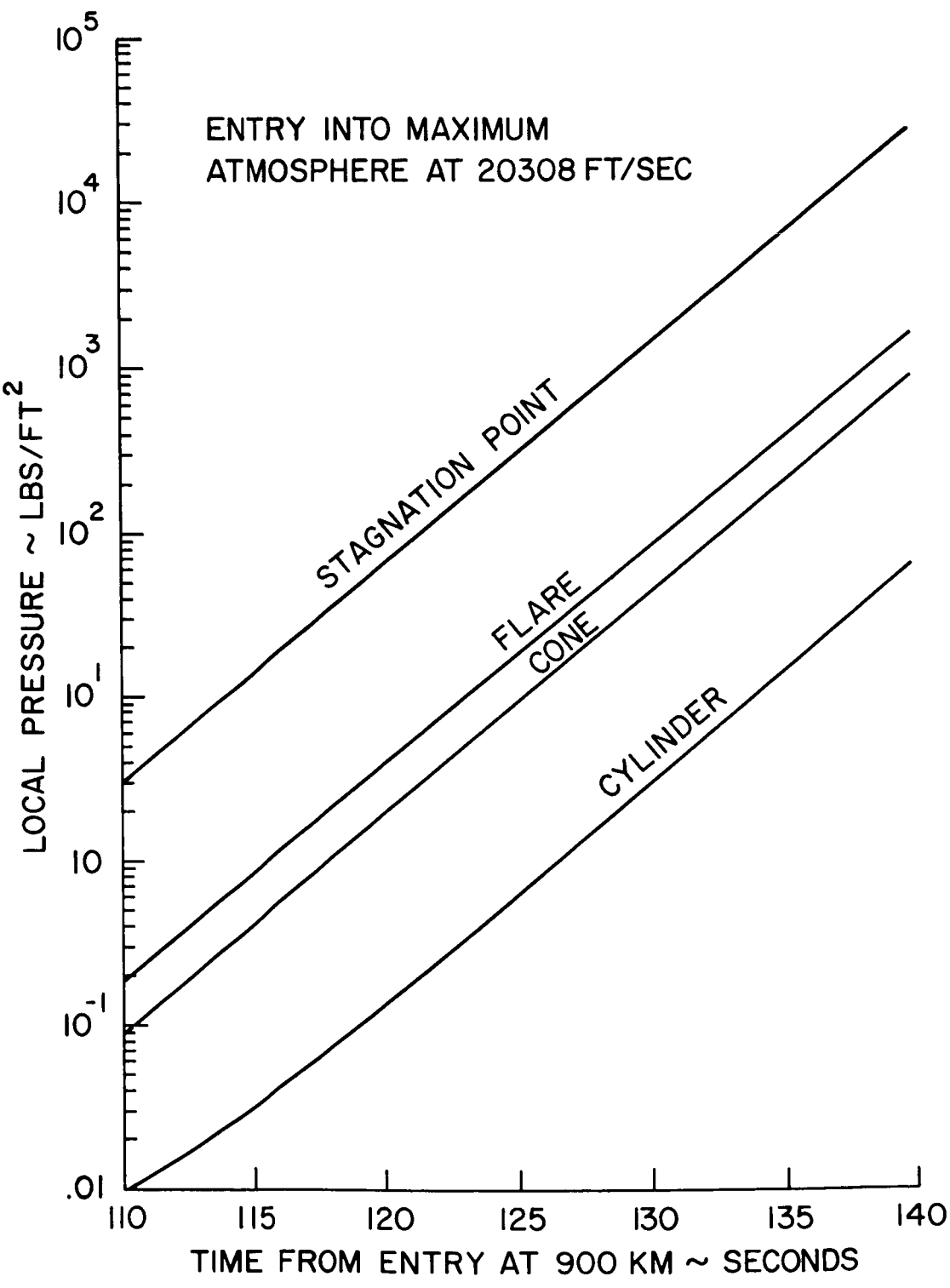
MARTIAN PRESSURE HISTORIES
ENTRY INTO MAXIMUM
ATMOSPHERE AT 20308 FT/SEC
STAGNATION POINT
FLARE CONE
CYLINDER
LOCAL PRESSURE ~ LBS/FT²
10⁵
10⁴
10³
10²
10⁻
10
10⁻¹
.01
110
115
120
125
130
135
140
TIME FROM ENTRY AT 900 KM ~ SECONDS

FIGURE 9

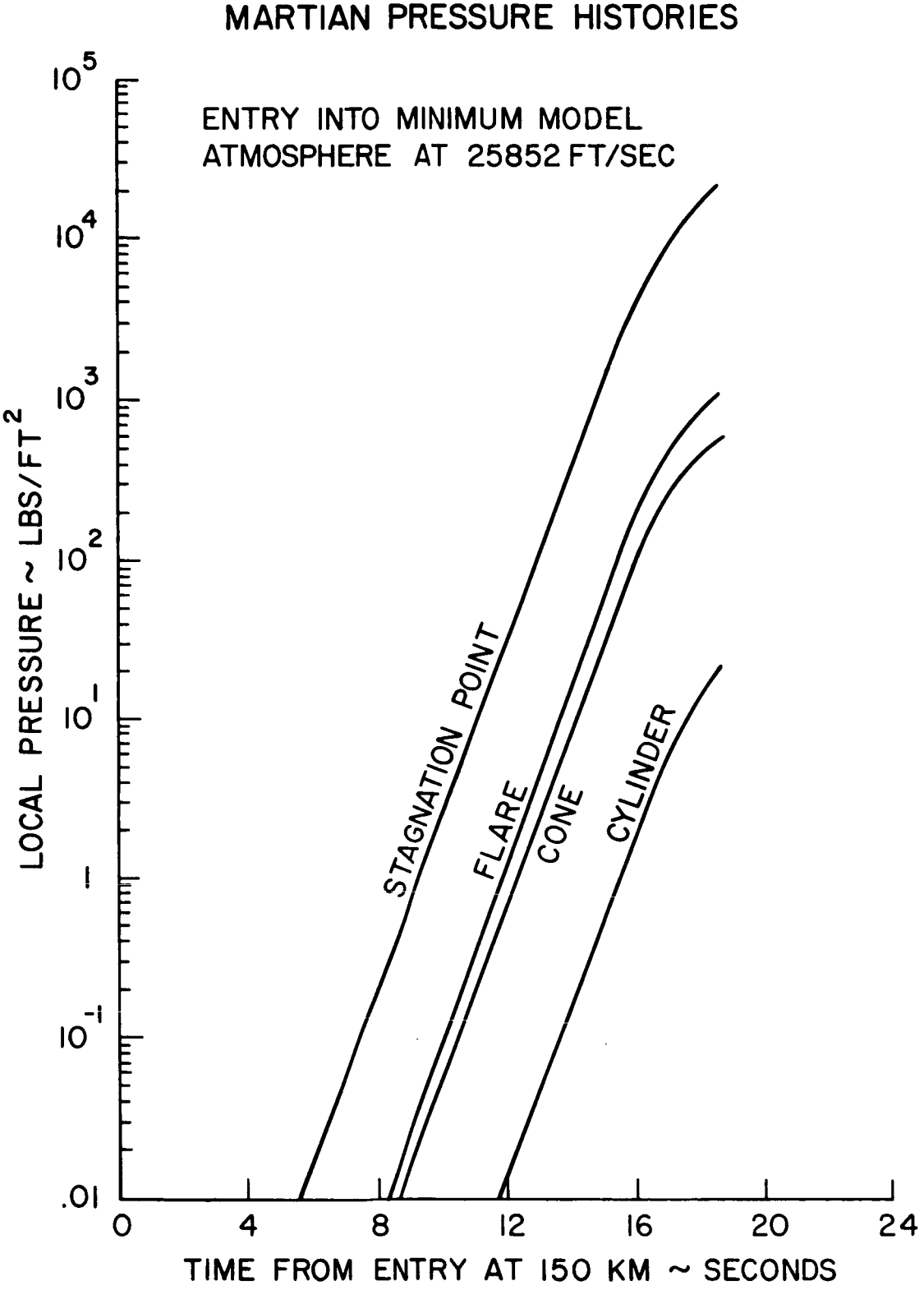
MARTIAN PRESSURE HISTORIES
ENTRY INTO MINIMUM MODEL
ATMOSPHERE AT 25852 FT/SEC
LOCAL PRESSURE ~ LBS/FT²
10⁵
10⁴
10³
10²
10
1
10⁻¹
.01
STAGNATION POINT
FLARE CONE
CYLINDER
0
4
8
12
16
20
24
TIME FROM ENTRY AT 150 KM ~ SECONDS

FIGURE 10

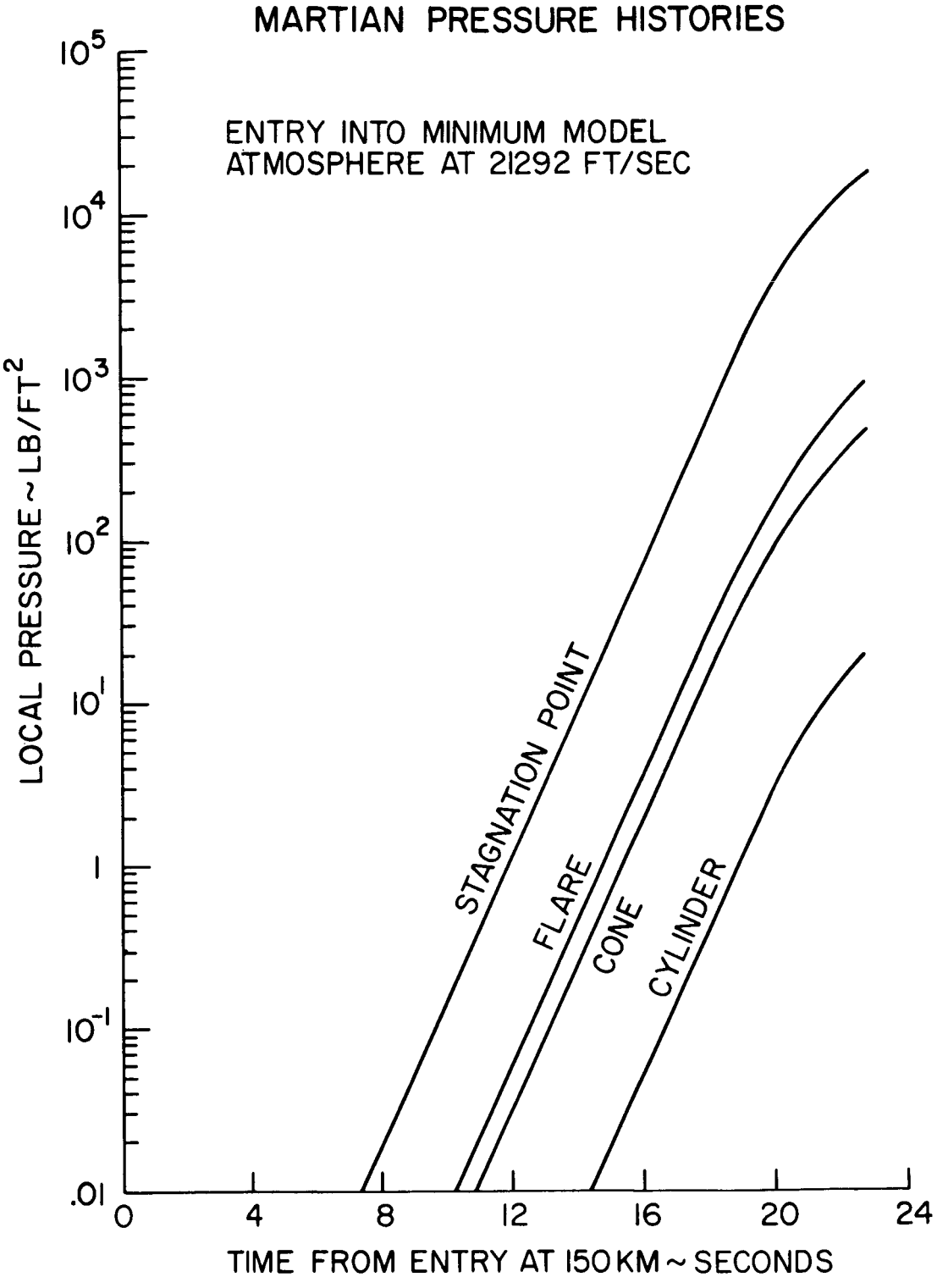
MARTIAN PRESSURE HISTORIES
ENTRY INTO MINIMUM MODEL ATMOSPHERE AT 21292 FT/SEC
LOCAL PRESSURE ~ LB/FT^2
10^5
10^4
10^3
10^2
10^1
1
10^{-1}
.01
0
4
8
12
16
20
24
TIME FROM ENTRY AT 150 KM ~ SECONDS
STAGNATION POINT
FLARE
CONE
CYLINDER

FIGURE 11

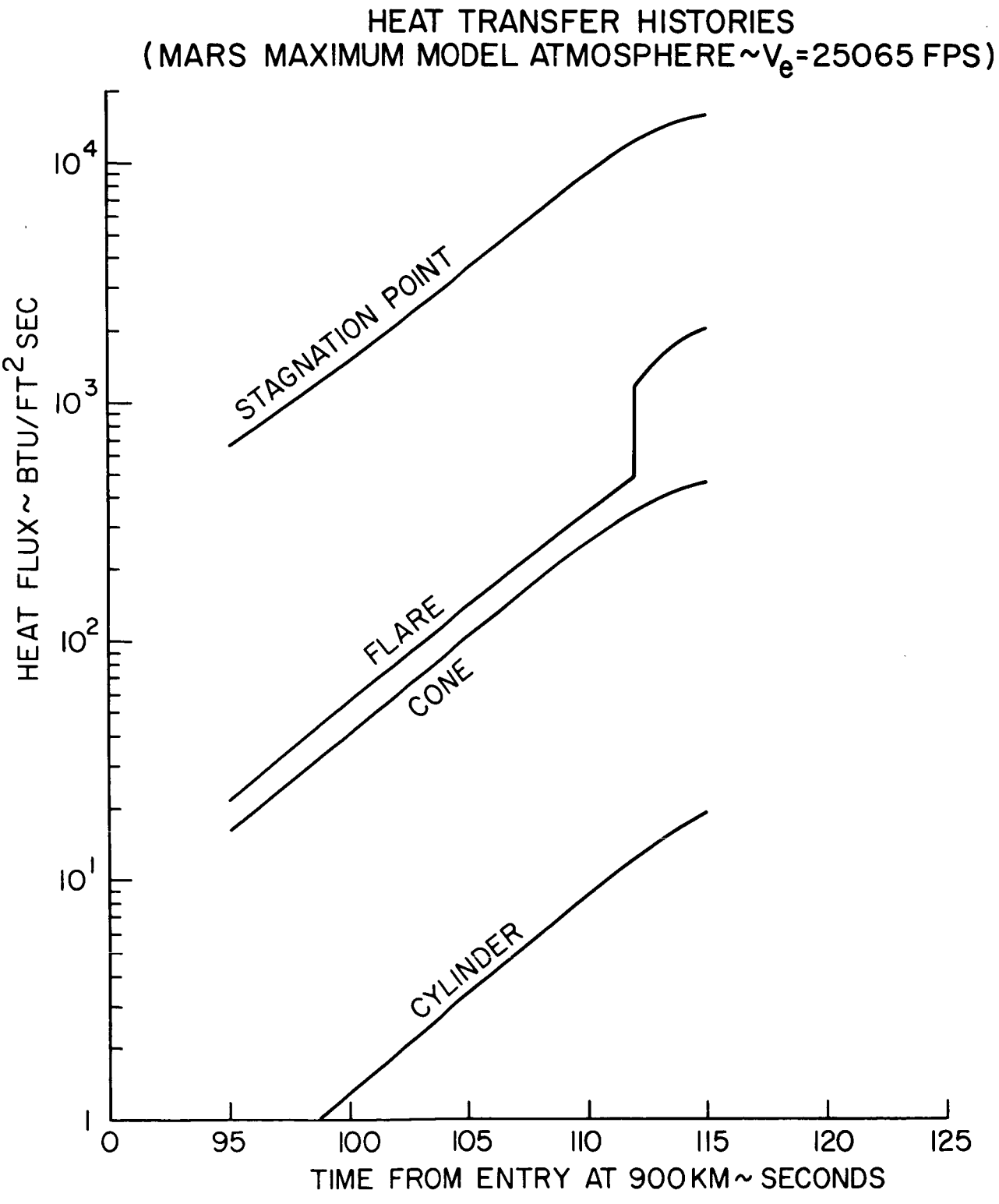
HEAT TRANSFER HISTORIES
(MARS MAXIMUM MODEL ATMOSPHERE ~ V_e = 25065 FPS)
HEAT FLUX ~ BTU/FT^2 SEC
10^4
10^3
10^2
10^1
1
STAGNATION POINT
FLARE
CONE
CYLINDER
0
95
100
105
110
115
120
125
TIME FROM ENTRY AT 900 KM ~ SECONDS

FIGURE 12

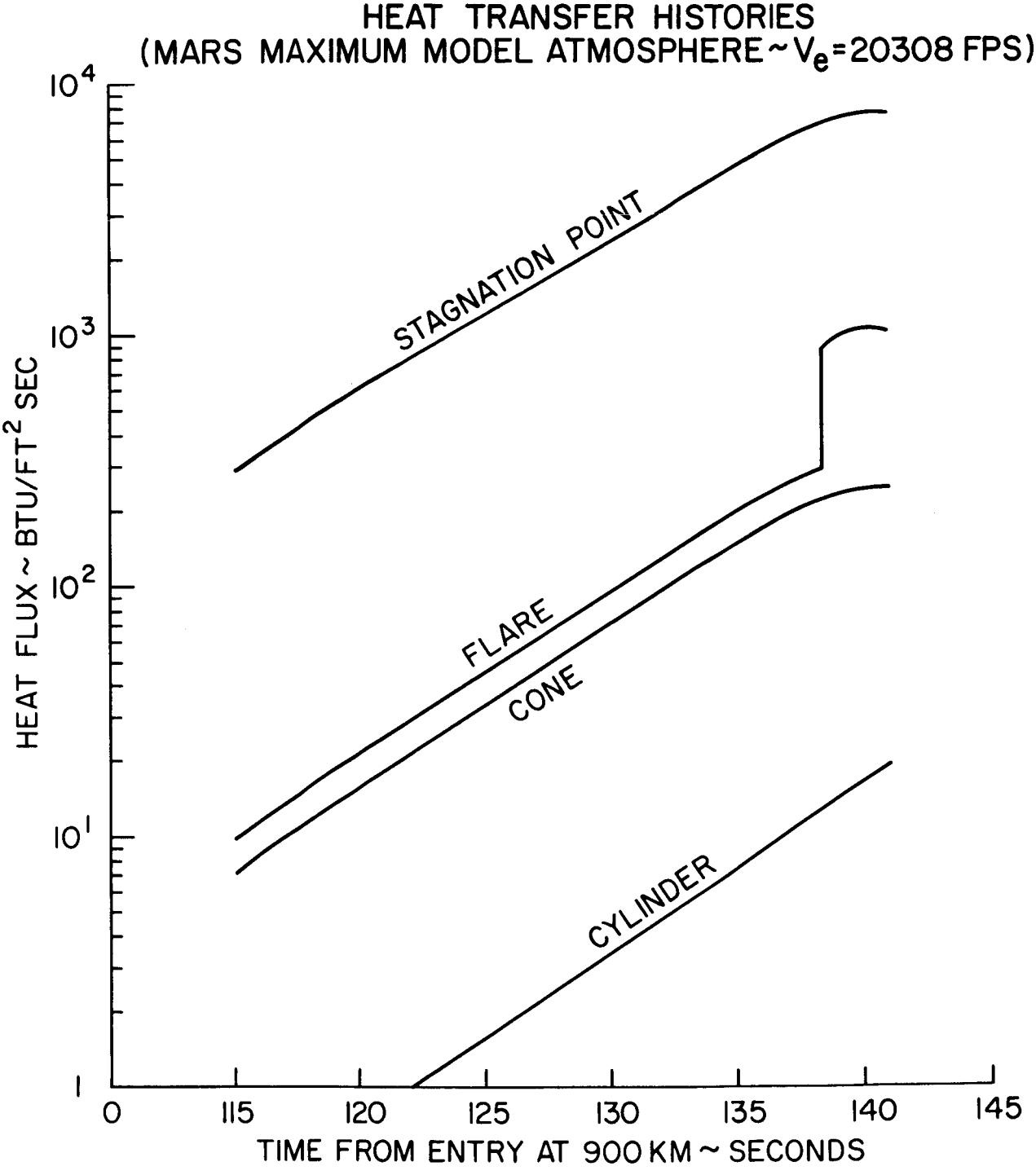
HEAT TRANSFER HISTORIES
(MARS MAXIMUM MODEL ATMOSPHERE ~ V_e = 20308 FPS)
10^4
10^3
10^2
10^1
1
HEAT FLUX ~ BTU/FT^2 SEC
STAGNATION POINT
FLARE
CONE
CYLINDER
0
115
120
125
130
135
140
145
TIME FROM ENTRY AT 900 KM ~ SECONDS

FIGURE 13

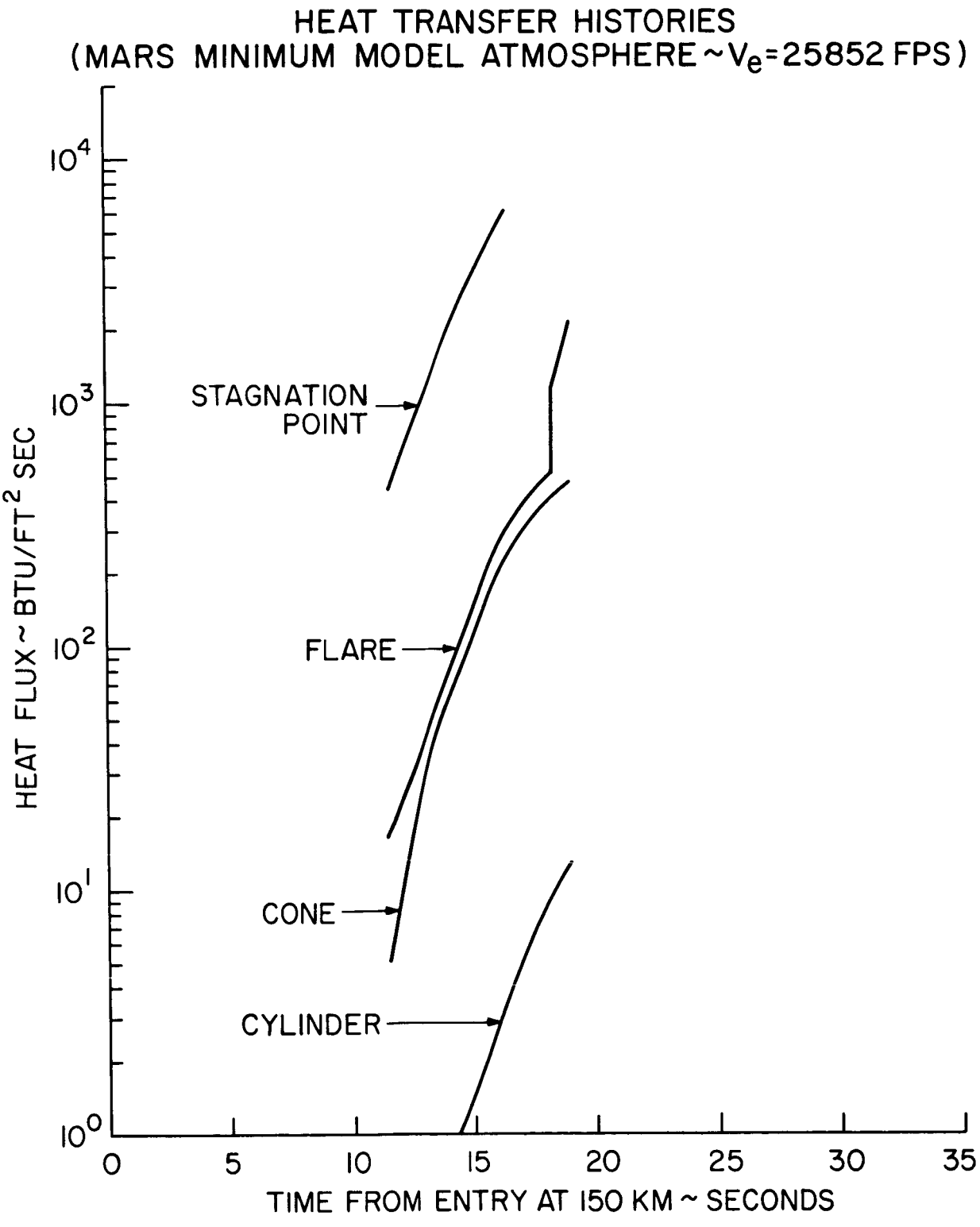
HEAT TRANSFER HISTORIES
(MARS MINIMUM MODEL ATMOSPHERE ~ V_e = 25852 FPS)
HEAT FLUX ~ BTU/FT^2 SEC
10^4
10^3
10^2
10^1
10^0
STAGNATION POINT
FLARE
CONE
CYLINDER
0
5
10
15
20
25
30
35
TIME FROM ENTRY AT 150 KM ~ SECONDS

FIGURE 14

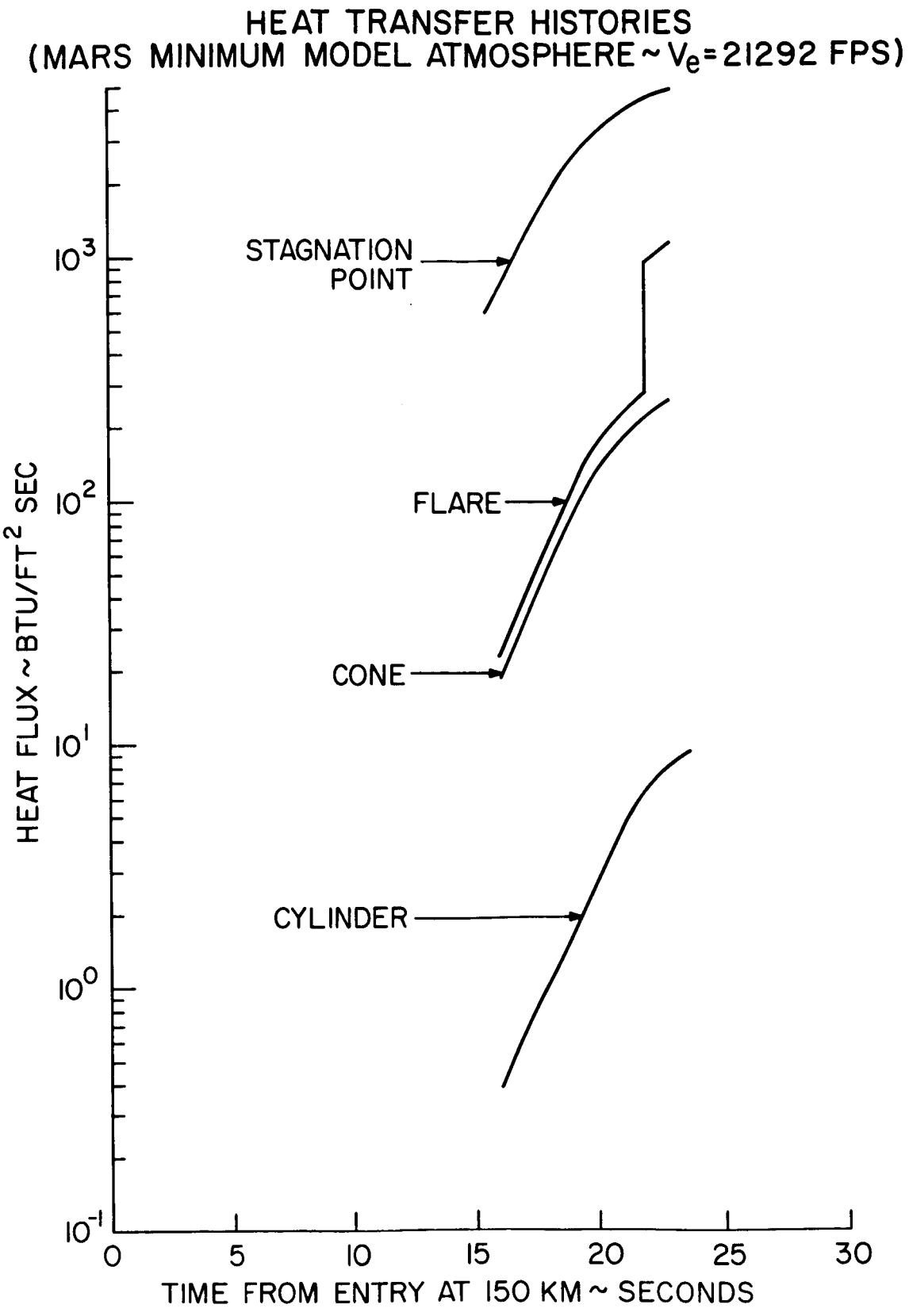
HEAT TRANSFER HISTORIES
(MARS MINIMUM MODEL ATMOSPHERE ~ V_e = 21292 FPS)
STAGNATION POINT
FLARE
CONE
CYLINDER
HEAT FLUX ~ BTU/FT^2 SEC
10^3
10^2
10^1
10^0
10^{-1}
0
5
10
15
20
25
30
TIME FROM ENTRY AT 150 KM ~ SECONDS

FIGURE 15

HEAT SHIELD RESPONSE CALCULATIONS

The heat shield (ATJ-Graphite) response to the predicted thermal environments was determined through the use of the Reaction Kinetics Ablation Program - REKAP[6,7]. Although the primary objective was to determine mass injection to and chemical interaction with the boundary layer, the related heat shield temperature response was also obtained.

The required solutions were obtained by solving an energy balance equation continuously through the heat shield, bond, and supporting structure*; with appropriate boundary conditions placed at both the front and backface of the system. For a non-charring heat shield material the energy balance equation assumed the form of the well known one-dimensional heat conduction equation:

$$\frac{\partial}{\partial \chi} \left(k \frac{\partial T}{\partial \chi} \right) = \rho C_P \frac{\partial T}{\partial t}$$

The heat balance at the front face is

---

* For the current study it was sufficient to assume an adiabatic boundary at the shield backface, thus eliminating considerations of the bond and supporting structure.

$$-k \frac{\partial T}{\partial \chi} = \dot{q}_C' + \dot{q}_{HGR} - \dot{q}_{RR}$$

where the net convective heat flux at the front face is calculated from,

$$\dot{q}_C' = \dot{q}_C \left(1 - s \left(A P_e^n e^{-B/T_W}\right)\right)^*$$

which inherently includes combustion processes. The total mass loss rates at the front face were obtained from[9]

$$\dot{m}_w = 1.15 \frac{\dot{q}}{(h_r - h_w)} \left[(\bar{C}_c)_w - (\bar{C}_c)_e \right]$$

where the carbon concentration at the wall $(\bar{C}_c)_w$ is given by

$$(\bar{C}_c)_w = (\bar{C}_c)_{w,D} + A(P_e)^n e^{-B/T_W}$$

where

	Maximum Model	Minimum Model
$(\bar{C}_c)_e$	0.021	0.161
$(\bar{C}_c)_{w,D}$	0.046	0.281
$A \times 10^{-6}$	0.62	2.85
$B \times 10^{-4}$	10.0	11.4
n	-0.605	-0.69

---

* The value of s was determined as a function of h_r by Scala and Gilbert[8].

and P_e is given in atmospheres. Using these techniques and the thermal environment from the Ablation Design Program calculations, mass loss predictions were made for (1) the stagnation point, (2) the cone (station 12), (3) the cylinder (station 30), and the flare (station 39) as shown in Figures 16-19. However, the heating rates on the cylinder were so small that no mass loss resulted for any trajectory.

In addition mass loss predictions were made for the quartz ring located at station 21. These predictions were based upon the heats of ablation quoted by Scala[10], and are presented in Figures 20 and 21.

Typical heat shield temperature profiles are shown in Figures 22-29. A summary of the heat shield backface temperatures at impact for all the cases analyzed is presented in Table 2. Surface temperature variations with altitude are provided in Figures 30-33.

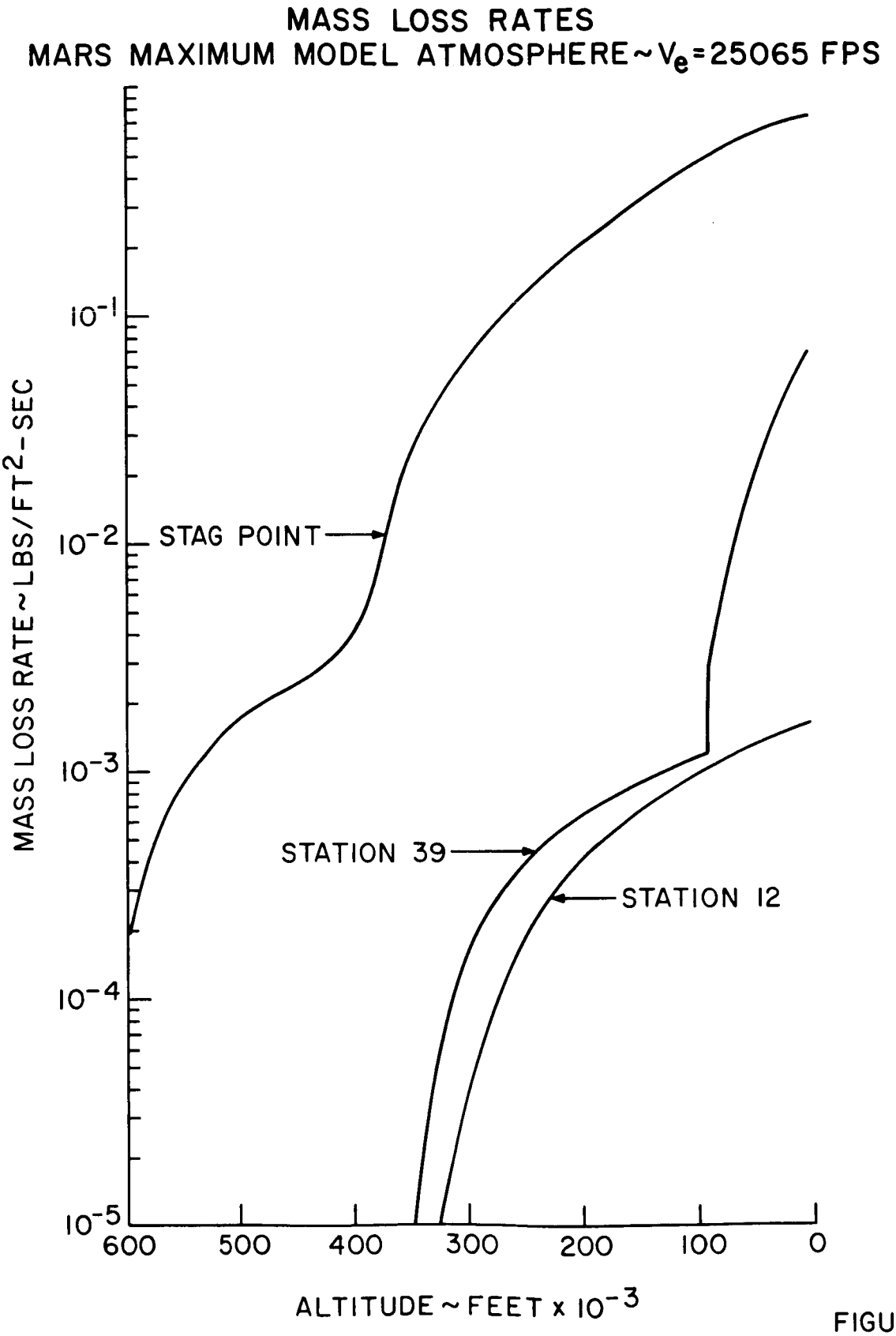
MASS LOSS RATES
MARS MAXIMUM MODEL ATMOSPHERE ~ V_e = 25065 FPS
MASS LOSS RATE ~ LBS/FT^2-SEC
10^{-1}
10^{-2}
10^{-3}
10^{-4}
10^{-5}
STAG POINT
STATION 39
STATION 12
600
500
400
300
200
100
0
ALTITUDE ~ FEET x 10^{-3}

FIGURE 16

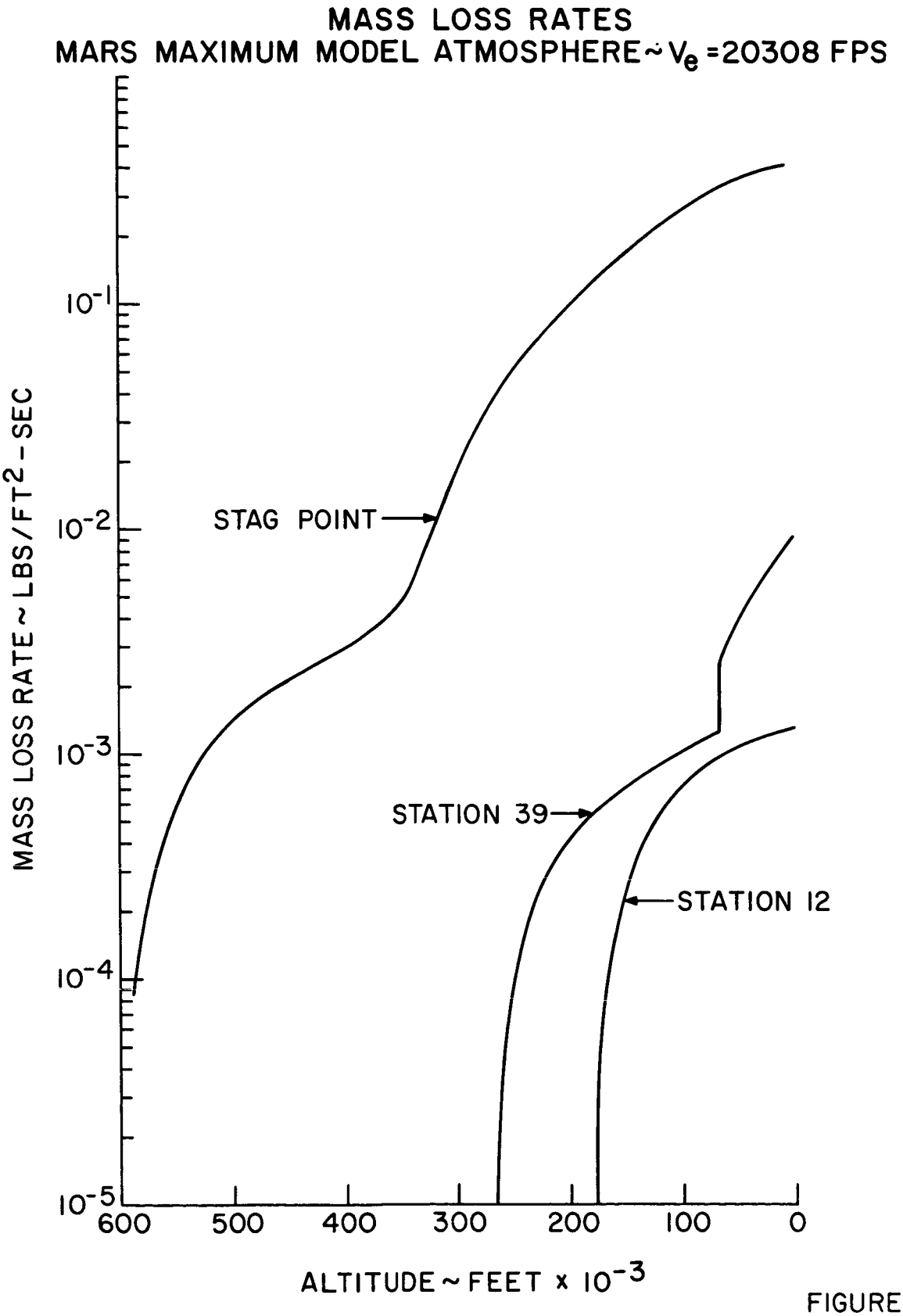
MASS LOSS RATES
MARS MAXIMUM MODEL ATMOSPHERE ~ V_e = 20308 FPS
MASS LOSS RATE ~ LBS/FT^2-SEC
10^{-1}
10^{-2}
10^{-3}
10^{-4}
10^{-5}
STAG POINT
STATION 39
STATION 12
600
500
400
300
200
100
0
ALTITUDE ~ FEET x 10^{-3}

FIGURE 17

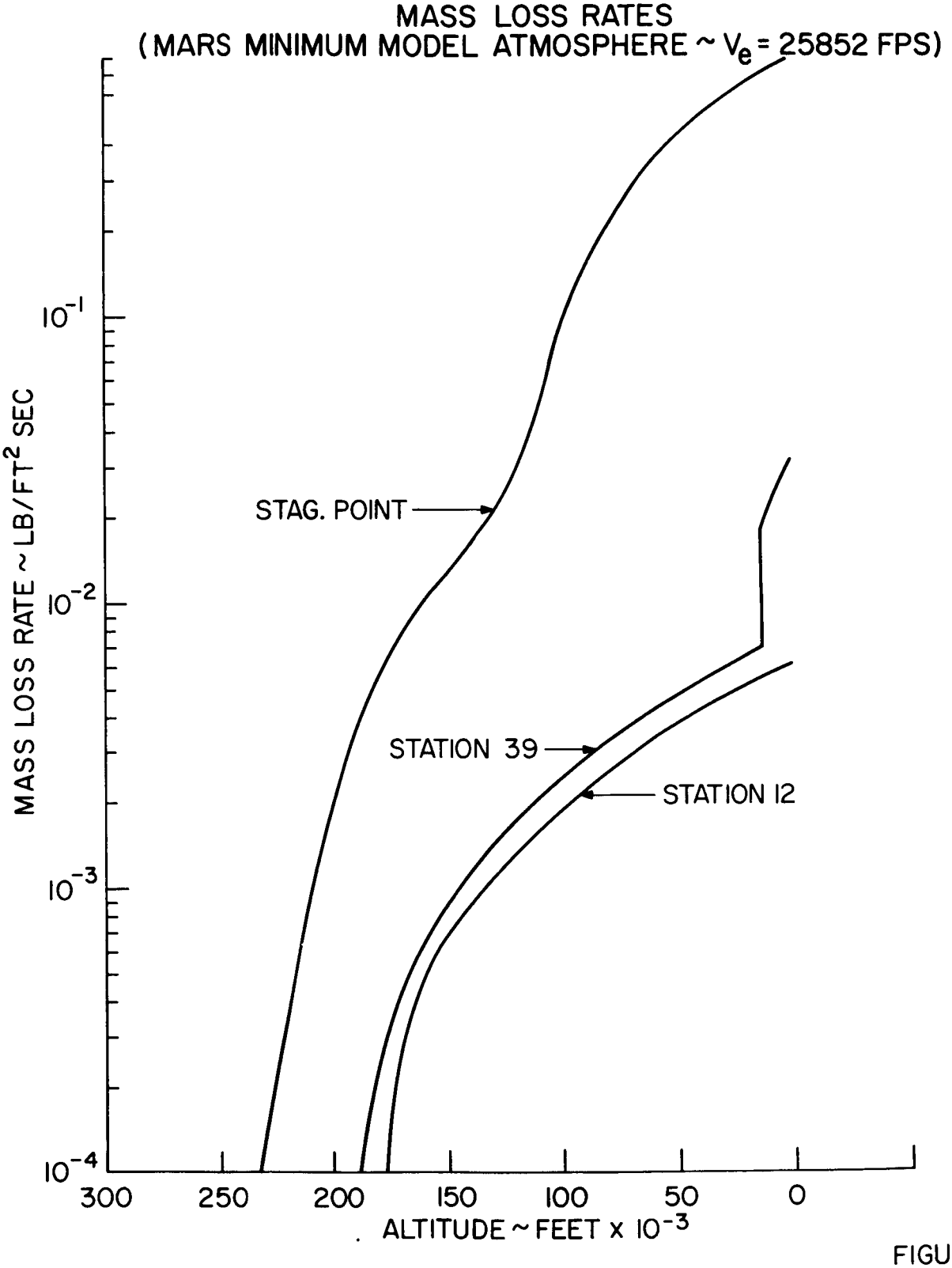
MASS LOSS RATES
(MARS MINIMUM MODEL ATMOSPHERE ~ V_e = 25852 FPS)
MASS LOSS RATE ~ LB/FT^2 SEC
10^{-1}
10^{-2}
10^{-3}
10^{-4}
STAG. POINT
STATION 39
STATION 12
300
250
200
150
100
50
0
ALTITUDE ~ FEET x 10^{-3}

FIGURE 18

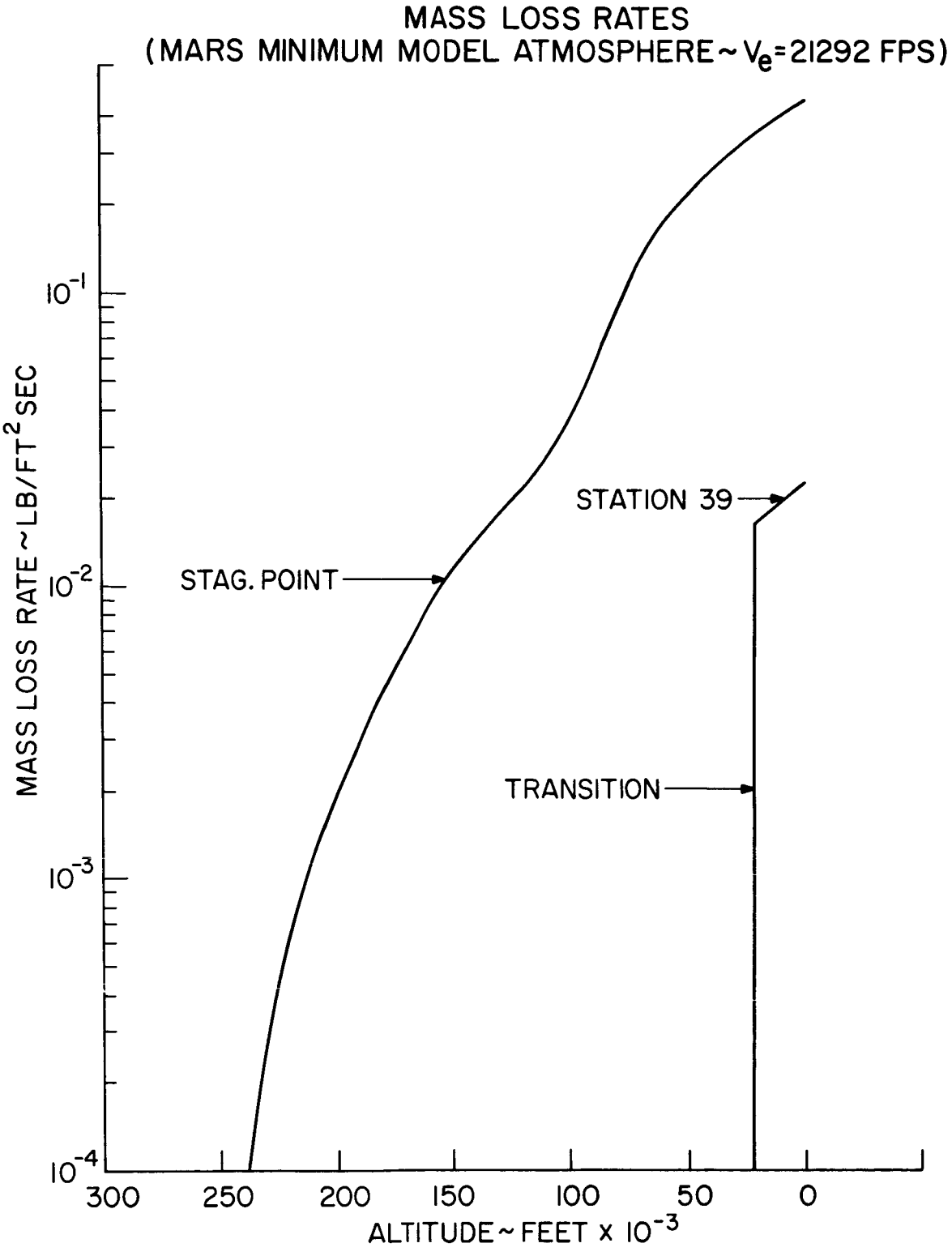
MASS LOSS RATES
(MARS MINIMUM MODEL ATMOSPHERE ~ V_e=21292 FPS)
MASS LOSS RATE ~ LB/FT^2 SEC
10^{-1}
10^{-2}
10^{-3}
10^{-4}
STAG. POINT
STATION 39
TRANSITION
300
250
200
150
100
50
0
ALTITUDE ~ FEET x 10^{-3}

FIGURE 19

MARS MASS SPECTROMETER PROBE
QUARTZ ANTENNA WINDOW
MASS LOSS RATES

TRAJECTORY PARAMETERS			
	VELOCITY	γ	ATMOSPHERE N_2 CO_2
1	25065 FT/SEC	90	MAXIMUM
2	20308 FT/SEC	90	MAXIMUM
3	25852 FT/SEC	90	MINIMUM
4	21292 FT/SEC	90	MINIMUM

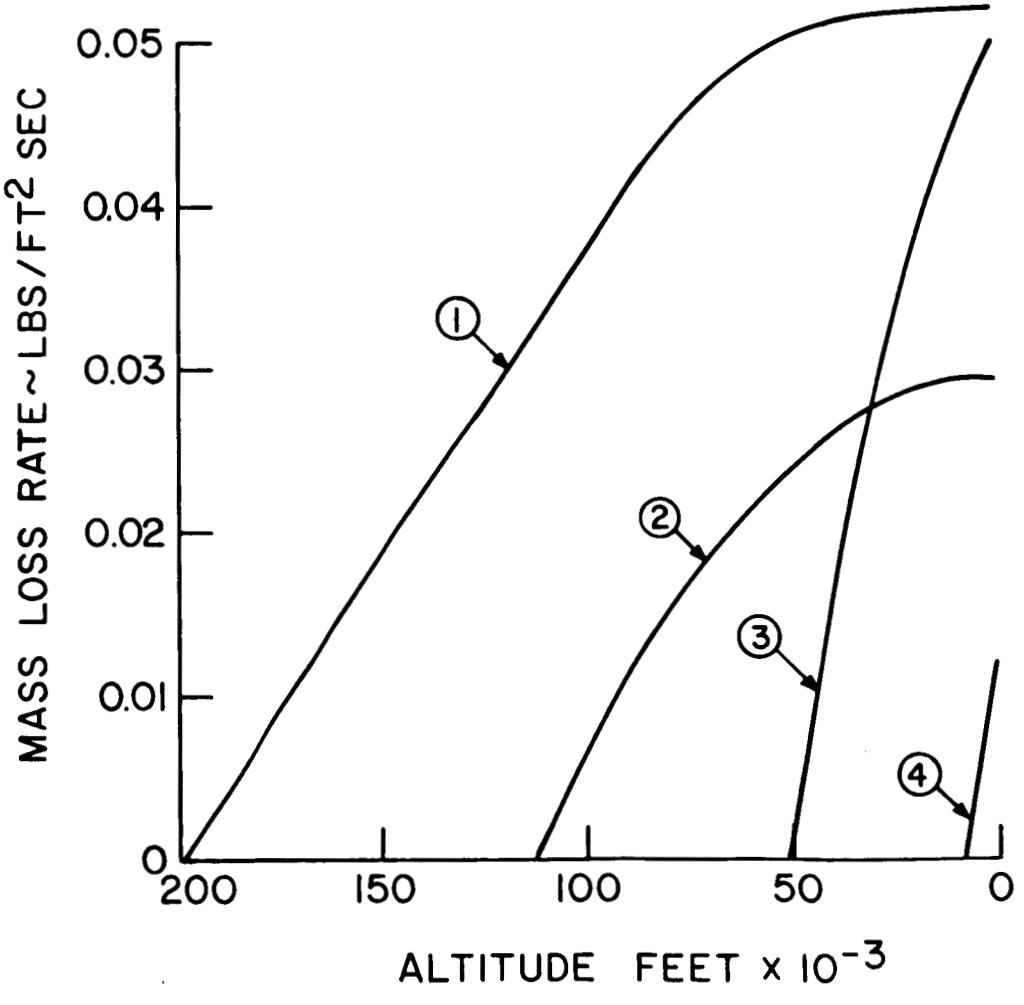

FIGURE 20

MARS MASS SPECTROMETER PROBE
QUARTZ ANTENNA WINDOW SURFACE TEMPERATURE HISTORIES

TRAJECTORY PARAMETERS			
	VELOCITY	γ	ATMOS (N_2-CO_2)
1	25065 FT/SEC	90	MAXIMUM
2	20308 FT/SEC	90	MAXIMUM
3	25852 FT/SEC	90	MINIMUM
4	21292 FT/SEC	90	MINIMUM

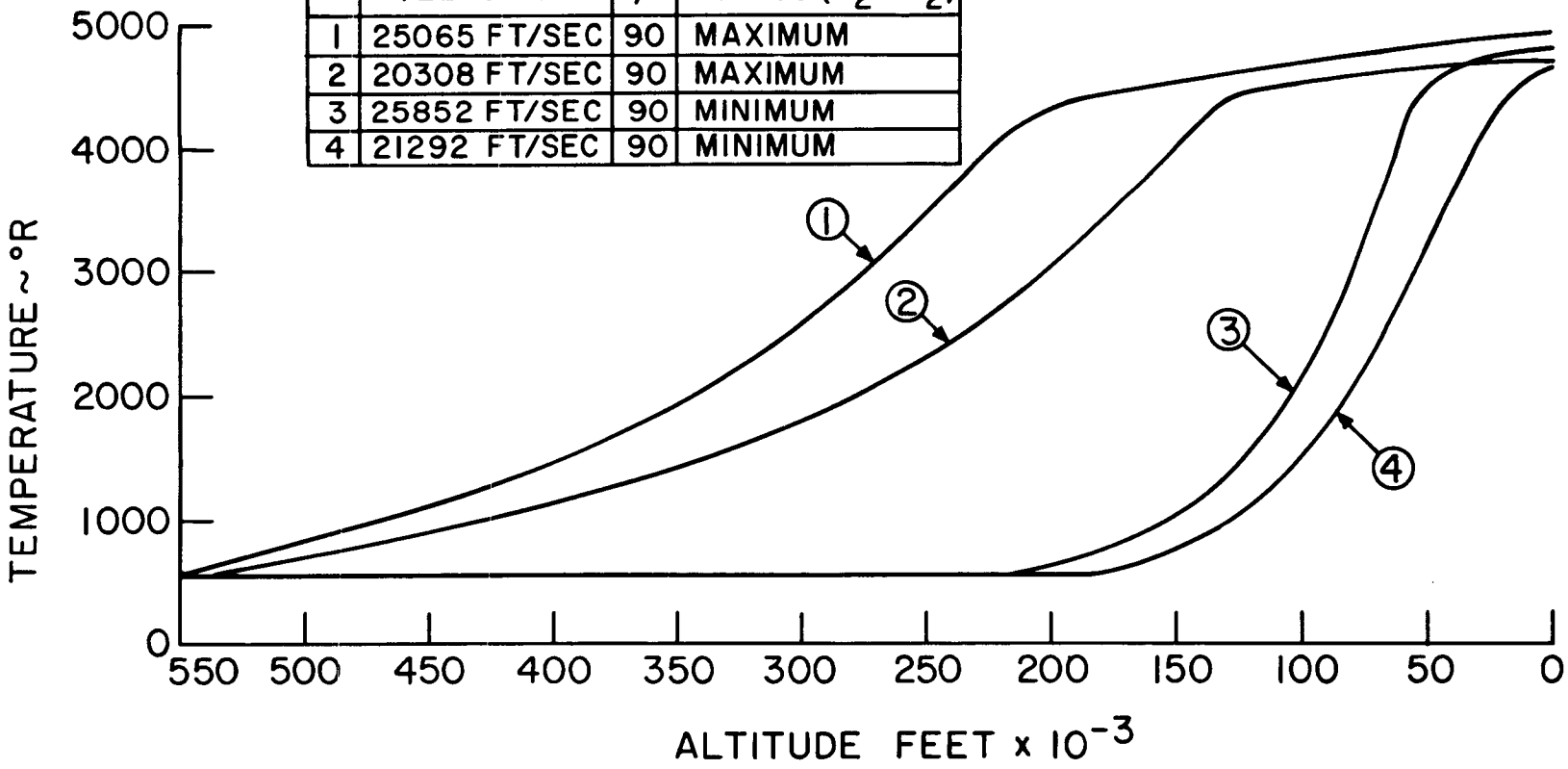

FIGURE 21

TEMPERATURE PROFILES
STAGNATION POINT
MARS MINIMUM MODEL ATMOSPHERE
V_e = 25852 FT/SEC

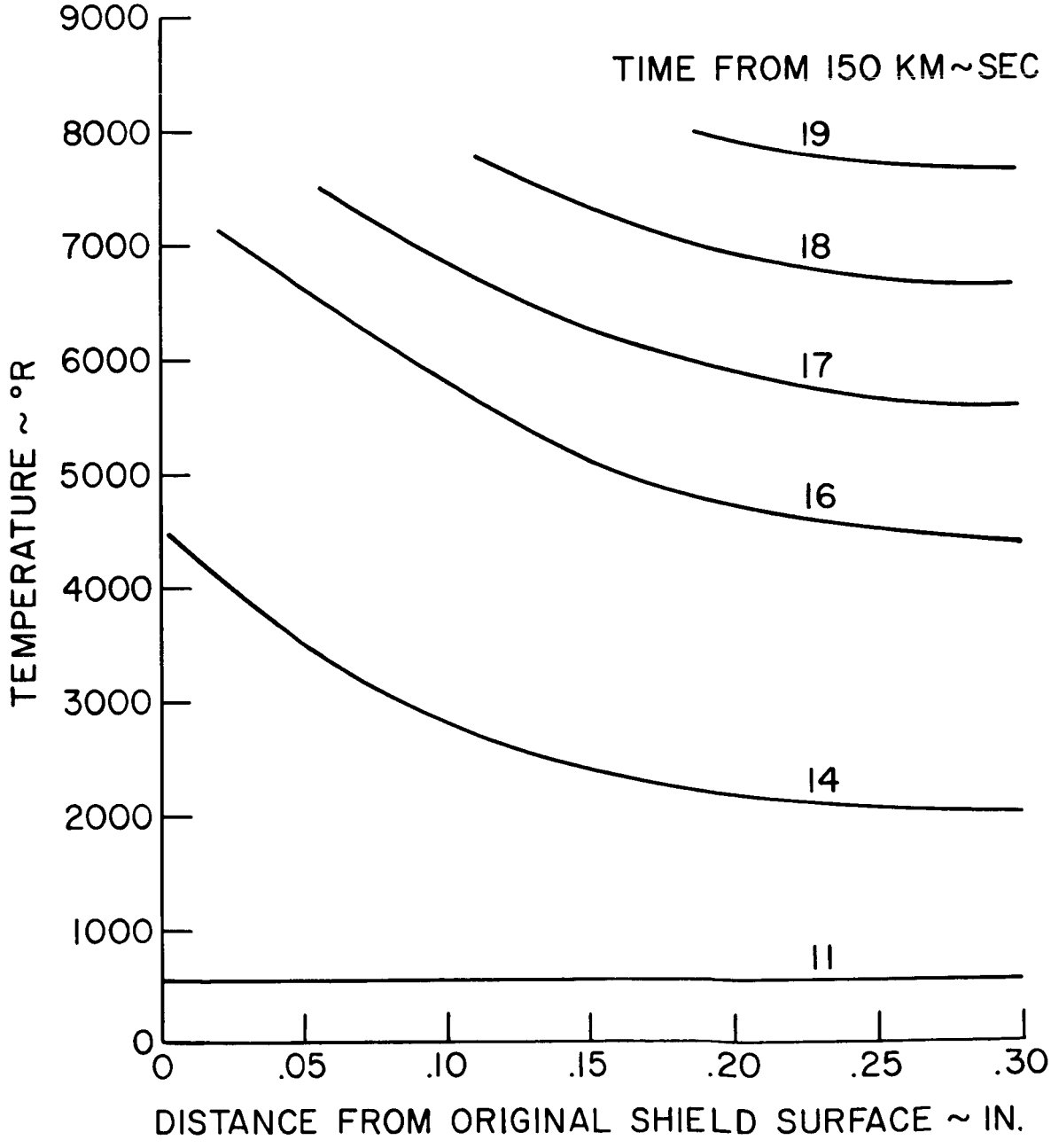

FIGURE 22

TEMPERATURE PROFILES
STAGNATION POINT
MARS MINIMUM MODEL ATMOSPHERE
V_e = 21292 FT/SEC

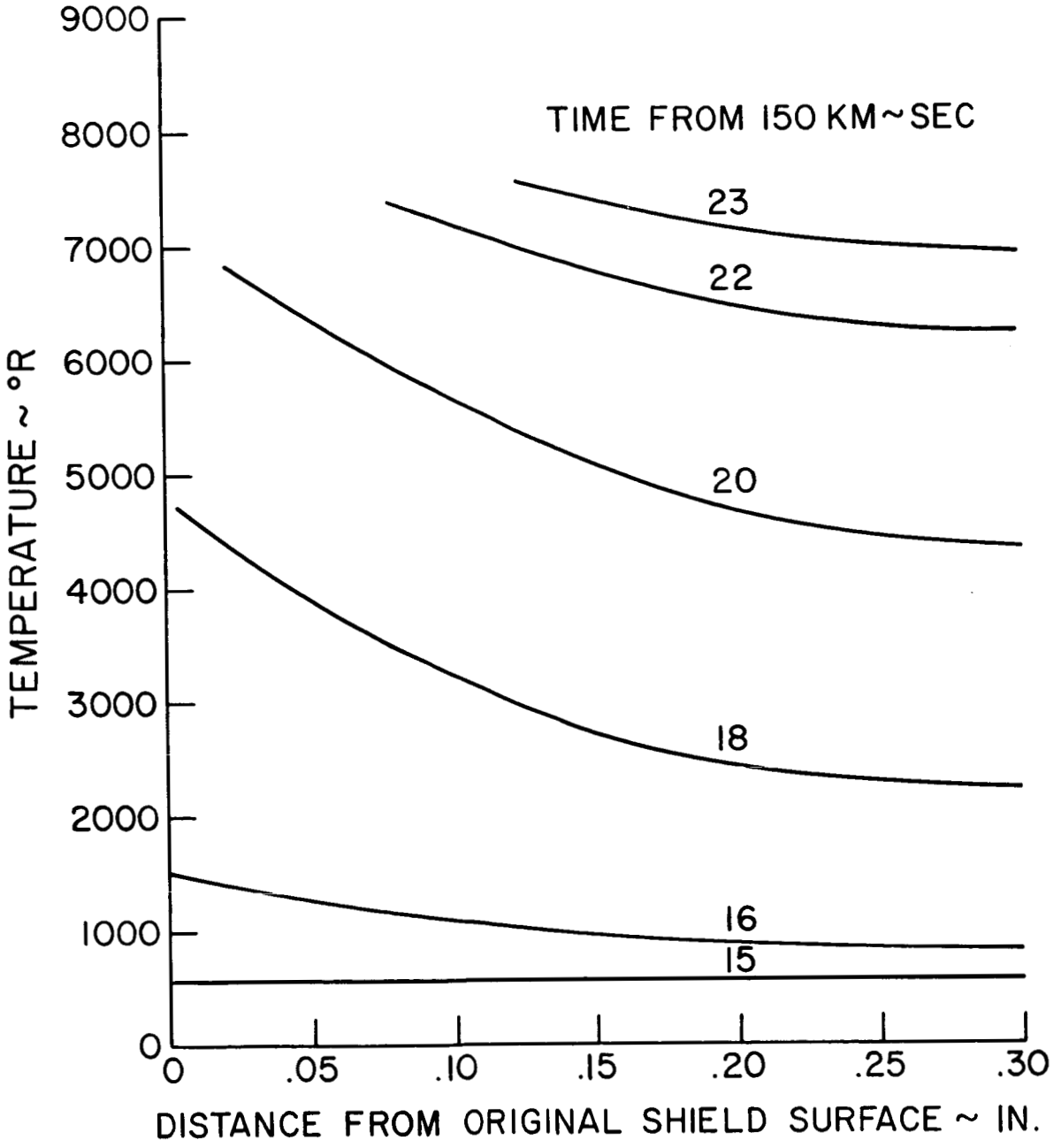

FIGURE 23

TEMPERATURE PROFILES
AT STATION 12
MARS MINIMUM MODEL ATMOSPHERE
V_e = 25852 FT/SEC

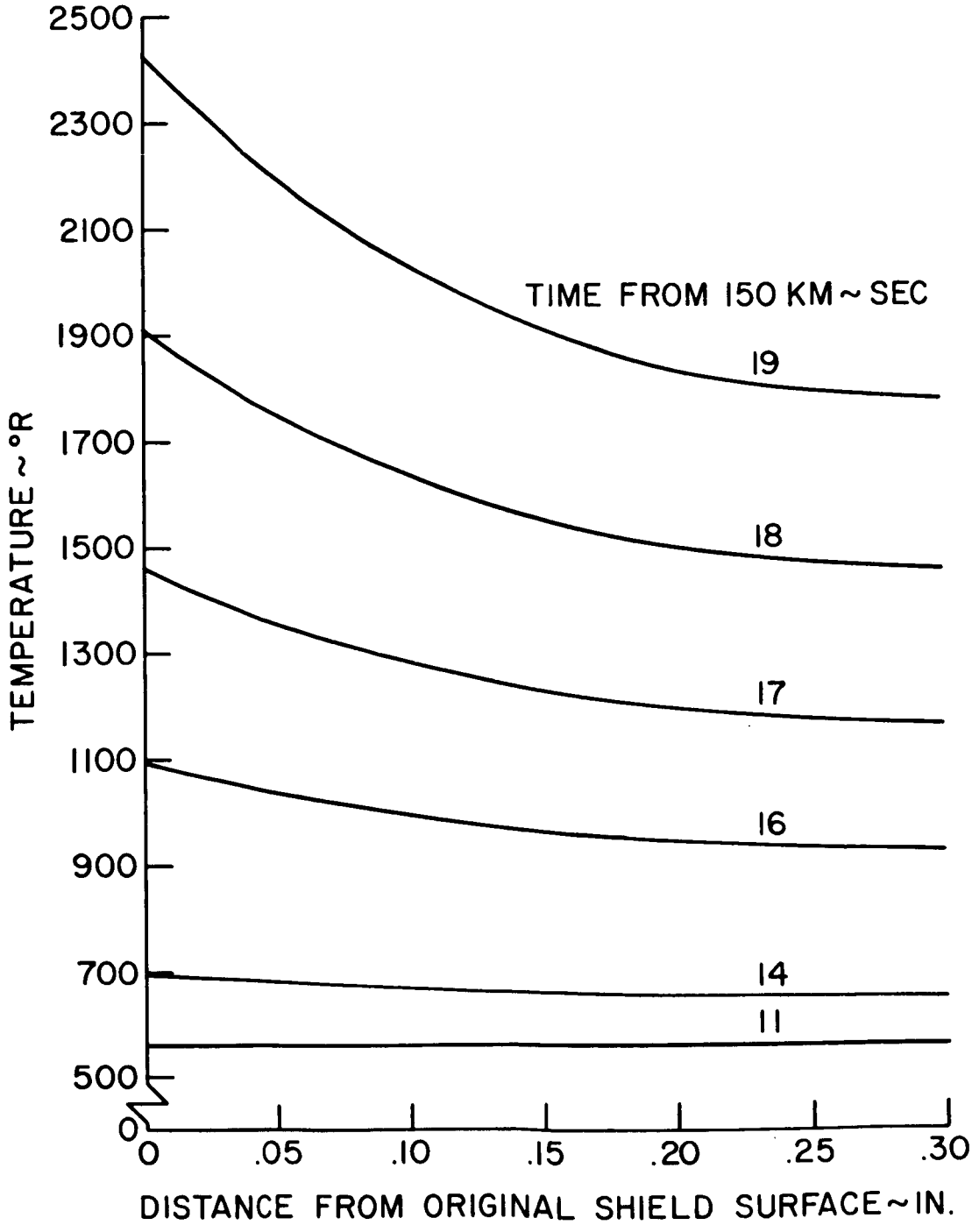

FIGURE 24

TEMPERATURE PROFILES
AT STATION 12
MARS MINIMUM MODEL ATMOSPHERE
V_e = 21292 FT/SEC

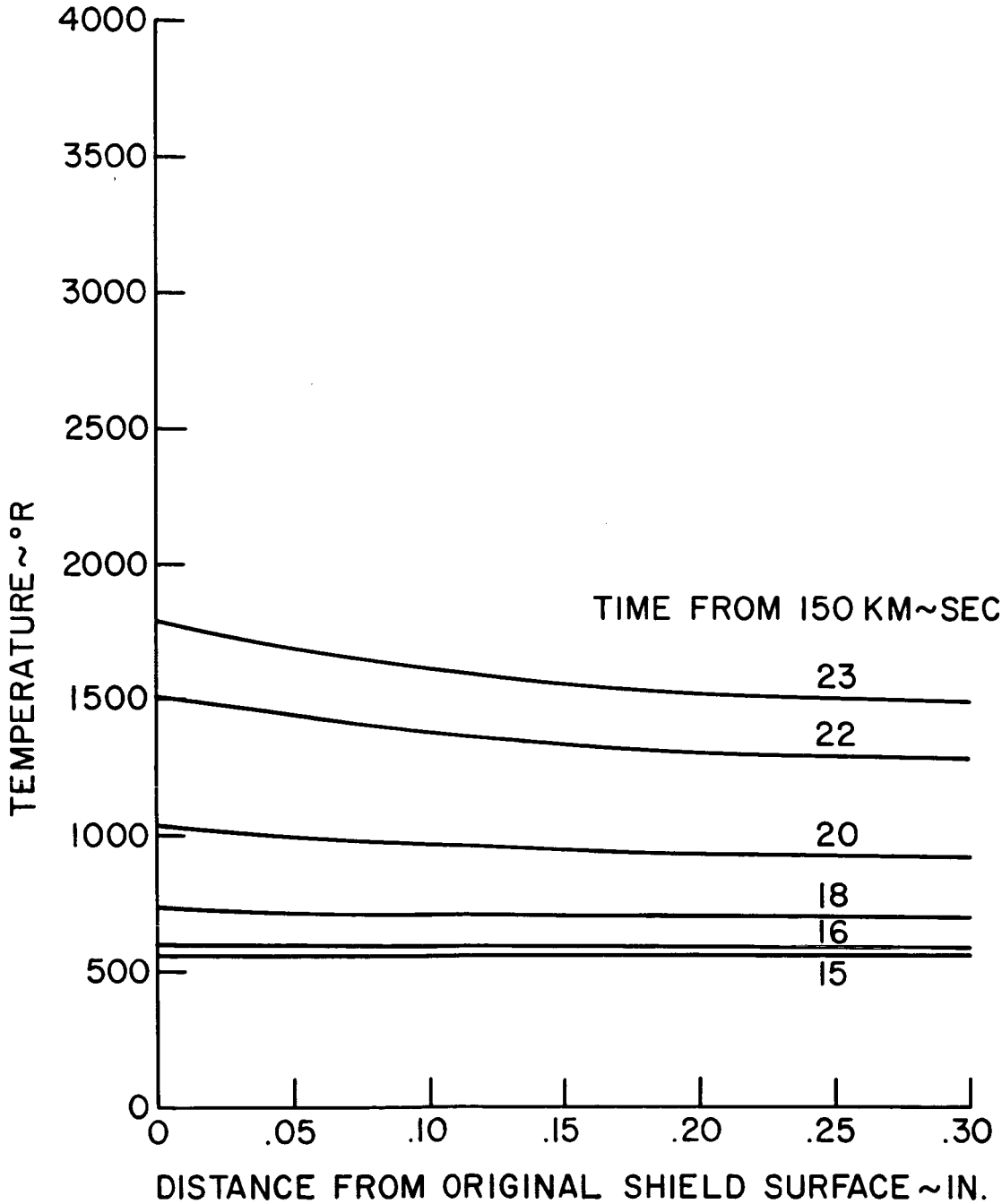

FIGURE 25

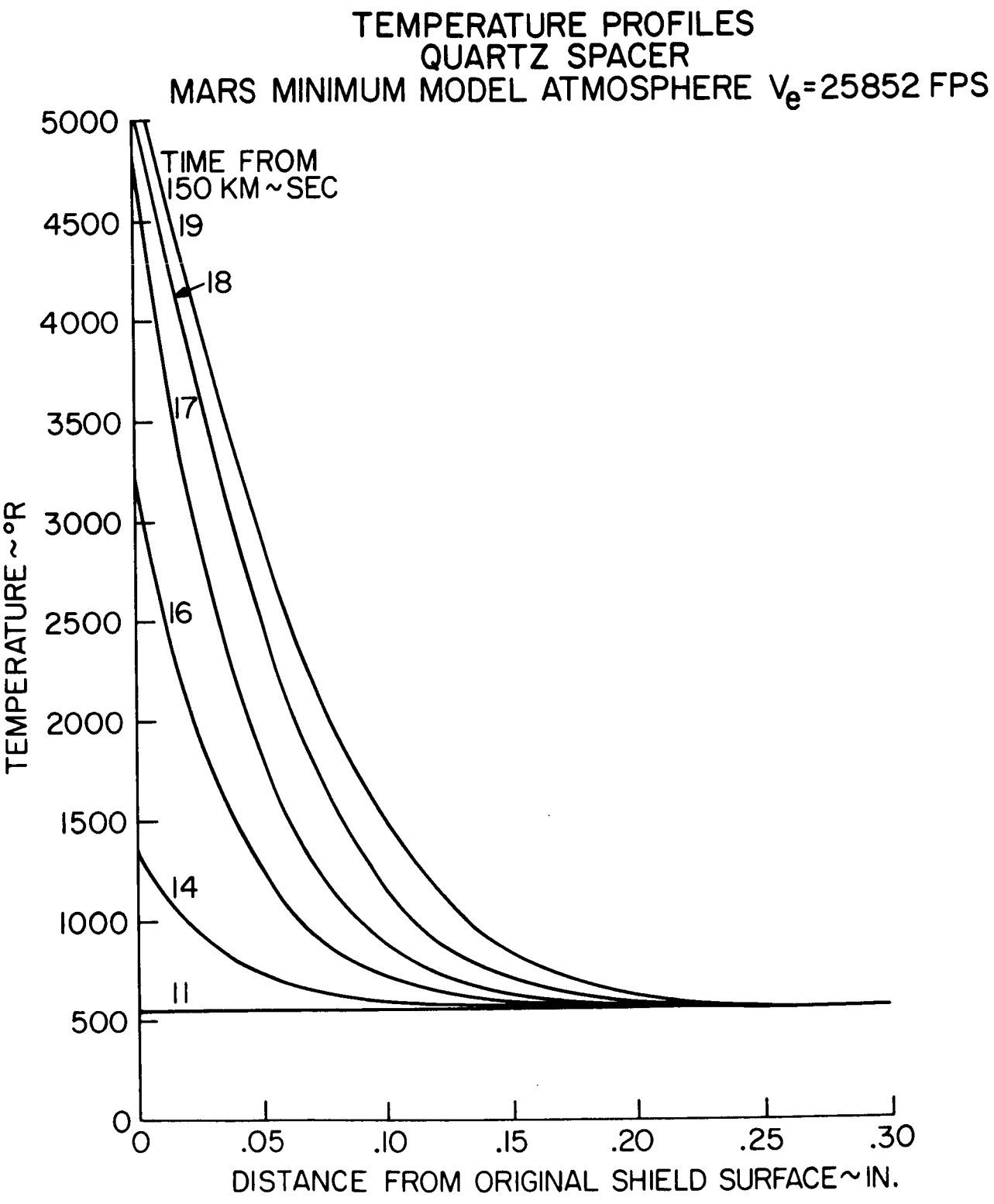
TEMPERATURE PROFILES
QUARTZ SPACER
MARS MINIMUM MODEL ATMOSPHERE V_e=25852 FPS
TIME FROM
150 KM~SEC
19
18
17
16
14
11
TEMPERATURE~°R
5000
4500
4000
3500
3000
2500
2000
1500
1000
500
0
0
.05
.10
.15
.20
.25
.30
DISTANCE FROM ORIGINAL SHIELD SURFACE~IN.

FIGURE 26

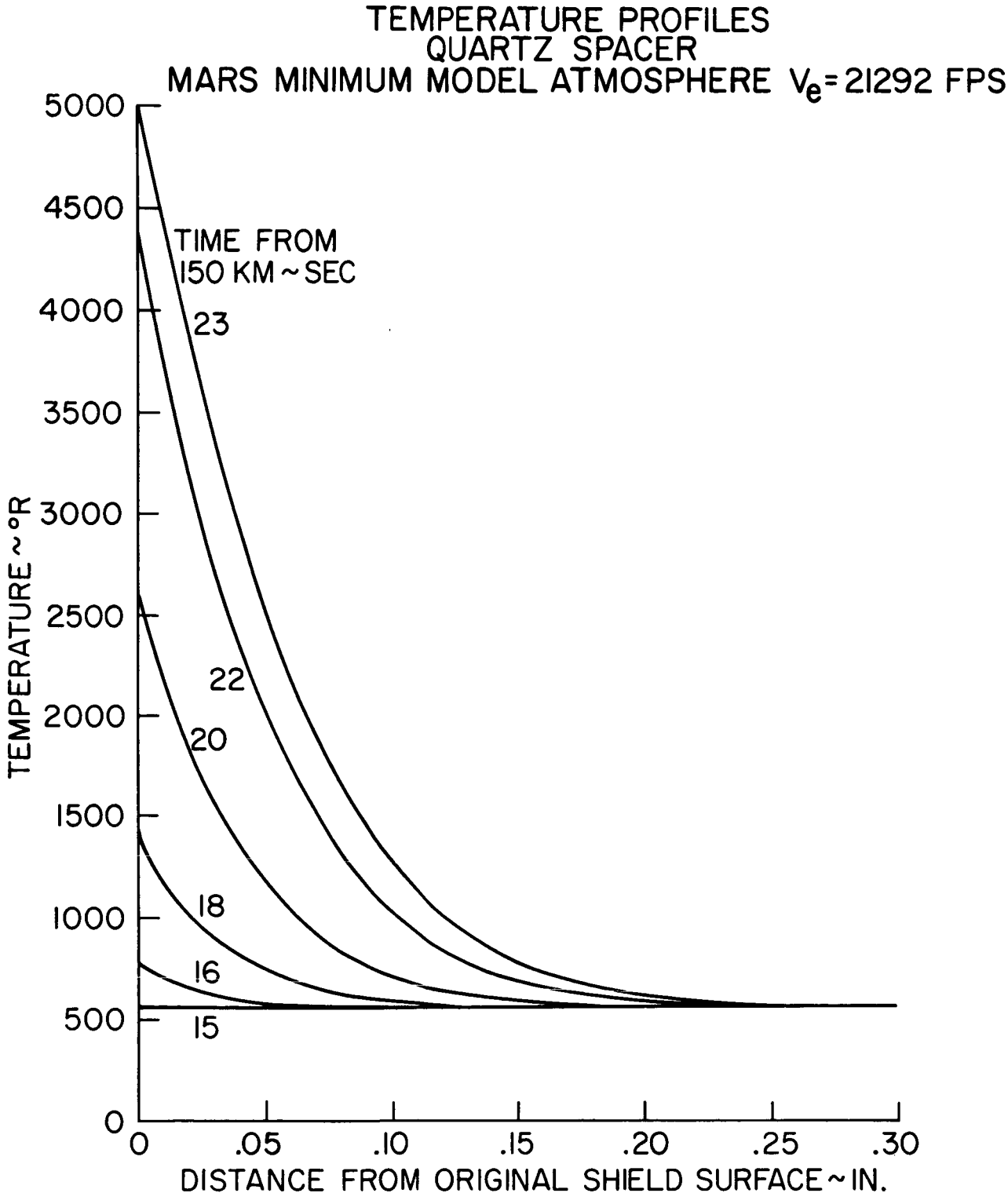
TEMPERATURE PROFILES
QUARTZ SPACER
MARS MINIMUM MODEL ATMOSPHERE V_e = 21292 FPS
TIME FROM
150 KM ~ SEC
23
22
20
18
16
15
TEMPERATURE ~ °R
5000
4500
4000
3500
3000
2500
2000
1500
1000
500
0
0
.05
.10
.15
.20
.25
.30
DISTANCE FROM ORIGINAL SHIELD SURFACE ~ IN.

FIGURE 27

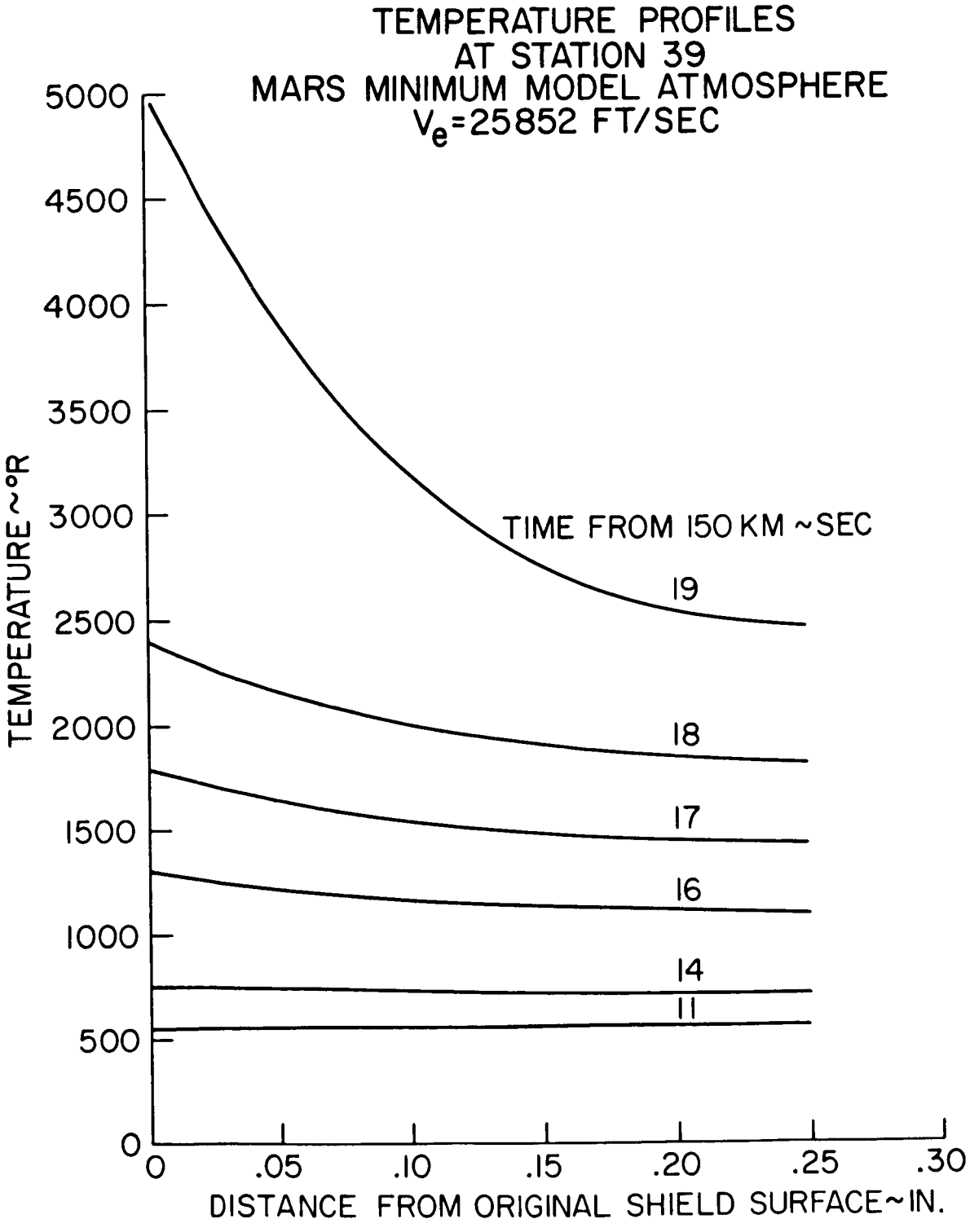
TEMPERATURE PROFILES
AT STATION 39
MARS MINIMUM MODEL ATMOSPHERE
V_e=25852 FT/SEC
TEMPERATURE ~ °R
5000
4500
4000
3500
3000
2500
2000
1500
1000
500
0
TIME FROM 150 KM ~ SEC
19
18
17
16
14
11
0
.05
.10
.15
.20
.25
.30
DISTANCE FROM ORIGINAL SHIELD SURFACE ~ IN.

FIGURE 28

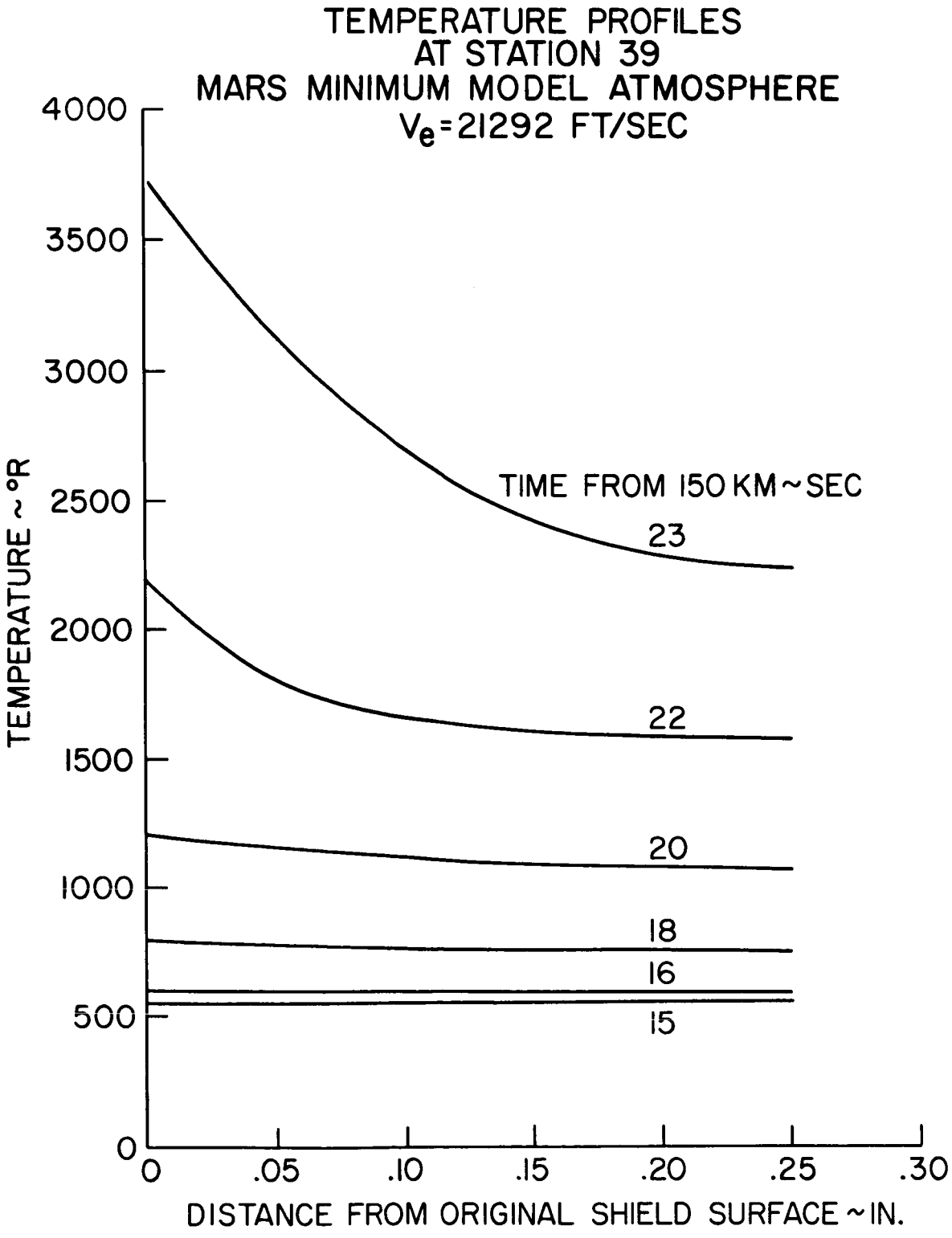
TEMPERATURE PROFILES
AT STATION 39
MARS MINIMUM MODEL ATMOSPHERE
V_e=21292 FT/SEC
TEMPERATURE ~ °R
4000
3500
3000
2500
2000
1500
1000
500
0
TIME FROM 150 KM ~ SEC
23
22
20
18
16
15
0
.05
.10
.15
.20
.25
.30
DISTANCE FROM ORIGINAL SHIELD SURFACE ~ IN.

FIGURE 29

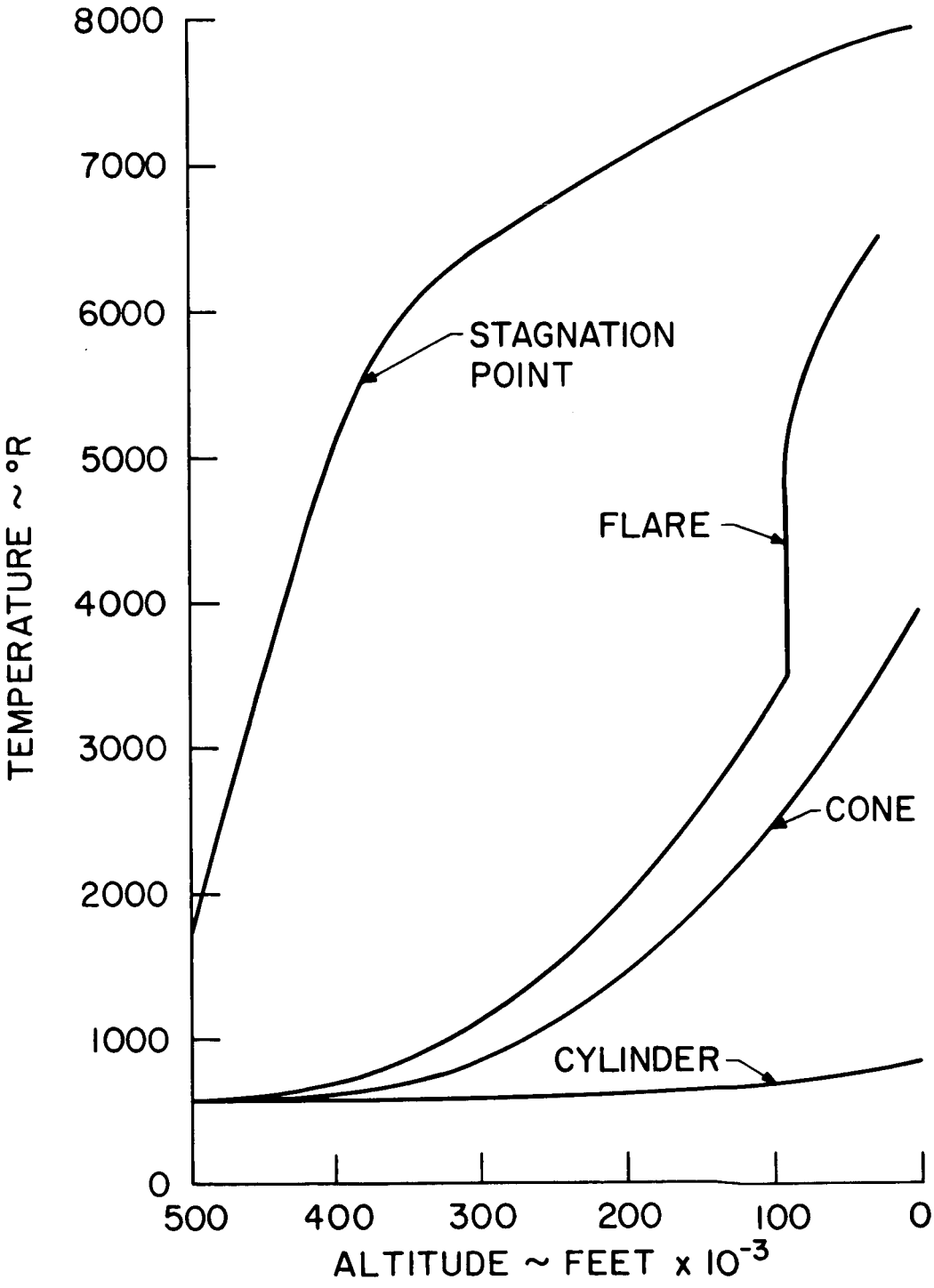
SURFACE TEMPERATURE HISTORIES
MARS MAXIMUM MODEL ATMOSPHERE V_e = 25065 FPS
TEMPERATURE ~ °R
8000
7000
6000
5000
4000
3000
2000
1000
0
STAGNATION POINT
FLARE
CONE
CYLINDER
500
400
300
200
100
0
ALTITUDE ~ FEET x 10^{-3}

FIGURE 30

SURFACE TEMPERATURE HISTORIES
MARS MAXIMUM MODEL ATMOSPHERE ~ V_e = 20308

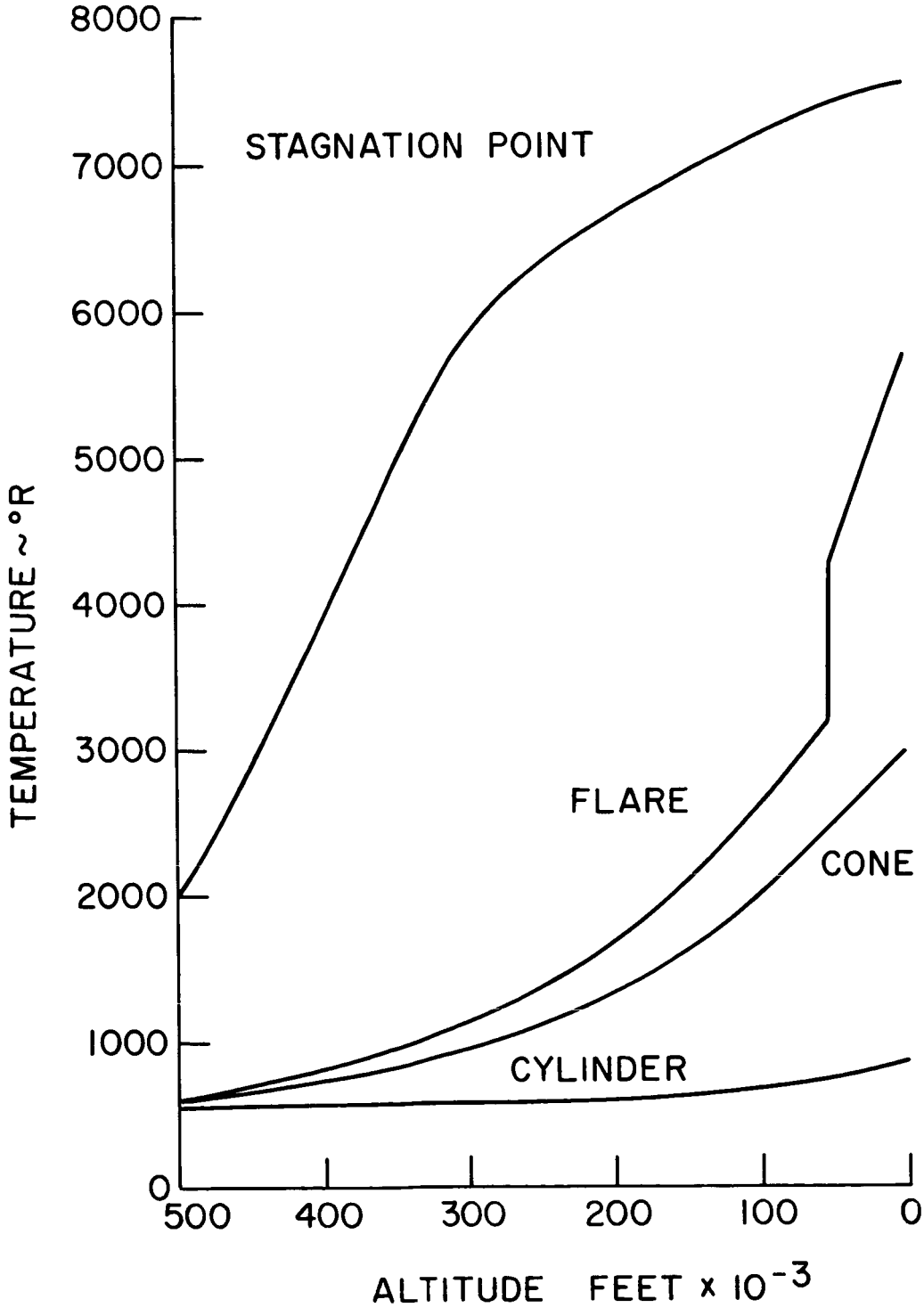

FIGURE 31

SURFACE TEMPERATURE HISTORIES
MARS MINIMUM MODEL ATMOSPHERE ~ V_e = 25852 FPS

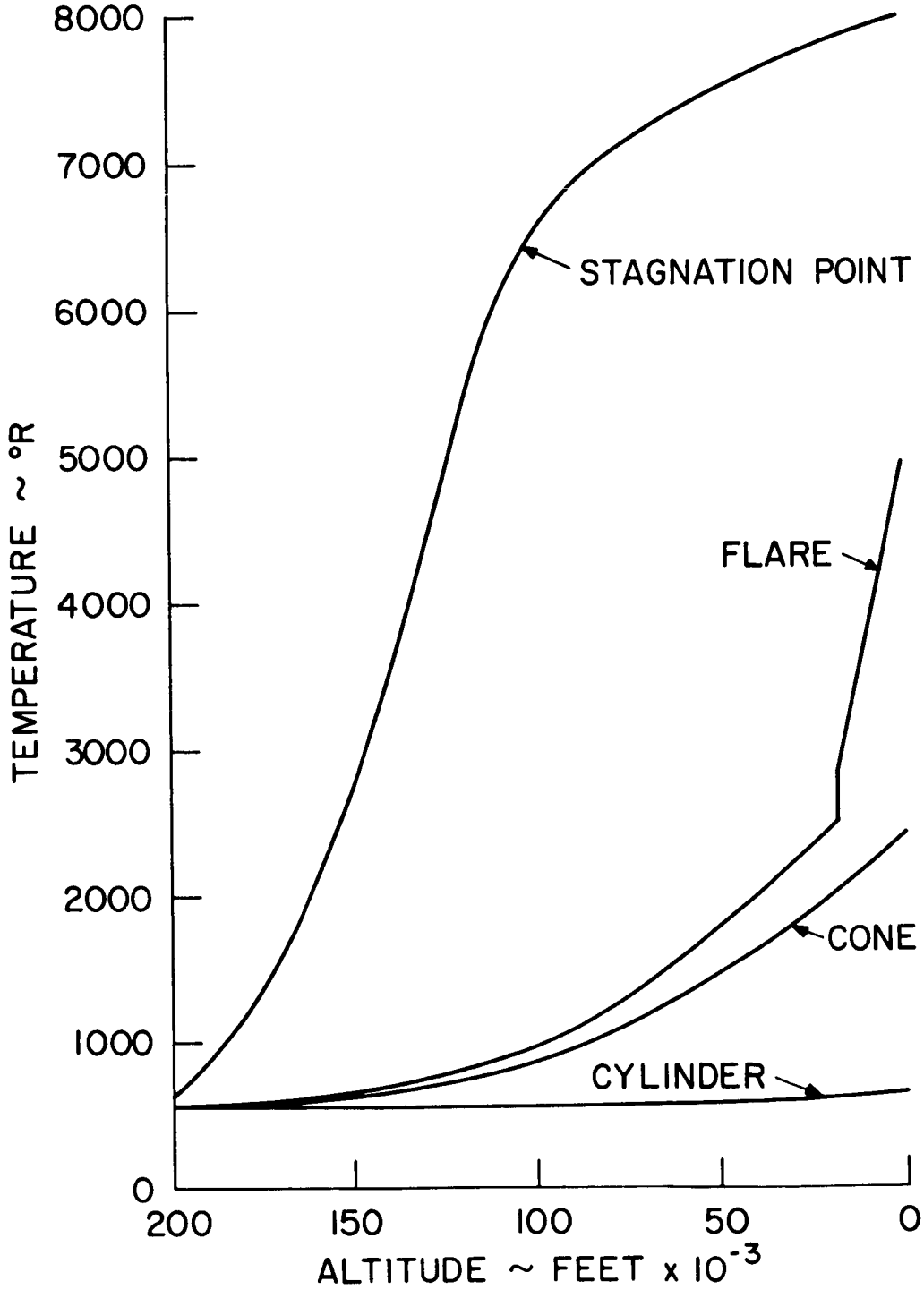

FIGURE 32

SURFACE TEMPERATURE HISTORIES
MARS MINIMUM MODEL ATMOSPHERE $V_e = 21292$ FPS

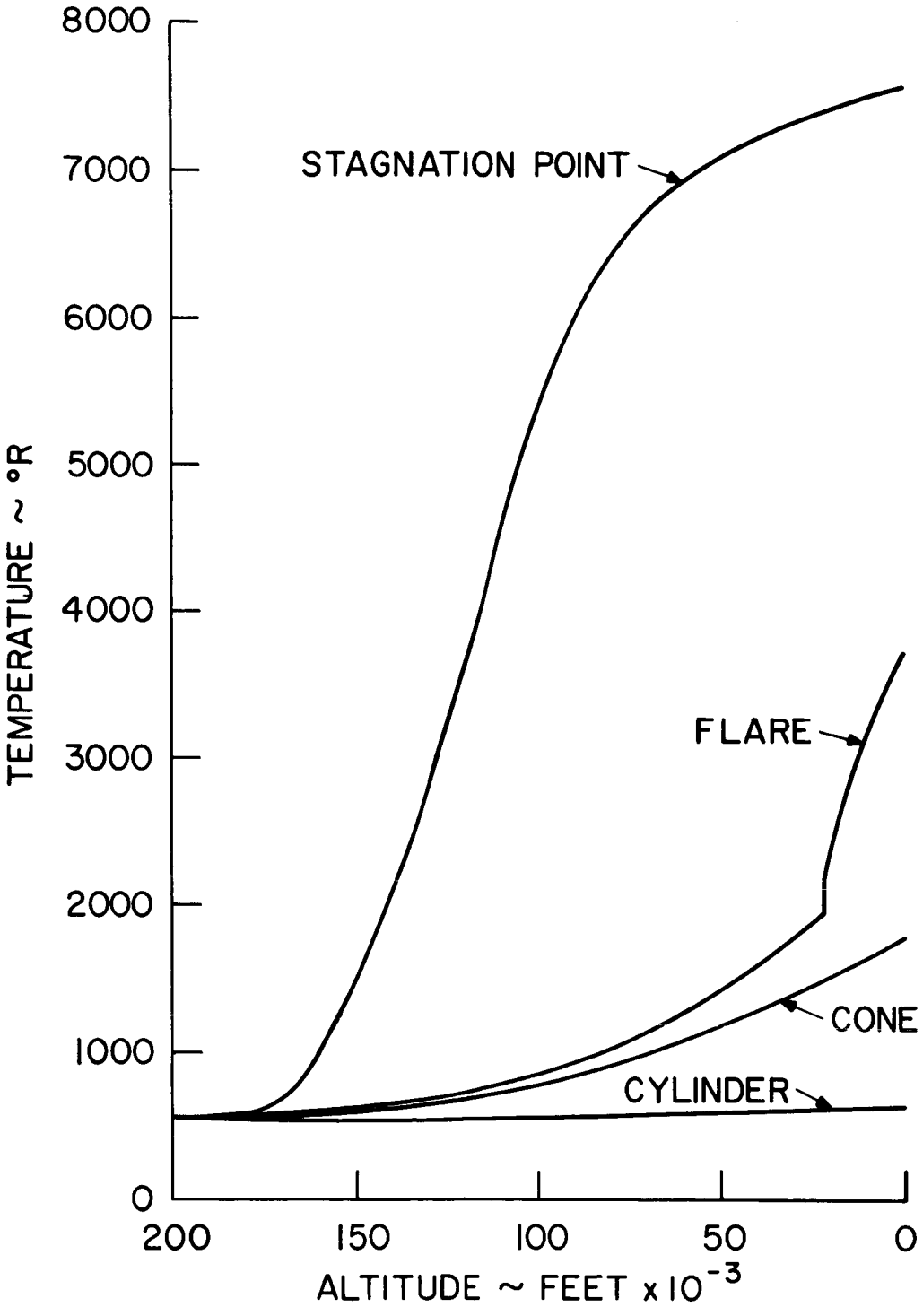

FIGURE 33

TABLE 2 - SUMMARY OF MAXIMUM BACKFACE TEMPERATURES

MODEL ATMOSPHERE	MARS MAXIMUM		MARS MINIMUM	
ENTRY VELOCITY (FPS)	25065	20308	25852	21292
BODY LOCATION				
CONE STATION 12 x = 0.30 IN.	2390°F	2021°F	1316°F	1026°F
CYLINDER STATION 30 x = 0.20 IN.	302°F	350°F	170°F	155°F
FLARE STATION 39 x = 0.25 IN.	4900°F	3859°F	2005°F	1767°F
QUARTZ RING STATION 21 x = 0.30 IN.	528°F	458°F	104°F	104°F

NOTE: CALCULATIONS BASED UPON AN INITIAL TEMPERATURE OF 100°F AND AN ADIABATIC BACKFACE.

MAXIMUM BACKFACE TEMPERATURES OCCUR AT THE SURFACE OF MARS.

x IS THE ORIGINAL THICKNESS OF THE HEAT SHIELD MATERIAL.

CALCULATIONS OF CHEMICAL REACTIONS IN THE BOUNDARY LAYER

Based upon the previously predicted local pressures and surface temperatures, the aerothermochemical interactions between the graphite surface and the Martian atmosphere were treated by means of a nine-component model which included: N_2, N, O_2, O, C, C_3, CO, CO_2 and CN. Scala and Gilbert[8] found that the contribution to the total enthalpy of the species NO,* C_2H_2 and C_2 was less than that of a trace species in Earth atmosphere calculations and were, therefore, neglected in this analysis.

$$N_2 \rightleftharpoons 2\,N \quad ; \qquad K_{P_N} = \frac{p_N^2}{p_{N_2}}$$

$$O_2 \rightleftharpoons 2\,O \quad ; \qquad K_{P_O} = \frac{p_O^2}{p_{O_2}}$$

$$CO + O \rightleftharpoons CO_2 \; ; \qquad K_{P_{CO_2}} = \frac{p_{CO_2}}{p_{CO}\, p_O}$$

$$C + O \rightleftharpoons CO \quad ; \qquad K_{P_{CO}} = \frac{p_{CO}}{p_C\, p_O}$$

---

* Although NO is expected to be a more prevalent component in Martian entry than for Earth, it is still expected to be present at a small level. Since its inclusion was not in the scope of the programs that were used, and consideration of sample chamber kinetics indicate that no significant quantity would reach the mass spectrometer leak, its omission is though to be reasonable.

$$C + N \rightleftharpoons CN \; ; \qquad K_{P_{CN}} = \frac{p_{CN}}{p_C \, p_N}$$

$$3\,C \rightleftharpoons C_3 \; ; \qquad K_{P_{C_3}} = \frac{p_{C_3}}{p_C{}^3}$$

$$C(s) \rightleftharpoons C(g); \qquad K_{P_C} = p_C$$

where p_i is the partial pressure of species i.

From Dalton's Law we obtain

$$\sum_i p_i = P_e$$

where P_e is the boundary layer edge pressure.

The elemental mass balance for nitrogen across the boundary layer may be shown to be[11]

$$(\bar{C}_N)_w = \frac{(\bar{C}_N)_e}{1 + B}$$

where B is a function of the dimensionless mass loss rate parameter $(\dot{m}_w/\rho_e U_e \, C_{HO})$ and $(\bar{C}_N)_w$ and $(\bar{C}_N)_e$ are the effective mass fraction of the element nitrogen at the wall and boundary layer edge, respectively.

For the final condition the mass transfer compatibility restraint may be shown to be

$$(\bar{C}_c)_w = \frac{(\bar{C}_c)_e + B}{1 + B}$$

where $\bar{C}_c$ is the effective mass fraction of the element carbon.

Based on the foregoing analysis, the equilibrium chemical

composition at the stagnation point, the cone, and the flare surfaces of the probe were determined. The results are presented in Figures 34-43. Cases where no ablation occurred due to very low heating rates were omitted. These included the cylinder for all atmosphere models and velocities and the cone for the minimum atmosphere and low velocity. The flare has also been omitted for the minimum atmosphere and low velocity because significant ablation starts at about 23,000 ft. Because of the low wall temperatures in these six cases, the surface composition for each could be assumed to be the undissociated ambient atmosphere. The pertinent compositions, as would be sensed by the mass spectrometer, were determined later, using kinetic considerations.

VARIATION OF CHEMICAL COMPOSITION AT SURFACE WITH ALTITUDE

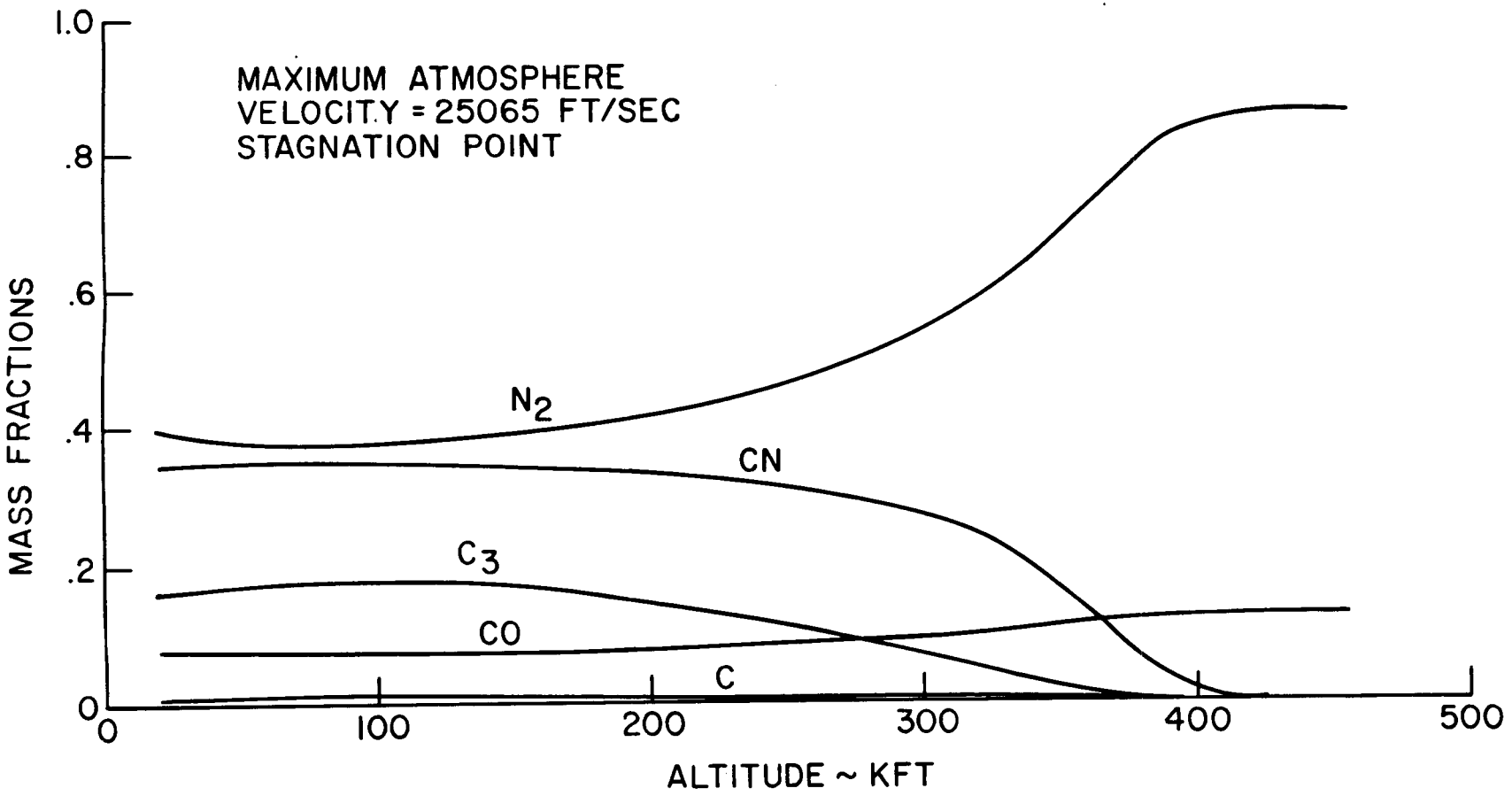

FIGURE 34

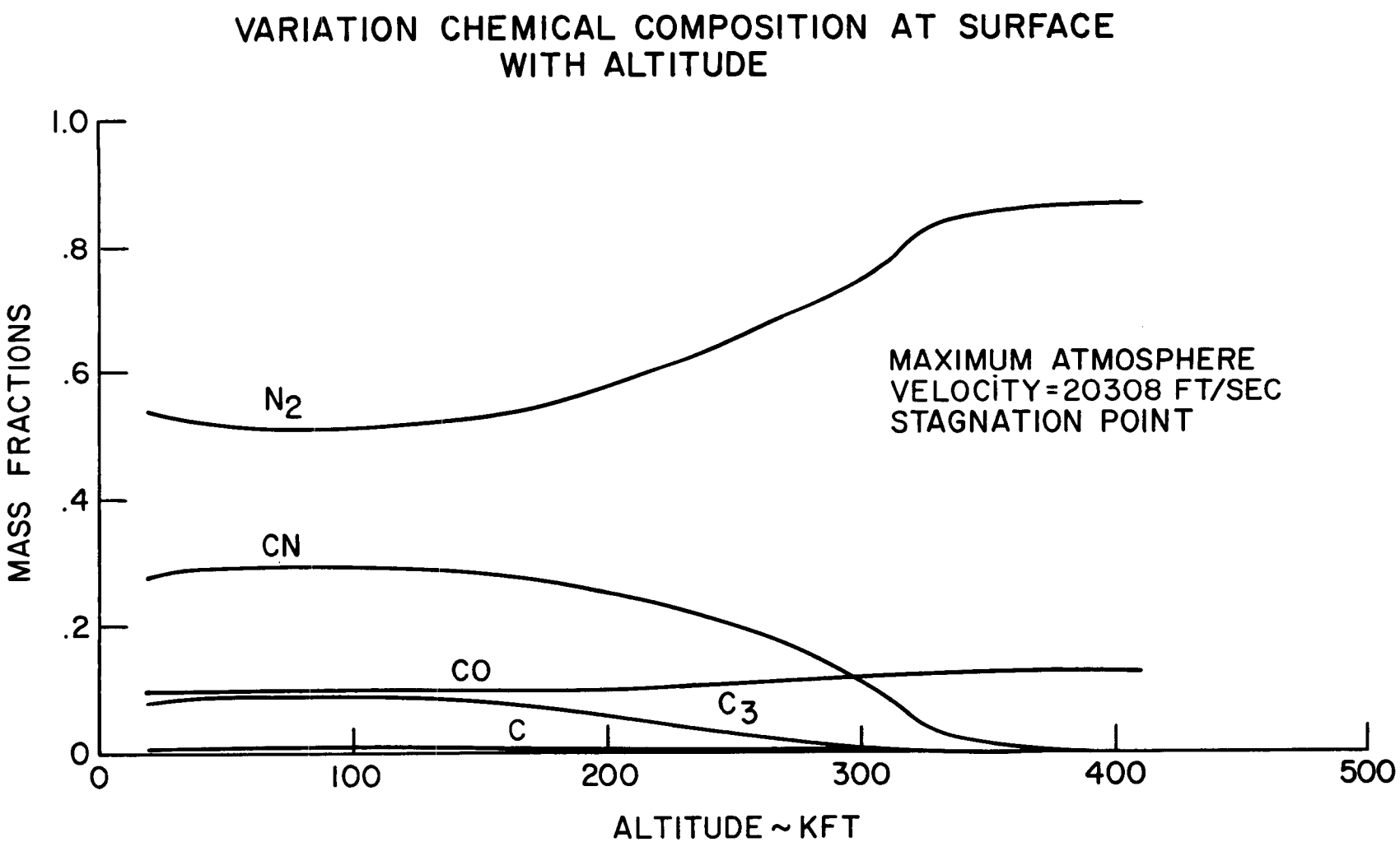
VARIATION CHEMICAL COMPOSITION AT SURFACE WITH ALTITUDE
MASS FRACTIONS
1.0
.8
.6
.4
.2
0
N_2
CN
CO
C_3
C
MAXIMUM ATMOSPHERE
VELOCITY=20308 FT/SEC
STAGNATION POINT
0
100
200
300
400
500
ALTITUDE ~ KFT

FIGURE 35

VARIATION OF CHEMICAL COMPOSITION AT SURFACE WITH ALTITUDE

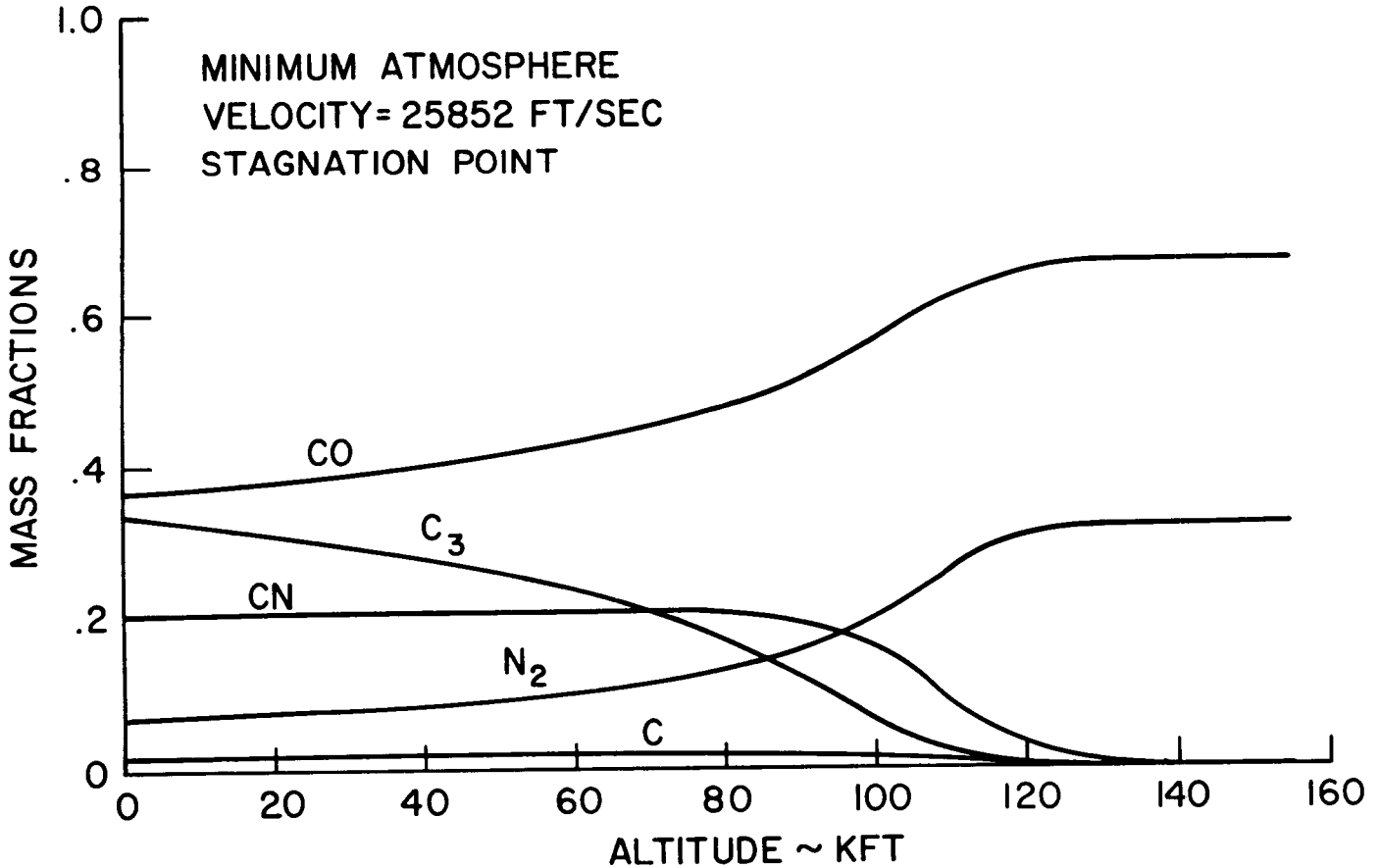

FIGURE 36

VARIATION OF CHEMICAL COMPOSITION AT SURFACE WITH ALTITUDE

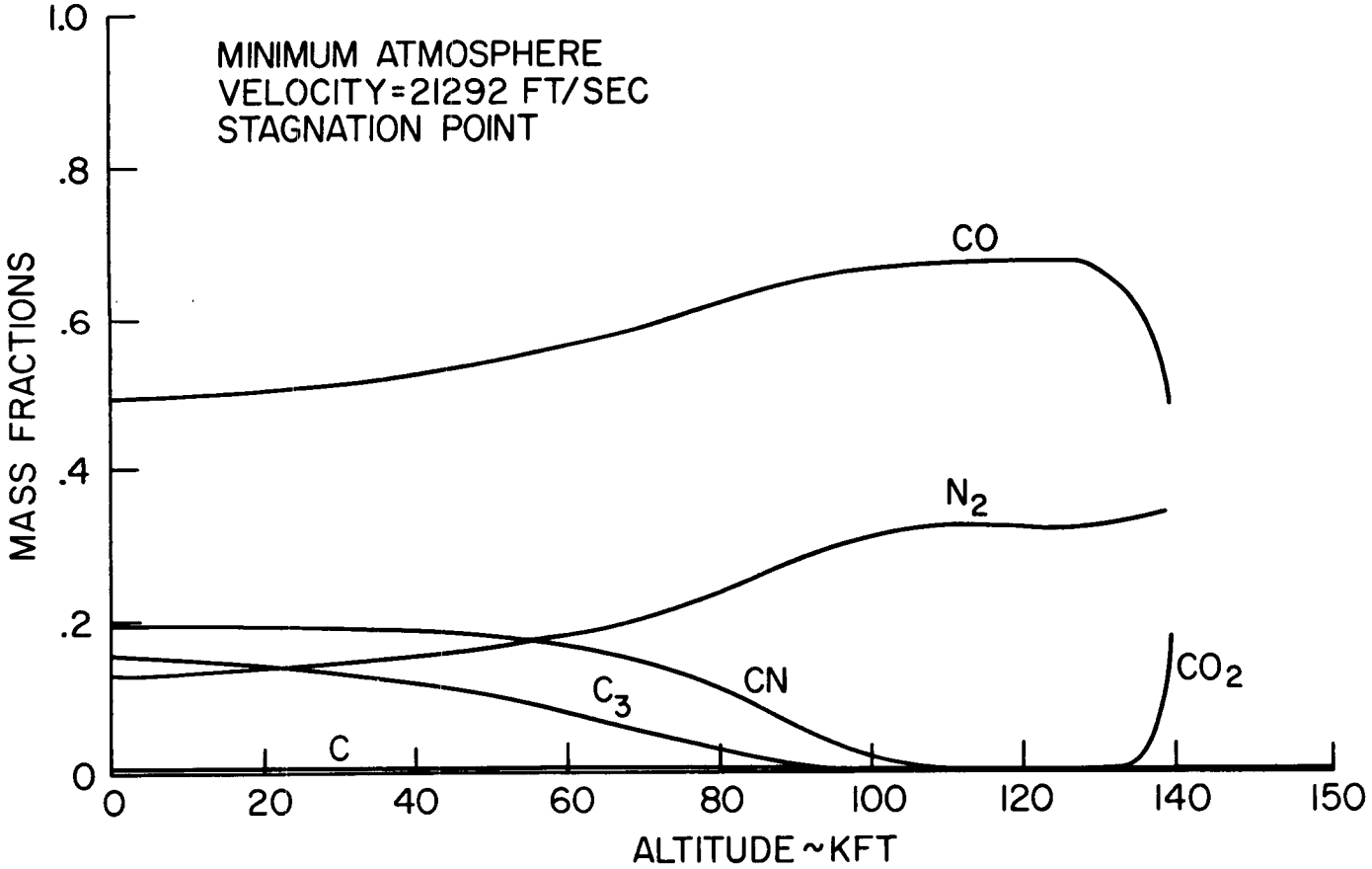

FIGURE 37

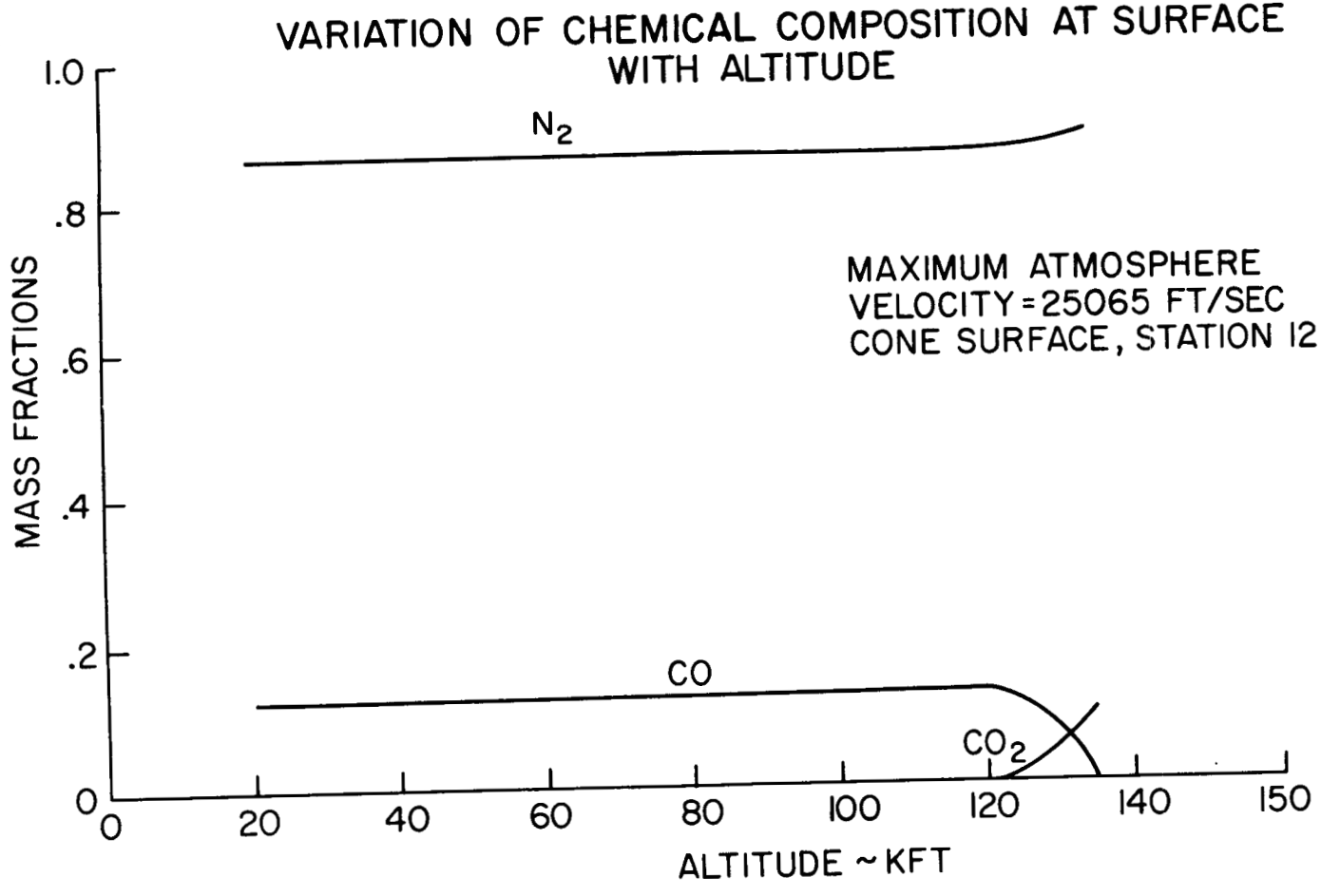
VARIATION OF CHEMICAL COMPOSITION AT SURFACE WITH ALTITUDE
MASS FRACTIONS
1.0
.8
.6
.4
.2
0
N_2
CO
CO_2
MAXIMUM ATMOSPHERE
VELOCITY = 25065 FT/SEC
CONE SURFACE, STATION 12
0
20
40
60
80
100
120
140
150
ALTITUDE ~ KFT

FIGURE 38

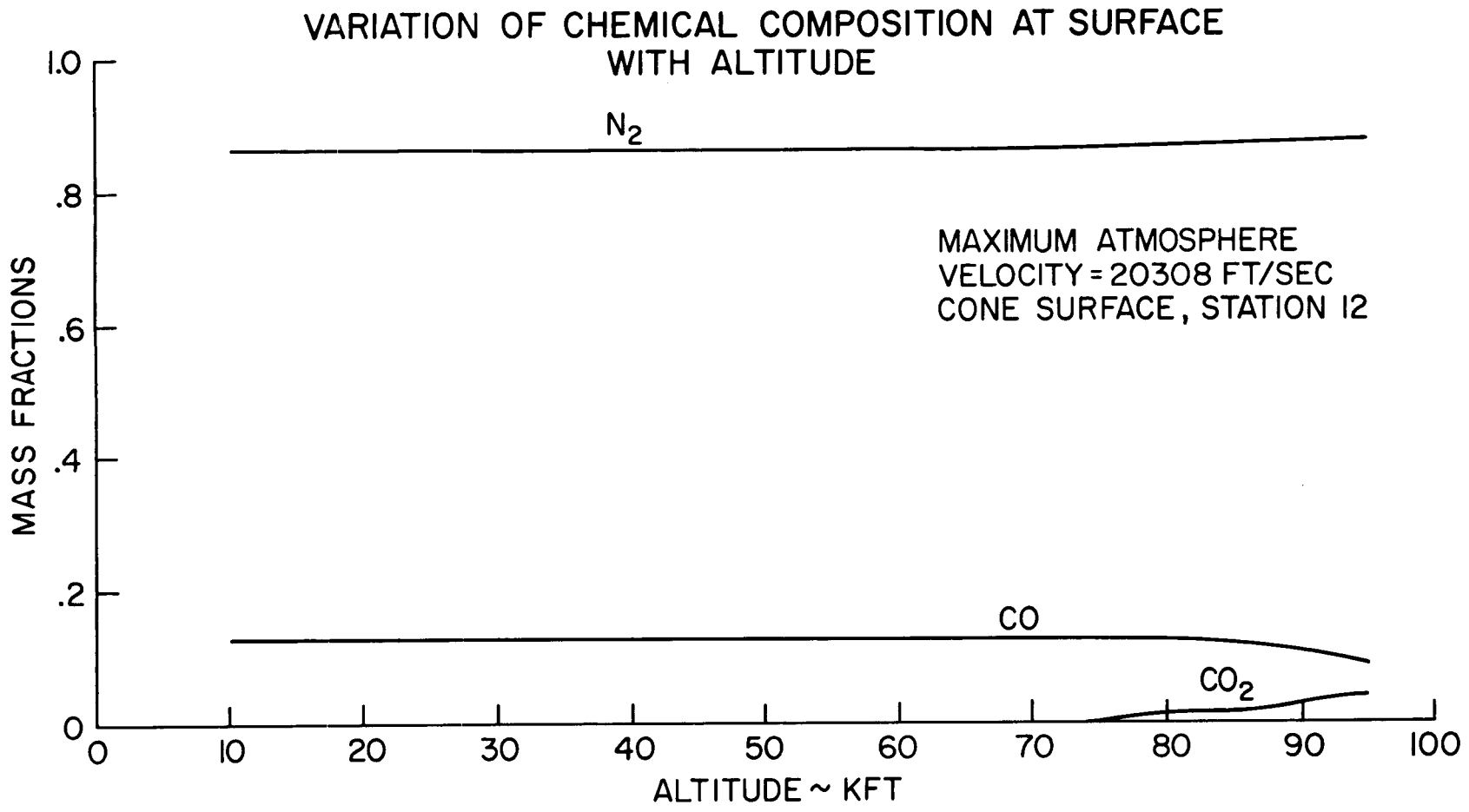
VARIATION OF CHEMICAL COMPOSITION AT SURFACE WITH ALTITUDE
MASS FRACTIONS
1.0
.8
.6
.4
.2
0
N_2
MAXIMUM ATMOSPHERE
VELOCITY = 20308 FT/SEC
CONE SURFACE, STATION 12
CO
CO_2
0
10
20
30
40
50
60
70
80
90
100
ALTITUDE ~ KFT

FIGURE 39

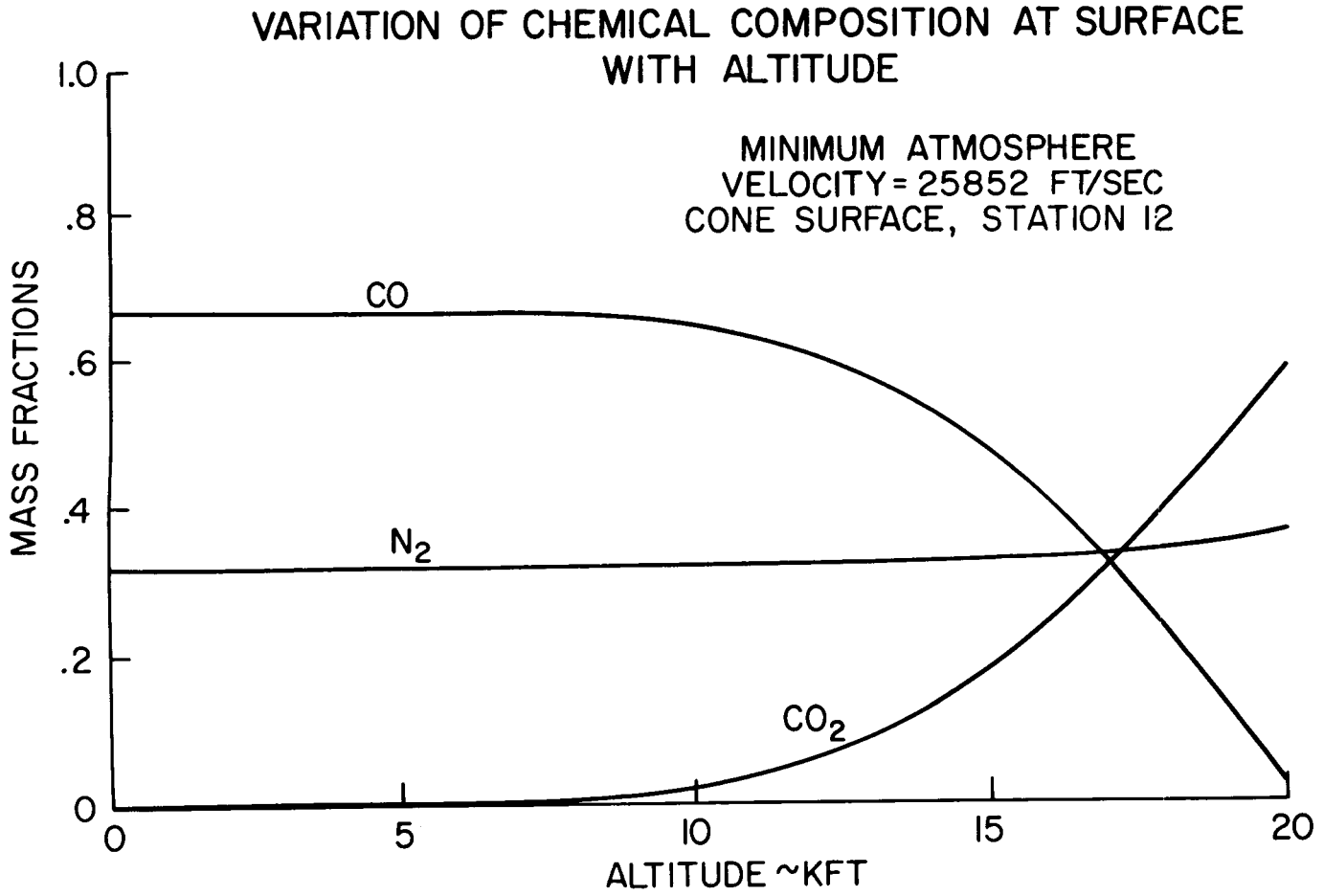
VARIATION OF CHEMICAL COMPOSITION AT SURFACE WITH ALTITUDE
MINIMUM ATMOSPHERE
VELOCITY = 25852 FT/SEC
CONE SURFACE, STATION 12
MASS FRACTIONS
1.0
.8
.6
.4
.2
0
CO
N_2
CO_2
0
5
10
15
20
ALTITUDE ~KFT

FIGURE 40

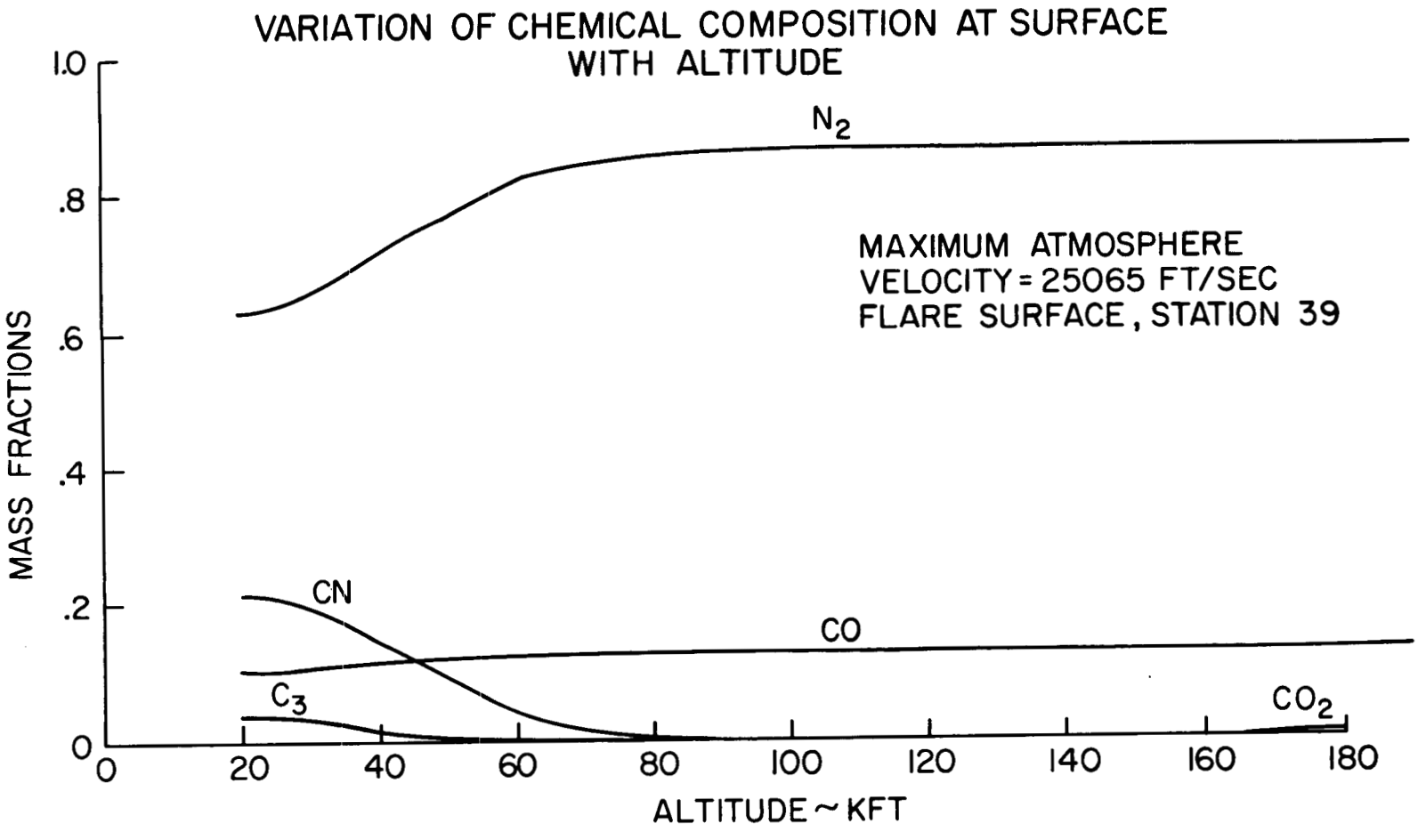
VARIATION OF CHEMICAL COMPOSITION AT SURFACE WITH ALTITUDE
MASS FRACTIONS
1.0
.8
.6
.4
.2
0
N_2
MAXIMUM ATMOSPHERE
VELOCITY = 25065 FT/SEC
FLARE SURFACE, STATION 39
CN
CO
C_3
CO_2
0
20
40
60
80
100
120
140
160
180
ALTITUDE ~ KFT

FIGURE 41

VARIATION OF CHEMICAL COMPOSITION AT SURFACE WITH ALTITUDE

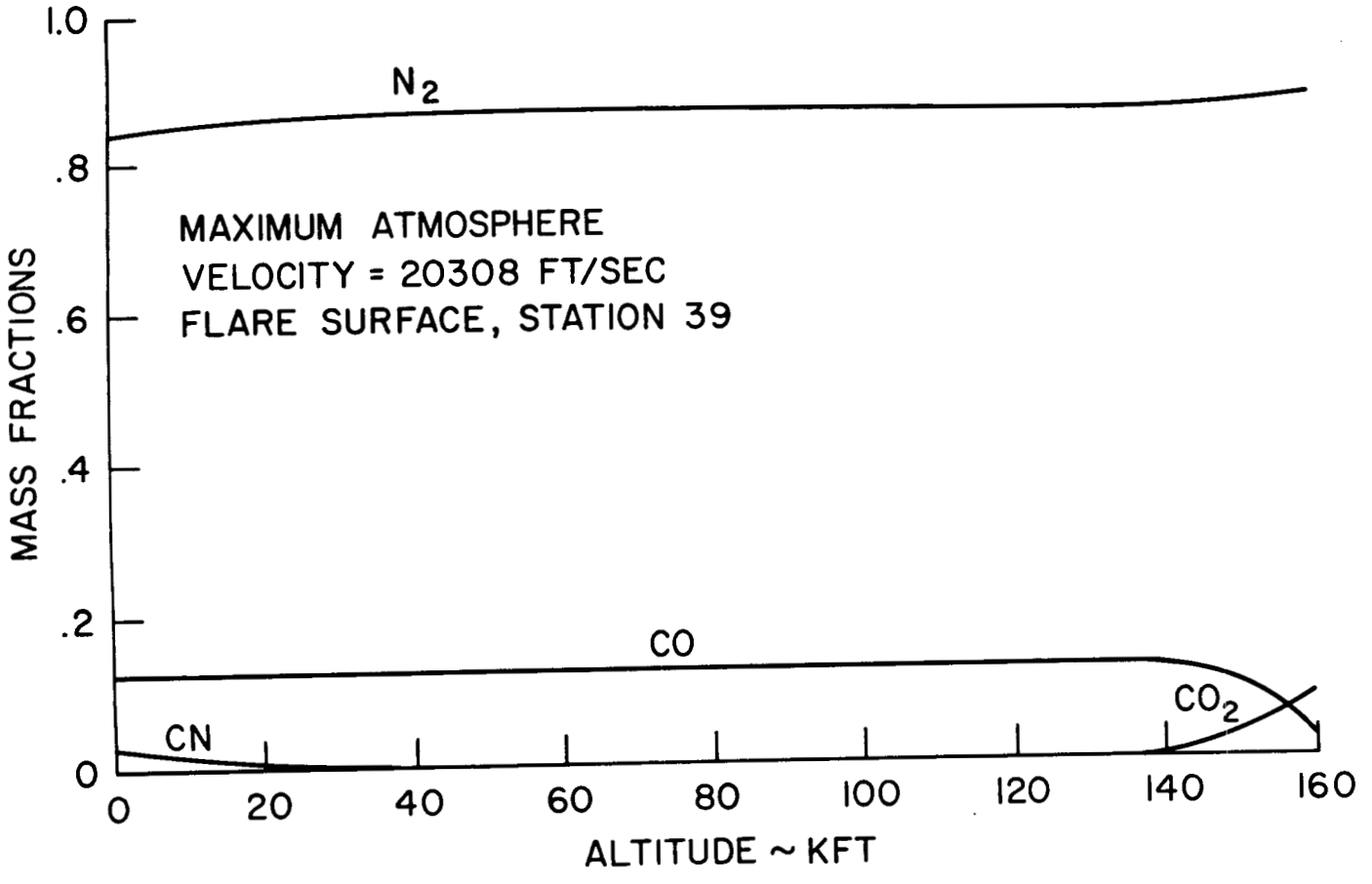

FIGURE 42

VARIATION OF CHEMICAL COMPOSITION AT SURFACE WITH ALTITUDE

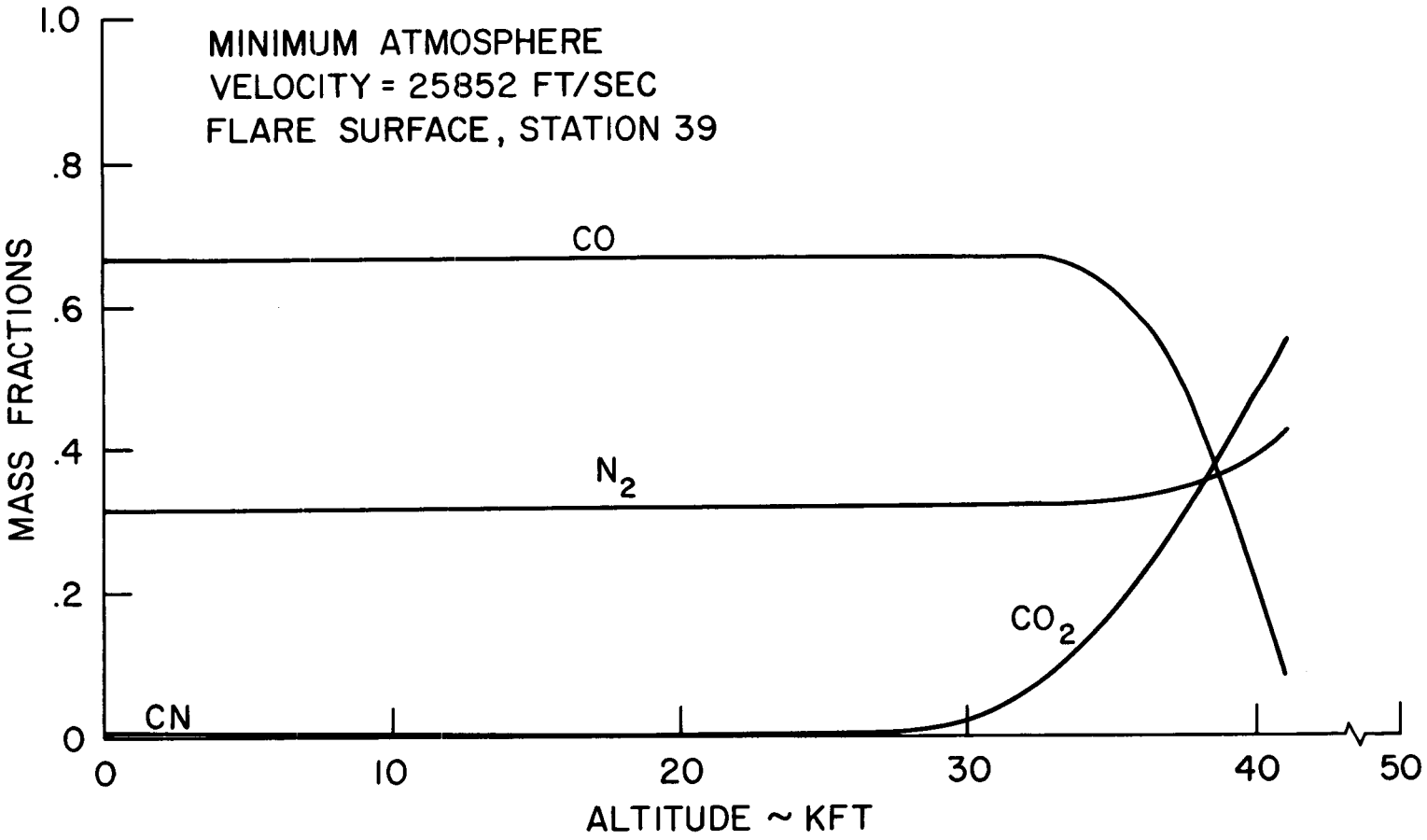

FIGURE 43

ESTIMATE OF CARBON CONTAMINATION FROM UPSTREAM ABLATION

The aerodynamic heat transfer calculations account for upstream atmosphere gases as they are swept back in the boundary layer. Since no programs are available to account for the contributions to the boundary layer of upstream ablation, the earlier calculations assumed that only carbon which was released at the station that was being considered contributed to the chemical composition in that area. In order to determine if this assumption was reasonable, a model was developed to estimate upstream contributions. The following assumptions were used: (1) All ablation products appear at the site that is being examined at the instant of evolution from all upstream sites; (2) No ablation products escape from the boundary layer; (3) The ablation products distribute themselves equally throughout the boundary layer. Ablation that was considered for these calculations occurred only at the stagnation point and on the cone. Stagnation point ablation was assumed to be constant over the whole spherical region. The rate of cone ablation was assumed to be constant over its entire surface, and at the rate calculated for station 12. Thus, $\dot{M}$ (total rate of upstream ablation, lb/sec) was calculated for stations 12, 30, and 39. $\dot{M}$'s were

compared to $\rho_e U_e A_\delta$ at each station, where ρ_e is the boundary layer density at its interface with the atmosphere, U_e is the velocity at that point, and A_δ is the area of the boundary layer. These parameters were determined during the earlier aerodynamic calculations. The results of these computations are shown in Table 3. It is clear that the input of upstream ablation products is not significant in most cases. In those where they are significant (principally the cylinder for the minimum atmosphere model at higher velocity) the ablation products have been included for further computations.

Note that the computations in Table 3 are the best that can be done with the present state-of-the-art, but are still very approximate. Therefore, they should be used as an indication of the effect of upstream carbon contaminants, rather than as exact values.

TABLE 3

CARBON CONTAMINATION FROM UPSTREAM ABLATION

Station	Altitude ft.	$\rho_e U_e A_\delta$ lb./sec.	$\dot{M}$ lb./sec.	$\dot{M}/\rho_e U_e A_\delta$
Minimum Atmosphere at V_e = 21,292 ft./sec.				
12	85,500	1.027×10^{-1}	4.566×10^{-5}	4×10^{-4}
12	64,034	1.611×10^{-1}	9.872×10^{-5}	6×10^{-4}
12	324	2.625×10^{-1}	2.838×10^{-4}	1×10^{-3}
30	85,500	1.158×10^{-2}	4.566×10^{-5}	4×10^{-3}
30	64,034	2.032×10^{-2}	9.872×10^{-5}	5×10^{-3}
30	324	6.105×10^{-2}	2.838×10^{-4}	5×10^{-3}
39	85,500	6.692×10^{-1}	4.566×10^{-5}	7×10^{-5}
39	64,034	1.154×10^{0}	9.872×10^{-5}	9×10^{-5}
39	324	3.969×10^{0}	2.838×10^{-4}	7×10^{-5}
Minimum Atmosphere at V_e = 23,852 ft./sec.				
12	103,040	7.726×10^{-2}	1.062×10^{-3}	1×10^{-2}
12	51,095	2.473×10^{-1}	2.295×10^{-3}	9×10^{-3}
12	0	3.516×10^{-1}	3.854×10^{-3}	1×10^{-2}
30	103,040	6.217×10^{-3}	3.203×10^{-3}	5×10^{-1}
30	51,095	2.112×10^{-2}	6.624×10^{-3}	3×10^{-1}
30	0	5.407×10^{-2}	1.099×10^{-2}	2×10^{-1}
39	103,040	5.000×10^{-1}	3.203×10^{-3}	6×10^{-3}
39	51,095	1.587×10^{0}	6.624×10^{-3}	4×10^{-3}
39	0	5.259×10^{0}	1.099×10^{-2}	2×10^{-3}

TABLE 3 (Continued)

Station	Altitude ft.	$\rho_e U_e A_\delta$ lb./sec.	$\dot{M}$ lb./sec.	$\dot{M}/\rho_e U_e A_\delta$
Maximum Atmosphere at V_e = 20,308 ft./sec.				
12	367,410	5.770×10^{-2}	2.406×10^{-6}	4×10^{-5}
12	153,020	2.659×10^{-1}	2.195×10^{-4}	8×10^{-4}
12	8,608	5.641×10^{-1}	9.368×10^{-4}	2×10^{-3}
30	367,410	1.849×10^{-2}	2.406×10^{-6}	1×10^{-4}
30	153,020	9.028×10^{-2}	4.769×10^{-4}	5×10^{-3}
30	8,608	2.625×10^{-1}	2.399×10^{-3}	9×10^{-3}
39	367,410	4.160×10^{-1}	2.406×10^{-6}	6×10^{-6}
39	153,020	1.784×10^{0}	4.769×10^{-4}	3×10^{-4}
39	8,608	4.625×10^{0}	2.399×10^{-3}	5×10^{-4}
Maximum Atmosphere at V_e = 25,630ft./sec.				
12	350,720	9.059×10^{-2}	1.597×10^{-5}	2×10^{-4}
12	168,860	3.401×10^{-1}	4.726×10^{-4}	1×10^{-3}
12	18,176	7.924×10^{-1}	1.288×10^{-3}	2×10^{-3}
30	350,720	1.936×10^{-2}	1.843×10^{-5}	1×10^{-3}
30	168,860	6.363×10^{-2}	1.128×10^{-3}	2×10^{-2}
30	18,176	2.069×10^{-1}	6.988×10^{-4}	3×10^{-3}
39	350,720	6.820×10^{-1}	1.843×10^{-5}	3×10^{-5}
39	168,860	2.236×10^{0}	1.128×10^{-3}	5×10^{-4}
39	18,176	5.848×10^{0}	6.988×10^{-4}	1×10^{-4}

CHEMICAL KINETIC ANALYSIS

Introduction

Chemical kinetic factors which influence reactions in the flow field and boundary layer and in the sampling chamber will be considered separately. In the flow field and boundary layer the temperatures are high and endothermic reactions will proceed at high rates. In the flow field the chemical kinetics are at least fairly well understood and one can have some confidence in the results of calculations. The boundary layer chemical kinetics are less well known and the results of calculations are less reliable. Still, order of magnitude results can be considered reasonably reliable.

Flow Field & Boundary Layer Chemical Kinetics

For the flow field region where the ambient atmosphere is considered to be mainly N_2 and CO_2 with small amounts of O_2, H_2O and A, the chemical system is only slightly more complex than that of the earth's atmosphere. The first reactions are the dissociation reactions of N_2 and CO_2. Data for the rate constant for N_2 dissociation are reasonably well known but for CO_2 dissociation there is conflicting evidence and its rate is therefore uncertain. However, since the CO_2 is largely dissociated for the conditions of interest here, for either extreme of this rate,

the uncertainty involved is not great. The oxygen atoms resulting from the CO_2 dissociation can react further with CO_2 by the reaction

$$O + CO_2 \longrightarrow CO + O_2$$

The CO and O_2 molecules can also be dissociated by collision. The inclusion of water in the atmospheric composition introduces several other reactions. In addition to the dissociation and other reactions of the hydrogen-oxygen system, the reaction of hydrogen atoms with CO_2

$$H + CO_2 \longrightarrow CO + OH$$

may be quite important.

Several other rearrangement reactions are important. These include

$$O + N_2 \longrightarrow N + NO$$

$$C + N_2 \longrightarrow N + CN$$

The NO and CN can, of course, undergo numerous reactions including further rearrangements and dissociation.

The ionization reactions include direct collisional ionization of all of the species, and those of the major species, N_2 and CO_2 are of most importance. The high temperatures the gases reach immediately on crossing the shock front cause these reactions to

be fast in this region. After significant numbers of free atoms are formed, associative ionization reactions form O_2^+, N_2^+, NO^+ and other molecular ions as well as free electrons.

All of the reactions discussed can occur in the reverse direction. In general, the gases immediately after crossing the shock front, being heated greatly, undergo endothermic reactions since many molecules have the required energy. These reactions cause the gas to cool. After the gases reach cooler regions the exothermic reactions become more important, in some cases being faster than the reverse endothermic reactions. Equilibrium may be approached from the endothermic direction by some species and from the exothermic direction by others.

The flow field reactions are summarized in Table 4. The rate constants which were used are given. The sources of the data have been discussed elsewhere.[12]

In the boundary layer of a graphite nose cone, much carbon is introduced mostly in the form of C and C_3. These, of course, react with the atmospheric species. These can also be surface reactions of the graphite with atmospheric species. These reactions result in the formation of CN, CO and other important species. In general these reactions are not well studied. It is

TABLE 4

FLOW FIELD REACTIONS AND RATE CONSTANTS*

	a	b	10^{-3}c	a'	b'	10^{-3}c'
$CO_2 + M = CO + O + M$	1^{-8}	0	86.4	1^{-36}	0	0
$N_2 + M = N + N + M$	5.2^{-6}	-.5	113	3.4^{-31}	-.5	0
$O + N_2 = N + NO$	1.3^{-10}	0	38.5	2.5^{-11}	0	0
$CO + M = C + O + M$	1^{-8}	0	125	1^{-35}	0	0
$H_2O + M = H + OH + M$	1^{-11}	0	50.3	1^{-31}	0	0
$CO_2 + H = CO + OH$	5^{-12}	0	16.8	3.8^{-14}	0	5.2
$N_2 + M = N_2^+ + e + M$	2^{-20}	1.5	181	5^{-26}	0	0
$N + M = N^+ + e + M$	2^{-20}	1.5	158	1^{-27}	0	0
$CO_2 + M = CO_2^+ + e + M$	2^{-20}	1.5	160	5^{-26}	0	0
$CO + M = CO^+ + e + M$	2^{-20}	1.5	169.5	5^{-26}	0	0
$O + M = O^+ + e + M$	2^{-20}	1.5	140	1^{-27}	0	0
$N + O = NO^+ + e$	1.2^{-12}	0	32	1^{-8}	0	0
$N + N = N_2^+ + e$	1.9^{-14}	1	67.7	1^{-5}	-.5	0
$O + O = O_2^+ + e$	2.8^{-15}	.65	80.8	9^{-5}	-1	0
$O + CO_2 = CO + O_2$	1^{-12}	0	29.5	1^{-15}	0	25
$O_2 + M = O + O + M$	9.2^{-7}	-.5	59.8	6.1^{-32}	-.5	0
$OH + M = O + H + M$	1^{-8}	0	50	1^{-32}	0	0
$CO + N = CN + O$	4^{-12}	.5	46	2^{-13}	.5	5.3

*Rate constant values are given by the values of a, b, and c in the expression $k = a\ T^b\ e^{-c/T}$. The unprimed values are for the forward (left to right) reaction as written; the primed values are for the reverse reaction. The values are in units appropriate for expressing concentrations in molecules cm^{-3}.

*The exponents given in the table are the powers of ten by which the accompanying entry is to be multiplied. Thus 1^{-8} is 1×10^{-8}. (This system used also for Tables 6-10).

probably safe to assume, however, that along the surface at altitudes where significant ablation occurred, these carbon-containing species are essentially in local equilibrium with each other. Some of the reactions which would be expected to play a significant role are listed in Table 5.

These flow field reactions were used in calculations to determine the regions in which equilibrium composition would be a reasonable assumption. In such regions the equilibrium compositions, whose calculation is described elsewhere in this report, were used as a starting point for the calculation of the chemical kinetics which occur in the sampling region. At higher altitudes the composition was calculated, using the chemical kinetics shown in Table 4, by a one-dimensional flow field calculation.

The Chemical Kinetics of the Sampling Chamber

The calculations of the composition of the gases at the inlet leak of the mass spectrometer were made assuming the following picture of the mechanism of sampling the boundary layer gases. Since the geometry and precise operation of the sampling system are not yet established, uncertainties in the chemical kinetics in this region are present.

TABLE 5

SOME BOUNDARY LAYER REACTIONS

$C + C + M$	=	$C_2 + M$
$C + C_2 + M$	=	$C_3 + M$
$C + N + M$	=	$CN + M$
$C_2 + N$	=	$C + CN$
$C_2 + O$	=	$C + CO$
$C_3 + O$	=	$C_2 + CO$
$CN + N$	=	$C + N_2$
$CN + O$	=	$CO + N$
$C + O_2$	=	$CO + O^*$
$C_2 + O$	=	$CO + C^*$
$C + OH$	=	$CO + H$
$C + OH$	=	$CH + O$
$CH + O$	=	$CO + H$
$CH + N$	=	$CN + H$

* Represents electronically excited states

The gas which is to be analyzed by the mass spectrometer enters the sampling chamber from the boundary layer through one or more orifices in the body. The gas resides in this chamber at the same density as that in the boundary layer at the body orifice. The residence time (the average transit time from body orifice to the mass-spectrometer inlet leak) was assumed to be between .01 and 1 second. Calculations of composition were made for both times. The reaction rates depend on the density. The rates, of course, increase with increasing density. The residence time is also important in determining the amount of reaction and, hence, concentrations.

The chemical kinetics in this region are not strongly dependent on the temperatures. The important reactions are exothermic. The temperatures were assumed to be below $1000^{\circ}K$ so that no appreciable amount of endothermic reaction occurred.

The reactions mainly involved the consumption of the unstable species, e.g., N, O, C, CN, and C_2. The N and O atoms were consumed by reaction with CN and three-body atom-atom recombination. Cyanide radicals were removed by the three-body formation of C_2N_2. Carbon atoms disappeared by the three-body reactions forming C_2 and C_3.

The reactions which were found to be of importance are given in Table 6 together with the rate constants used. Many other reactions were also considered. Most of the reactions have not beenstudied to obtain rate data. The concentrations of the species are exponentially dependent upon certain reaction rate constants and considerably dependent on the concentration of others and thus can be in error by orders of magnitude. Thus the calculated concentrations can only be said to be the best estimates, but may be considerably in error.

Results

The results for which the chemical kinetics calculations were made were the concentrations of the species at the inlet leak of the mass spectrometer. However, since the flow field and boundary layer chemical kinetics calculations had to be made first, these intermediate results should also be considered.

For the altitudes and conditions of interest in these calculations most of the species were close to equilibrium. This was more nearly true for the maximum than for the minimum atmosphere. The nitrogen, however, tended to overshoot the equilibrium degree of dissociation. This resulted in more atomic nitrogen than would be predicted by equilibrium. At altitudes where there was

no ablation there also tended to be more atomic oxygen than at equilibrium. If a one second reaction time is actually available in the sampling chamber some of this departure from equilibrium may be decreased by reaction in this region.

Probably the largest uncertainty in the boundary layer chemical kinetics calculations made was that of the CN kinetics. In the program used for the atmospheric kinetics calculations the CN reaction system was not as complete as would have been desired. For conditions where the concentrations of N atoms were high, the CN should probably be lower than calculated. This would result in less C_2N_2 at the mass-spectrometer inlet leak and other changes in concentrations.

Some of the calculated concentrations at the inlet leak are extremely dependent on rate constants, some of which were only estimated. Among the more important of these are $N + CN \longrightarrow C + N_2$ and $C + N + M \longrightarrow CN + M$. Reactions involving certain other species, e.g., C_2 and CH appears to be fast enough to consume these species and leave little for analysis.

Ions and free electrons are formed in the flow field and boundary layer. Most of these are converted to NO^+ by charged rearrangement reactions and these ions will largely recombine

with the free electrons during the time in the sampling regime. Some negative ions may be formed (e.g., O^-, CN^-) and will probably be neutralized by the positive ions in this region. Thus ions and electrons are not expected to influence the operation of the mass spectrometer.

The results, which were obtained using the chemical kinetics described in the section on the kinetics of the sampling chamber and listed in Table 6, are best presented in tabular form. The concentrations are presented in Tables 7 through 10 for the four designated sampling points*. The data are presented for two atmospheres (denoted "Maximum" and "Minimum" for those of higher and lower densities, respectively), for two velocities (denoted "High" and "Low", respectively, for those of 25065 and 20308 feet sec^{-1} for the maximum atmosphere and 25852 and 21292 feet sec^{-1} for the minimum atmosphere), for three altitudes (given in km), and for two residence times in the sampling region. The uncertainties are large enough to prevent an accurate prediction of the composition. Hence, it is not practical to expect to interpret the mass spectrometer results by use of the chemical kinetics. Rather

---

* Only species that are expected in significant quantities are listed in Tables 7-10. Note that NO is not expected to be among them.

TABLE 6

REACTIONS IN THE SAMPLING CHAMBER

$N + N + M$	$\longrightarrow$	$N_2 + M$	2.2^{-32}
$N + O + M$	$\longrightarrow$	$NO + M$	3^{-32}
$O + O + M$	$\longrightarrow$	$O_2 + M$	5^{-33}
$C + N + M$	$\longrightarrow$	$CN + M$	1^{-32}
$C + C + M$	$\longrightarrow$	$C_2 + M$	1^{-32}
$C + C_2 + M$	$\longrightarrow$	$C_3 + M$	1^{-32}
$CN + CN + M$	$\longrightarrow$	$C_2N_2 + M$	3^{-33}
$N + NO$	$\longrightarrow$	$N_2 + O$	2.5^{-11}
$N + O_2$	$\longrightarrow$	$NO + O$	$3^{-16}T^{3/2}e^{-30}$ w/t
$N + CN$	$\longrightarrow$	$C + N_2$	1^{-13}
$N + CO_2$	$\longrightarrow$	$CO + NO$	1^{-14}
$CO + OH$	$\longrightarrow$	$CO_2 + H$	1^{-14}
$CN + O_2$	$\longrightarrow$	$CO + NO$	1^{-11}
$C_3 + O$	$\longrightarrow$	$C_2 + CO$	1^{-13}
$C + O_2$	$\longrightarrow$	$CO + O^1$	1^{-14}
$C_2 + N$	$\longrightarrow$	$C + CN$	1^{-13}
$C_2 + O$	$\longrightarrow$	$C + CO$	1^{-13}

TABLE 7

CONCENTRATIONS AT THE MASS SPECTROMETER INLET OF GASES SAMPLED AT THE STAGNATION POINT

Atm.	Vel.	Alt. (km.)	Time (sec.)	$n^*_{N_2}$ (cm^{-3})	n_N (cm^{-3})	n_{CO} (cm^{-3})	n_C (cm^{-3})	n_{C_3} (cm^{-3})	n_{CN} (cm^{-3})	$n_{C_2N_2}$ (cm^{-3})
Max	High	0	.01	1.3^{19}	0	2.6^{18}	2^{16}	2.7^{18}	1.2^{15}	6^{18}
Max	High	0	1	1.3^{19}	0	2.6^{18}	2^{14}	2.7^{18}	1.2^{13}	6^{18}
Max	High	50	.01	2.1^{18}	0	4.2^{17}	2^{14}	6.7^{17}	6^{15}	1^{18}
Max	High	50	1	2.1^{18}	0	4.2^{17}	2^{12}	6.7^{17}	6^{13}	1^{18}
Max	High	110	.01	2.7^{17}	0	4.3^{16}	1.9^{14}	3.8^{15}	3.4^{16}	1^{16}
Max	High	110	1	2.7^{17}	0	4.3^{16}	6^{13}	3.8^{15}	7.7^{15}	2.3^{16}
Max	Low	0	.01	1.3^{19}	0	2.3^{18}	1.4^{14}	8.1^{17}	1.4^{15}	7.2^{17}
Max	Low	0	1	1.3^{19}	0	2.3^{18}	1.4^{12}	8.1^{17}	1.4^{13}	7.2^{17}
Max	Low	50	.01	2.0^{18}	0	3.6^{17}	8.8^{14}	2.2^{17}	8.9^{15}	5.4^{17}
Max	Low	50	1	2.0^{18}	0	3.6^{17}	8.9^{12}	2.2^{17}	8.9^{13}	5.4^{17}
Max	Low	110	.01	2.8^{17}	3.1^{12}	4.2^{16}	0	2.6^{13}	3.1^{15}	5^{13}
Max	Low	110	1	2.8^{17}	0	4.2^{16}	0	2.6^{13}	7.7^{14}	1.2^{15}
Min	High	0	.01	1.4^{18}	0	7.7^{18}	1.6^{12}	5.7^{18}	1.7^{15}	2.3^{18}
Min	High	0	1	1.4^{18}	0	7.7^{18}	1.6^{10}	5.7^{18}	1.7^{13}	2.3^{18}
Min	High	20	.01	5.3^{17}	0	2.2^{18}	6.7^{14}	9.1^{18}	6.7^{15}	5.6^{17}
Min	High	20	1	5.3^{17}	0	2.2^{18}	6.7^{12}	9.1^{18}	6.8^{13}	5.6^{17}
Min	High	30	.01	2.4^{17}	0	7.3^{17}	2.3^{15}	7.2^{16}	2.4^{16}	9.2^{16}
Min	High	30	1	2.4^{17}	0	7.3^{17}	2.6^{13}	7.2^{16}	2.6^{14}	1.1^{17}
Min	Low	0	.01	2.0^{18}	0	7.3^{18}	2.3^{14}	1.9^{18}	2.3^{15}	1.6^{18}
Min	Low	0	1	2.0^{18}	0	7.3^{18}	2.3^{12}	1.9^{18}	2.3^{13}	1.6^{18}
Min	Low	20	.01	6.5^{17}	0	1.9^{18}	7.8^{14}	1.6^{17}	9.9^{15}	2.7^{17}
Min	Low	20	1	6.5^{17}	0	1.9^{18}	1.0^{13}	1.6^{17}	1.0^{14}	2.7^{17}
Min	Low	30	.01	3.6^{17}	4^{1}	7.9^{17}	0	7.4^{14}	1.4^{16}	6.5^{13}
Min	Low	30	1	3.6^{17}	0	7.9^{17}	0	7.4^{14}	2.8^{14}	1.3^{16}

* n's are in units of particles/cm^3. To convert to pressure in atmospheres, multiply by 6.8×10^{-20}.

TABLE 8

CONCENTRATIONS AT THE MASS SPECTROMETER INLET OF GASES SAMPLED AT THE CONE SURFACE

Atm.	Vel.	Alt. (km)	Time (sec.)	$n^*_{N_2}$ (cm^{-3})	n_N (cm^{-3})	n_{CO_2} (cm^{-3})	n_{CO} (cm^{-3})
Max	High	0	.01	1.67^{18}	1.2^{15}	0	2.44^{17}
Max	High	0	1	1.67^{18}	1.2^{13}	0	2.44^{17}
Max	High	50	.01	8.2^{16}	1.0^{15}	0	1.9^{16}
Max	High	50	1	8.6^{16}	9.2^{15}	0	1.9^{16}
Max	High	110	.01	1.8^{14}	1.3^{16}	1.6^{15}	3.4^{15}
Max	High	110	1	1.8^{14}	1.3^{16}	1.6^{15}	3.4^{15}
Max	Low	0	.01	1.62^{18}	1.2^{15}	0	2.37^{17}
Max	Low	0	1	1.62^{18}	1.2^{13}	0	2.37^{17}
Max	Low	50	.01	3.4^{15}	7.8^{17}	0	2.1^{16}
Max	Low	50	1	3.4^{17}	1.0^{17}	0	2.1^{16}
Max	Low	110	.01	4.5^{16}	3^{15}	1.0^{15}	1.5^{15}
Max	Low	110	1	4.5^{16}	3^{15}	1.0^{15}	1.5^{15}
Min	High	0	.01	5.77^{16}	1.2^{15}	0	1.2^{18}
Min	High	0	1	5.77^{16}	1.2^{13}	0	1.2^{18}
Min	High	20	.01	2.5^{15}	6.2^{17}	0	3.1^{17}
Min	High	20	1	2.5^{17}	1.3^{17}	0	3.1^{17}
Min	High	30	.01	7.9^{16}	2.4^{16}	2^{16}	2.3^{16}
Min	High	30	1	8.0^{16}	2.3^{16}	2^{16}	2.3^{16}
Min	Low	0	.01	7.7^{17}	2^{16}	0	8^{17}
Min	Low	0	1	7.8^{17}	0	0	8^{17}
Min	Low	20	.01	1.9^{15}	5^{17}	0	2.6^{17}
Min	Low	20	1	1.9^{17}	1.3^{17}	0	2.6^{17}
Min	Low	30	.01	5.3^{16}	9.3^{15}	1.7^{16}	4.2^{16}
Min	Low	30	1	5.3^{16}	9.2^{15}	1.7^{16}	4.2^{16}

* n's are in units of particles/cm^3. To convert to pressure in atmospheres, multiply by 6.8×10^{-20}.

TABLE 9

CONCENTRATIONS AT THE MASS SPECTROMETER INLET OF GASES SAMPLED AT THE CYLINDER SURFACE

Atm.	Vel.	Alt. (km)	Time (sec.)	$n^*_{N_2}$ (cm^{-3})	n_N (cm^{-3})	n_{CO} (cm^{-3})	n_O (cm^{-3})	n_{O_2} (cm^{-3})	n_{CN} (cm^{-3})	$n_{C_2N_2}$ (cm^{-3})	n_C (cm^{-3})	n_{C_3} (cm^{-3})
Max	High	0	.01	5.9^{17}	4^{15}	3.2^{16}	3.1^{16}	8^{15}	1^{15}	2^{13}	0	0
Max	High	0	1	5.9^{17}	4^{13}	3.2^{16}	3.1^{14}	2.2^{16}	3^{14}	3^{14}	0	0
Max	High	50	.01	5.5^{16}	3^{16}	3.8^{15}	5.3^{15}	0	1^{14}	0	0	0
Max	High	50	1	7^{16}	3^{14}	3.8^{15}	1.8^{15}	1.8^{15}	1^{14}	5^{11}	0	0
Max	High	110	.01	1.9^{15}	5^{15}	2.4^{14}	3.4^{14}	1^{12}	1^{13}	0	0	0
Max	High	110	1	4.4^{15}	5^{13}	2.4^{14}	3.4^{14}	1^{12}	1^{13}	0	0	0
Max	Low	0	.01	6.34^{17}	3^{15}	3.4^{16}	1.8^{16}	1.5^{16}	1^{15}	2^{13}	0	0
Max	Low	0	1	6.35^{17}	3^{13}	3.4^{16}	3.1^{14}	2.4^{16}	3^{14}	3^{14}	0	0
Max	Low	50	.01	5.5^{16}	3^{16}	3.8^{15}	5.3^{15}	0	1^{14}	0	0	0
Max	Low	50	1	7.0^{16}	3^{14}	3.8^{15}	1.1^{15}	2.1^{15}	1^{14}	5^{11}	0	0
Max	Low	110	.01	2.1^{15}	5^{15}	2.5^{14}	3.5^{14}	1^{12}	1^{13}	0	0	0
Max	Low	110	1	4.6^{15}	5^{13}	2.5^{14}	3.5^{14}	1^{12}	1^{13}	0	0	0
Min	High	0	.01	1.3^{17}	1^{17}	1^{17}	1^{16}	2^{16}	1^{16}	1^{14}	2^{14}	7^{13}
Min	High	0	1	1.3^{17}	1^{15}	1^{17}	1^{14}	2.5^{16}	1^{15}	5^{15}	2^{12}	1^{14}
Min	High	20	.01	1.5^{16}	3^{15}	1^{16}	5^{15}	1^{14}	1^{16}	0	0	0
Min	High	20	1	1.5^{16}	3^{13}	1^{16}	1^{14}	2.5^{15}	1^{16}	1^{15}	0	0
Min	High	30	.01	2.2^{15}	7^{14}	3^{15}	4^{15}	1^{12}	1^{16}	0	0	0
Min	High	30	1	2.6^{15}	7^{12}	3^{15}	4^{15}	1^{12}	1^{16}	1^{14}	0	0
Min	Low	0	.01	1.1^{17}	1.1^{17}	1.1^{17}	4^{16}	3.5^{16}	1^{15}	2^{13}	1.4^{16}	4^{16}
Min	Low	0	1	1.1^{17}	1.1^{15}	1.1^{17}	5^{14}	5^{16}	1^{15}	5^{16}	1.4^{14}	4^{16}
Min	Low	20	.01	1.4^{16}	3^{15}	1.6^{16}	1.6^{16}	0	4^{15}	0	0	0
Min	Low	20	1	1.5^{16}	3^{13}	1.6^{16}	2.7^{15}	7^{15}	4^{15}	1.3^{16}	0	0
Min	Low	30	.01	3.1^{15}	7^{14}	3.5^{15}	3.6^{15}	1^{12}	9^{15}	0	0	0
Min	Low	30	1	3.5^{15}	7^{12}	3.5^{15}	3.6^{15}	1^{12}	9^{15}	5^{14}	0	0

* n's are in units of particles/cm^3. To convert to pressure in atmospheres, multiply by 6.8×10^{-20}.

TABLE 10

CONCENTRATIONS AT THE MASS SPECTROMETER INLET OF GASES SAMPLED AT THE FLARE SURFACE

Atm.	Vel.	Alt. (km)	Time (sec.)	$n^*_{N_2}$ (cm^{-3})	n_N (cm^{-3})	n_{CO_2} (cm^{-3})	n_{CO} (cm^{-3})	n_{CN} (cm^{-3})	$n_{C_2N_2}$ (cm^{-3})	n_C (cm^{-3})	n_{C_3} (cm^{-3})
Max	High	0	.01	1.3^{18}	0	0	2.2^{17}	7.8^{15}	8.0^{13}	1.4^{15}	6.4^{16}
Max	High	0	1	1.3^{18}	0	0	2.2^{17}	2.3^{17}	2.4^{17}	1.6^{13}	6.5^{16}
Max	High	50	.01	7.6^{17}	3^{15}	0	1.1^{17}	0	0	0	0
Max	High	50	1	7.6^{17}	3^{13}	0	1.1^{17}	0	0	0	0
Max	High	110	.01	1.4^{17}	2.5^{16}	2.7^{12}	8^{15}	0	0	0	0
Max	High	110	1	1.5^{17}	2.8^{15}	2.7^{12}	8^{15}	0	0	0	0
Max	Low	0	.01	1.4^{18}	4^{12}	0	2.0^{17}	8.2^{15}	2.2^{17}	0	0
Max	Low	0	1	1.4^{18}	0	0	2.0^{17}	8.3^{13}	2.2^{17}	0	0
Max	Low	50	.01	6.6^{17}	1^{9}	0	7.5^{15}	1.7^{16}	3.2^{16}	0	0
Max	Low	50	1	6.6^{17}	0	0	7.5^{15}	2.2^{14}	4.0^{16}	0	0
Max	Low	110	.01	4.9^{15}	6.8^{16}	3.8^{13}	4.4^{15}	0	0	0	0
Max	Low	110	1	8.0^{16}	4.7^{15}	3.8^{13}	4.4^{15}	0	0	0	0
Min	High	0	.01	5.2^{17}	3^{14}	0	1.1^{18}	3.9^{15}	1.2^{15}	0	0
Min	High	0	1	5.2^{17}	0	0	1.1^{18}	1.0^{14}	3.1^{15}	0	0
Min	High	20	.01	4.0^{17}	3^{17}	0	5.4^{17}	0	0	0	0
Min	High	20	1	5.5^{17}	4.2^{13}	0	5.4^{17}	0	0	0	0
Min	High	30	.01	1.5^{17}	1.3^{16}	0	1.6^{17}	0	0	0	0
Min	High	30	1	1.6^{17}	1.4^{14}	0	1.6^{17}	0	0	0	0
Min	Low	0	.01	5.0^{17}	1.5^{15}	0	1.1^{18}	0	0	0	0
Min	Low	0	1	5.0^{17}	1.5^{13}	0	1.1^{18}	0	0	0	0
Min	Low	20	.01	4.6^{17}	5.4^{15}	0	4.1^{17}	0	0	0	0
Min	Low	20	1	4.0^{17}	5.4^{13}	0	4.1^{17}	0	0	0	0
Min	Low	30	.01	1.0^{17}	1.3^{16}	2.5^{12}	1.1^{17}	0	0	0	0
Min	Low	30	1	1.1^{17}	2.1^{14}	2.5^{12}	1.1^{17}	0	0	0	0

* n's are in units of particles/cm^3. To convert to pressure in atmospheres, multiply by 6.8×10^{-20}.

the chemical kinetics are useful only in predicting an order of magnitude composition to be expected in the mass spectrometer assuming an atmospheric composition. The mass spectrometer can thus be expected to mainly given an elemental analysis (i.e., carbon, nitrogen, oxygen) from which it is necessary to reconstruct the undisturbed ambient atmosphere.

DISCUSSION

General Mass Spectrometry Considerations

From the kinetic analysis (Tables 7-10) the main species to be expected are N_2, N, CO_2, CO, C_2N_2, CN, O_2, O, C_3, and C. Sufficient quantities of gases to provide adequate samples for the mass spectrometer appear to be available at all altitudes that were considered. The quantities of ions and electrons that would be present would be trivial. Argon would be present in all cases at the level that is present in the atmosphere. Typical mass spectra may be found in the literature for N_2, CO_2, CO, O_2, and A. Calibration for these substances and C_2N_2 should present no problems. Rather sophisticated experiments would have to be performed in order to calibrate for N, CN, O, C_3, and C. In order to do a good job on C_2N_2 and CN, the mass spectrometer would probably have to reach m/e-52.

Mass spectrometer data for some of the gases of interest are listed in Table 11 for a Consolidated Model 21-611 Mass Spectrometer. Although it is not the same one that would be flown, the data can be used to illustrate analytical considerations. C_2N_2, CO_2, A, C_3, O_2, and H_2O would be determined directly from ion signals at

TABLE 11

MASS SPECTROMETER CALIBRATION*

m/e	A	N_2	CO	Air	CO_2	H_2O
2						.03
12			1.02		3.62	
13			.07		.03	
13½	.42					
14		6.98	1.21	38.53		
15		.14	.03	.75		
16			.10	5.54	8.36	1.43
17					.10	22.35
18						100.00
19						.16
20	28.75			2.00		.21
22					4.51	
28		100.00	100.00	566.57	8.88	
29		.90		5.14	.28	
30			.22			
32				100.00		
34				.40		
36	.37			.14		
38	.09			.05		
40	100.00			6.93		
44					100.00	
**Sensitivity	292.92	281.89	290.21	40.25	237.96	45.11

* For Consolidated Electrodynamics Corp. Model 21-611 (Figure 3.06 of CEC Operation and Maintenance Manual 21-611, Nov. 1957).

** Sensitivity in divisions per micron at 10 micro-amps ionizing current.

masses 52, 44, 40, 36, 32, and 18, respectively. Fragment ion signals could then be evaluated for all fragment peaks due to these substances. CN and OH would be determined from residual signals at masses 26 and 17, respectively. Quantities of N_2, CO, and C at the stagnation point (Table 7) would be evaluated from the signals at masses 28, 14, and 12. At the cone surface (Table 8) accurate determination of N_2, CO, and N could be hampered because 28 and 14 would be the two most significant peaks for the three unknowns. One would, therefore, have to employ weaker signals at masses 29, 16, 15, 13, and 12 to estimate the most probable analysis. N_2, N, CO, O, and C would have to be considered at the cylinder surface (Table 9). Masses 28, 16, 14, and 12 would be most useful for this analysis, but could cause some problems where the N atom signal at mass 14 is strong. For this reason, it would probably be helpful to allow the gases to stand for about one second so that N atoms would have an opportunity to react before carrying out the analysis. The same considerations would also apply to the flare surface (Table 10).

The lowest contribution to ablation products occurs at the surface of the cylinder. Thus, the further back towards the flare, the lower would be the level of effect of upstream ablation

products. Since the surface temperature would also be lowest in this region, it seems appropriate to recommend it for location of the surface inlet. The sampling chamber should be designed with sufficient impedance to allow the products about a second of contact in advance of analysis.

It is impossible to calculate the errors to be expected because so many factors are uncertain. It seems reasonable to expect that a reasonably accurate element analysis would be expected. However, one will have to rely more on plausible chemistry of the Martian atmosphere than on kinetic information in order to extrapolate to the actual atmospheric composition.

Gaseous impurities normally present in ATJ graphite could cause additional errors in interpretation of mass spectrometric data unless special purification techniques are employed. Several varieties of high purity graphite are commercially available, as is specially purified ATJ graphite. A study of the various graphites should be undertaken to select the one best suited for the intended usage.

Mass Spectrometric Analysis of Water

A factor which could not be looked into thoroughly was the chemical kinetics of water. In the time available, most of

the complex calculations had to be done with existing programs. The program which calculated the composition of the gases resulting from the mixing of the atmosphere and the ablation products lumped all species arising from the water together with the argon in one term.

Water reactions comprise a complex system. It can be expected that for various conditions, different species arising from this system would predominate. These species would include H, H_2, OH, and H_2O with some of the oxygen ending up on other species (O, O_2, CO_2, etc.) or with some oxygen from other species ending up bound to hydrogen. In general, in the systems which have more ablation and thus more carbon, it can be expected that there will be more H_2 while in those with little ablation, there should be more OH. At the lower altitudes there will be more time to reform H_2O. Such general statements are all that can be made without a considerably longer time to make a more complete analysis.

In principle, the accuracy of water analysis could be assured by providing means of determining the total quantity of elemental hydrogen that is present in the gases analyzed by the mass spectrometer if no hydrogen arises from any other source than water. In order to do this properly, one would have to determine

ion signals at m/e-1,2, and the heavier peaks that would result from combination of hydrogen with the other elements. Therefore, one may conjecture that in the case of very accurate qualitative and quantitative analysis of all species, one should be able to obtain a rather accurate analysis for water. Reduction in either category would tend to increase errors. With little ablation, determination of OH (m/e-17) would be important, while with more ablation, determination of H_2 (m/e-2) would be desirable.

Condensation of Carbon Vapor

The condensation of carbon vapor cannot be assessed quantitatively for a variety of temperatures and surfaces because of lack of experimental information.

Recent mass spectrometric data reported[13] for two substrate temperatures indicate that the reflection coefficients* of C and C_3 on solid carbon are different from zero.

It was found that the apparent reflection coefficient of C atoms from polycrystalline graphite surface is 0.6 ± 0.2 at temperatures of $2300^{\circ}K$ while at the same conditions the reflection coefficient of C_3 molecules is 0.9 ± 0.2. At a temperature of

---

* Number reflected/number impinging

about 800°K (which approaches the anticipated temperature of the leak) the reflection coefficients of C and C_3 are 0.3 ± 0.15 and 1 ± 0.2 respectively. This information indicates that there might be some fractionation of C during the sampling process. Therefore, possible errors from this source must be investigated.

Differentiating Between Carbon from Vehicle and Atmosphere

Carbon will originate from both the atmosphere and surface of the vehicle in some cases. When the quantity from the surface is appreciable, it would be desirable to determine the relative quantities that arose from each source. Having such information will not be absolutely essential, if accurate analysis of all of the other elements is available for all altitudes, especially since the gases at the higher altitudes will be free of surface carbon. However, the availability of such information could improve accuracy and credibility of the results by providing a check.

About 1% of the earth's carbon is made up of the 13-isotope. Spectroscopic observation of the skies indicate that it may be similar for Mars[14]. A heat shield fabricated from about 10% of a uniform dispersion of C^{13} should provide such information under conditions where sufficient ablation occurs. Since it would

be necessary to account for C^{12} and C^{13} in all molecules which contain carbon, it would be necessary to examine additional masses and have good mass resolution for the heavier molecules. This requirement is likely to be in advance of the current state-of-the-art for appropriate mass spectrometers. In addition, the cost of fabricating such a heat shield would be high. Another approach would be to seed the heat shield with a material that would volatilize at the same rate as graphite, and would thus serve as an ablation indicator. This substance should be inert, have a mass in the range that could be handled by the mass spectrometer, and should produce peaks that would not interfere with expected peaks. Obviously a research program would have to be carried out to develop such a material. These approaches should be evaluated to determine their potential value in the light of being able to carry out suitable experiments with ordinary pure graphite.

REFERENCES

1. Goodman, M., "Ablation Design Program (Deck 9)", GE-RSD Report, unpublished.
2. Helsel, W., "User's Manual for the Ablation Design Program", GE-RSD Report, July, 1964.
3. Lees, L., "Laminar Heat Transfer Over Blunt-Nosed Bodies at Hypersonic Speeds", Jet Propulsion, April, 1956.
4. Eckert, E., "Engineering Relationships for Heat Transfer and Turbulent Boundary Layer Flow Over Surfaces With Constant Pressure and Temperature", ASME Paper No. 55-A-31, 1955.
5. Walker, G., "Some Comments on Laminar and Turbulent Heat Transfer Equations", GE-RSD AETM 147, December, 1959.
6. Gordon, P., "Analysis of One-Dimensional Heat Conduction Program", GE TIS 64SD201, January, 1964.
7. Grebey, C., "User's Manual for the One-Dimensional Heat Conduction Program", GE-RSD Report, June, 1964.
8. Scala, S., and Gilbert, L., "The Sublimation of Graphite at Hypersonic Speeds", GE TIS R64SD55, August, 1964.
9. Fogaroli, R., "Graphite Surface Chemistry in the Martian Atmosphere", PIR HTT-8151-452, August, 1965.
10. Scala, S., "A Study of Hypersonic Ablation", GE TIS R59SD438, September, 1959.
11. Dorrance, "Viscous Hypersonic Flow", McGraw-Hill, New York, 1962.

12. Bortner, M.H., "The Chemical Kinetics of Planetary Entry", Dynamics of Manned Lifting Planetary Entry (ed. S.Scala, A. Harrison and M. Rogers), Wiley, N.Y., 1963, pp. 172-184.

13. Chupka, W.A., Berkowitz, J., Meschi, D.J., and Tasman, H.A., "Mass Spectrometric Studies of High Temperature Systems", Advances in Mass Spectrometry, Vol. 2, Pergamon Press, N.Y., 1963, p. 99.

14. Owen, T., IITRI, Private Communication, July 1, 1965.